On some methods of downward continuation of mean free-air gravity anomaly

Hossein Nahavandchi

Royal Institute of Technology

Department of Geodesy and Photogrammetry

S-100 44 Stockholm, Sweden.

Abstract

This paper investigates four methods of downward continuation of free-air gravity anomalies to sea-level, an iterative process based on the Poisson's integral, a linear simple formula, a method based on the Pellinen approximation and the one based on the topographc-isostatic potential proposed by Sjöberg. Mean free-air gravity anomalies in $6' \times 10'$ cells from a test area with topographical heights between 71-396 metres have been successfully downward continued to sea-level. The effect of the downward continuation is everywhere positive on the geoid, while it is negative and positive on gravity anomalies. The results show some differences between these methods. The methods based on the Poisson's integral and topographic-isostatic potential have the smallest difference among the methods. A mean difference of 0.97 cm for the downward continuation effect on the geoid is computed between these two methods. In the Poissons' integral, long-wavelength contributions have been evaluated using a global gravity model and in the method based on topographc-isostatic potential, $30' \times 30'$ heights information over the world are used to consider the long-wavelength contributions. They are missing in the other two methods. The correctness of the solution has then been checked by back substitution of the gravity values at the geoid to estimate them at the surface of the Earth. The Poisson's integral uses the gravity anomalies, directly, for the downward continuation of them to the geoid, while the Sjöberg's method implies the height data. Also, because some approximation made in the latter, the iterative process of the Poisson's integral is preferred.

Key words: Downward continuation, Poisson's integral, topographic-isostatic potential, Pellinen approximation

1 Introduction

Geoid determination by Stokes well known formula requests that the gravity anomalies Δg represent boundary values at the geoid, which implies all topographic masses are removed or reduced and gravity anomalies Δg must refer to the geoid. For satisfying the second condition, as the observations (gravity values g) are available on the surface of the Earth, we have to reduce them from the Earth's surface to the geoid. This reduction is called "downward continuation". The main problem with the downward continuation is the masses between the surface level and the geoid and irregularity of the density distribution, which causes the disturbing potential

is non-harmonic outside the geoid. However, the reduction problem would only fail, if a fully analytical approach be used. As terrestrail gravity anomalies are only available at discrete points or as mean grid values, therefore a unique solution could be expected. The free-air model has been used in the solving of the Molodenskii's problem (Heiskanen and Moritz, 1967; Moritz, 1980).

Bjerhammar (1962) and (1963) pointed out that it is always possible to downward continue point gravity anomalies (at least for a limited set of observations Δg) to an internal sphere of radius R (the Bjerhammar sphere) embedded in the Earth. In this study, we carry out the downward continuation of mean free-air anomalies. Hence, the smooting (due to avergaing) in the methods studied herein are present.

Heiskanen and Moritz (1967) also proposed an iterative process to downward continue the free-air gravity anomalies from surface level to the geoid. This process uses Poisson's integral, directly, which is more accurate than the linear and planar approximations (see ibid). Assuming that the gravity anomalies Δg are linearly correlated with elevation, Moritz (1980) proposed a method to downward continue gravity anomalies to sea-level based on the Pellinen approximation.

Sjöberg (1998) has developed another way to downward continue the gravity anomalies. His study is based on the external type of topographic-isostatic potential and gravity anomaly and its vertical derivatives, derived from the Airy/Heiskanen model. The effect is estimated on the geoid for the downward continuation of gravity to sea-level in the application of Stokes formula.

We have also to mention that recent investigation by Vaníček et al. (1996) and Sun and Vaníček (1996) and (1998) concentrated on the downward continuation of mean Helmert grvaity. They showed that the downward continuation of mean Helmert's anomaly is a well posed problem with a unique solution in $5' \times 5'$ cells and can be done routinely to any accuracy desired in the geoid computation.

2 Downward continuation of free-air anomaly by the Poisson's integral

The Stokes's integral requires that the disturbing potential T is harmonic on the geoid, which implies that there are no masses outside the geoid. Assume a fictious field of gravity anomalies Δg^* on the geoid, which generate on the ground level the measured free-air anomalies Δg. These two anomalies can be related by the Poisson's formula (excluding the spherical harmonics of degrees zero and one)(Kellogg, 1929; MacMillan, 1930):

$$\Delta g = \frac{t^2(1-t^2)}{4\pi} \iint_\sigma \frac{\Delta g^*}{D^3} d\sigma \,, \tag{1}$$

where

$$t = \frac{R}{r} \;;\; r = R + H_P.$$

In this equation spherical approximation has been used; R is the mean radius of the Earth, H_P is the orthometric height of the surface point P, σ is the unit sphere and

$$D = \sqrt{1 - 2tcos\psi + t^2} = \frac{\ell}{r},$$

where ℓ and ψ are the spatial and spherical distances between the surface point P and the running points under integral. The observed values Δg at level surface are obtained by measurements, and the free-air anomalies Δg^* at sea-level are desired. In this sense, Eq. (1) can be solved in different ways; for example by a linear approximation as:

$$\Delta g_P^* = \Delta g_P - \frac{\partial \Delta g}{\partial H_P} H_P \, . \tag{2}$$

After Bjerhammar (1962), Heiskanen and Moritz (1967) proposed an iterative process to solve the integral (1), which is more accurate than linear approximation in Eq. (2). An alternative expression for Eq. (1) is (Heiskanen and Moritz, 1967):

$$\Delta g_P^* = \Delta g_P - \frac{t^2(1-t^2)}{4\pi} \iint_\sigma \frac{\Delta g^* - \Delta g_P^*}{D^3} d\sigma \, , \tag{3}$$

which can be used as the recursive formula that lends to an iterative solution. As a first approximation one can set

$$\Delta g^{*^1} = \Delta g \, , \tag{4}$$

i.e. taking the known free-air gravity anomalies at the surface level as the first iteration for all points in the area of interest. This iterative process downward continues the free-air anoamalis from surface level (Δg) to the geoid (Δg^*). If we convolve downward continuation correction on gravity anomaly with Stokes's kernel, the effect on the geoid for the downward continuation of gravity to sea-level is obtained. The physical interpretation of this process is that the free-air gravity anomalies Δg^* at geoid, computed by the iterative method, generate on the level surface gravity anomalies Δg, which are identical with actual grvaity anomalies generated by observations.

The convergence of the iterative process has to be paied enough attention, because the solution of integral equations of first kind (like the Poisson's integral) may be unstable and cause some errors in the sought free-air anomaly at the geoid (Vaníček et al., 1996). The prescribed limit of the convergence of the iterative process is set up to 10 μGal to guarantee the magic level 1 cm for the accuracy of the geoid (Vaníček and Martinec, 1994). The iterative process uses gravity anomalies as a main input data to downward continue them to the geoid. The height data used in the Poisson's integral is in second degree of importance compared with the gravity anomalies.

Fortunately, the Poisson's integration kernel vanishes quickly with growing the distance from the computation point P. It means that it is enough to integrate Eq. (3) over a small area of σ_0 around the computation point, instead of the whole Earth (over σ). But, limiting the area of integration to σ_0 causes an error which is, here, called truncation error. We have tested different radius of integration and found out that a radius of integration $\psi_0 = 1^\circ$ gives small truncation

error (see also, Vaníček et al., 1996) . To obtain accurate results for the downward continuation correction, we have also modified the Poisson's kernel by the minimizing the upper limit of the truncation error (see e.g. Molodenskii et al., 1962; Sjöberg, 1984; Vaníček and Sjöberg, 1991). Discribing the Poisson's kernel by

$$K(H,\psi) = \frac{R(r^2 - R^2)}{\ell^3} = \sum_{n=0}^{\infty}(2n+1)(\frac{R}{r})^{n+1}P_n(\cos\psi) \ , \tag{5}$$

the modified Poisson's kernel can be evaluated from

$$K^m(H,\psi,\psi_0) = K(H,\psi) - \sum_{n=0}^{L}\frac{2n+1}{2}s_n(H,\psi_0)P_n(\cos\psi) \ , \tag{6}$$

where s_n is the unknown coefficients to be computed from the following system of equations (Molodenskii et al., 1962)

$$\begin{aligned}\sum_{n=0}^{L}\frac{2n+1}{2}s_n(H,\psi_0)e_{in}(\psi_0) &= Q_i(H,\psi_0) \\ & \qquad i = 0,1,\cdots,L\end{aligned} \tag{7}$$

where

$$e_{in}(\psi_0) = \int_{\psi_0}^{\pi} P_i(\cos\psi)P_n(\cos\psi)\sin\psi d\psi \ , \tag{8}$$

$$Q_n(H,\psi_0) = \int_{\psi_0}^{\pi} K(H,\psi)P_n(\cos\psi)\sin\psi d\psi \ . \tag{9}$$

We have selected L=20 in our computations. The contribution of the rest of the world ($Tg(P)$=truncation error) is quite small (will be shown in numerical investigations) and can be evaluated using a global gravity model as (see, e.g. Vaníček et al., 1996):

$$Tg(P) = \frac{R\gamma}{2r}\sum_{n=2}^{\infty}\sum_{m=-n}^{n}(n-1)\bar{Q}_n(H,\psi_0)T_{nm}Y_{nm}(P) \tag{10}$$

where

$$\bar{Q}_n(H,\psi_0) = \int_{\psi_0}^{\pi} K^m(H,\psi,\psi_0)P_n(\cos\psi)\sin\psi d\psi \ , \tag{11}$$

and the modified Poisson's kernel in a spectral form is

$$K^m(H,\psi,\psi_0) = \sum_{n=0}^{\infty}\frac{2n+1}{2}\bar{Q}_n(H,\psi_0)P_n(\cos\psi) \ . \tag{12}$$

γ is the normal gravity, T_{nm} are the potential coefficients taken from a global gravity model and Y_{nm} are the fully normalized spherical harmonics.

We have also subtracted the low degree harmonics Δg_L from the gravity anomalies Δg at the surface of the Earth (see, also Vaníček et al., 1996). Δg_L have been computed from EGM96 global model (Lemoine et al, 1997). We have downward continued this long-wavelength part,

separately. Finally, the contributions from these long-wavelength part and corrections due to the truncation error are added to the short-wavelength downward continued part of free-air anomaly determined by the iterative process.

To have a simpler computing procedure, in opposite with the iterative process, Eq. (2) is used instead of the Poisson's integral. To downward continue the gravity anomalies by this simple expression, one need to know the vertical gradient of gravity anomalies. We have assumed that the free-air gravity anomaly changes linearly with elevation according to the Bouguer plate correction $2\pi G\rho h$, and this change is only dependent to the variations in computation point P. G is the gravitational constant and ρ is the density of the terrain. Hence, Eq. (2) can be written to

$$\Delta g_P^* = \Delta g_P - 2\pi G\rho H_P \ . \tag{13}$$

This formula will next be compared with the results of the iterative process.

3 Downward continuation of free-air anomaly by the Pellinen approximation

The vertical gradient of gravity anomaly in Eq. (2) is needed to be evaluated correctly for accurate computation of downward continuation of free-air gravity anomalies. It can be estimated from (Heiskanen and Moritz, 1967)

$$\frac{\partial \Delta g}{\partial r} = \frac{R^2}{2\pi} \iint_\sigma \frac{\Delta g - \Delta g_P}{\ell_0^3} d\sigma \ , \tag{14}$$

where $\ell_0 = 2R \sin \frac{\psi}{2}$. Assuming that there are linear correlation between gravity anomalies and heights, Moritz (1980) came to the following expression for the vertical gradient of gravity anomalies based on the Pellinen approximation:

$$\frac{\partial \Delta g}{\partial r} = 2\pi G\rho \frac{R^2}{2\pi} \iint_\sigma \frac{H - H_P}{\ell_0^3} d\sigma \ . \tag{15}$$

Inserting Eq. (15) into Eq. (2), one can estimate downward continuation effect of Δg to the geoid (Δg^*).

4 Downward continuation of gravity anomaly by a method based on topographic-isostatic compensation potential

Sjöberg (1998) has studied downward continuation of gravity anomalies on the geoid in a different way. His study would mainly apply the downward continuation of the gravity anomaly and its effect on the geoid, directly. Moritz (1980) assumed that the free-air anomaly changes linearly with elevation. This linear correlation derived based on the simplified Airy/Heiskanen compensation potential. In Sjöberg (1998), the effect on the geoid is considered for the downward continuation of free-air gravity to sea-level using original Airy/Heiskanen compensation

potential. The gravity anomaly can analytically be continued down to sea-level, e.g by the Taylor expansion

$$\Delta g^* = \Big(1 - H_P \frac{\partial}{\partial r_P} - \frac{1}{2} H_P^2 \frac{\partial^2}{\partial r_P^2} \cdots \Big) \Delta g \ . \tag{16}$$

Sjöberg (1998) used the external type of topographic-isostatic potential and gravity anomaly and its vertical derivatives, derived from the Airy/Heiskanen model for isostatic compensation. From the first and the second radial derivatives of the gravity anomaly, the effect on the geoid is estimated for the downward continuation of gravity to sea-level in the application of Stokes's formula. This effect is composed of two parts as

$$\begin{aligned} \delta N_{dwc} &= \frac{R}{4\pi\gamma} \iint_\sigma S(\psi) \delta g_{dwc} d\sigma \\ &= \delta N^1_{dwc} + \delta N^2_{dwc} \ , \end{aligned} \tag{17}$$

where $S(\psi)$ is Stokes function, γ is the normal gravity and δg_{dwc} is the downward continuation of free-air gravity anomaly to sea-level. The first part of the correction can be obtained from (Sjöberg, 1998):

$$\delta N^1_{dwc} = \frac{1}{4\pi} \iint_\sigma S(\psi)(A H_Q^3 + B H_Q^4) d\sigma_Q \tag{18}$$

or in spectral form

$$\delta N^1_{dwc} = \sum_{n=2}^{M} \frac{1}{n-1} \sum_{m=-n}^{n} [A(H^3)_{nm} + B(H^4)_{nm}] Y_{nm}(P) \ , \tag{19}$$

where

$$(H^\nu)_{nm} = \frac{1}{4\pi} \iint_\sigma H^\nu Y_{nm} d\sigma; \quad \nu = 3, 4 \ , \tag{20}$$

$A = 0.585 \ \ m/km^3$

$B = -4.9 \times 10^{-3} \ \ m/km^4$

and M is the maximum degree of expansion. We have used M=360 in our computations.

The first correction term has mostly short-wavelength nature and contributes locally. It is the dominent part of downward continuation. The second part of the correction, δN^2_{dwc}, expected to have a long-wavelength nature (see Sjöberg, 1998) and a spherical harmonic representation has been used for numerical investigations. It can be written (Sjöberg, 1998):

$$\delta N^2_{dwc} = -\sum_{n,m} \frac{2}{n-1} C_{nm} Y_{nm} \ , \tag{21}$$

where

$$C_{nm} = \frac{1}{4\pi} \iint_\sigma H \Big(\frac{\Delta g}{\gamma} + 2\frac{\zeta}{r} \Big) Y_{nm} d\sigma \ . \tag{22}$$

$\frac{\Delta g}{\gamma} + 2\frac{\zeta}{r}$ may be computed from:

$$\frac{\Delta g}{\gamma} + 2\frac{\zeta}{r} = \sum_{n,m}(n+1)T_{nm}\Big(\frac{R}{r}\Big)^{n+2}Y_{nm}\ , \tag{23}$$

where T_{nm} are the potential coefficients and ζ is the height anomaly. Formula (21) can also be written:

$$\delta N^2_{dwc} = -\frac{1}{2\pi}\iint_{\sigma} S(\psi)H\Big(\frac{\Delta g}{\gamma} + 2\frac{\zeta}{r}\Big)d\sigma\ . \tag{24}$$

Then the total effect on geoid from downward continuation of gravity anomalies to sea-level, can be computed from the summation of the local contribution δN^1_{dwc} and the global contribution δN^2_{dwc}. In the formula (17), the direct gravity anomaly effect, caused by the reduction of the terrain, has also been applied to the gravity anomalies at the surface level. In iterative process this direct effect has not been applied. It has also to be mentioned that in the main part of the downward continuation (δN^1_{dwc}) in formula (17), the input data needed for the computation is the height data. It is in opposite with the iterative process by the Poisson's integral, which the gravity anomalies are the main input data.

Equation (18) is an integral formula with the Stokes's kernel. One is supposed to evaluate this integral over the whole Earth, which is impractical. Therefore, a modification procedure, the same as for the Poisson's kernel, has been performed and the modified Stokes's kernel used in further computations. The inner zone integration area for the short-wavelength contributions is set to $\psi_0 = 6°$. The long-wavelength contributions of the rest of the world are computed from a global height data set using Eq. (19).

5 Numerical investigations

In this section, we have numerically investigated the downward continuation of free-air gravity anomaly by the Poisson's integral based on the iterative procedure (Eqs. 3-4), the simple formula (Eq. 13), the method based on the Pellinen approximation (see Eq. 15) and the one developed by Sjöberg based on the topographic-isostatic compensation potential (see Eqs. 17-24). In the last approach $\frac{\Delta g}{\gamma} + 2\frac{\zeta}{r}$ has been computed according to Eq. (23) in $30' \times 30'$ cells all over the whole Earth, which has then been used in Eq. (24). A test area of size $1° \times 1°$ is chosen in Sweden. It is limited by latitudes 57° N and 58° N and longitudes 13° E and 14° E, located in the north-west of Sweden. The mean free-air anomalies at the surface of the Earth are in $6' \times 10'$ cells. They vary between -32.17 mGal and 40.89 mGal. The mean heights, used in this test area, are in $2.5' \times 2.5'$ cells (GETECH, 1995a) and range from 70.92 to 395.60 metres. To reduce the effect of leakage of the data coverage for the integration cap (along the edge of the test area), we have increased the integration area 6° in each direction, so that the area for which the downward continuation would actually be computed is $13° \times 13°$. But, to escape from the edge effect, the original $1° \times 1°$ test area is used at the end. The potential coefficients used in this study are taken from EGM96 model .

First, the downward continuation correction by the Poisson's integral is determined. To do this, we define the modified Poisson's kernel and then compute the truncation error in the

test area. Figure 1 represents the correction due to the truncation error on geoid. This effect reaches to 3.64 mm. It should be mentioned that the effect of the truncation error on gravity anomalies ranges from -0.18 mGal to 0.26 mGal. To minimize this contribution from the rest of the world, low degree and order field is subtracted from the observed free-air anomalies and downward continued, separately. This long-wavelength contributions have also been added to the contributions from the iterative procedure (short-wavelength part). Downward continuation correction by the simple formula and the Pellinen approximation as well as by the method based on the topographic-isostatic potential are also determined. In the last method, second part of

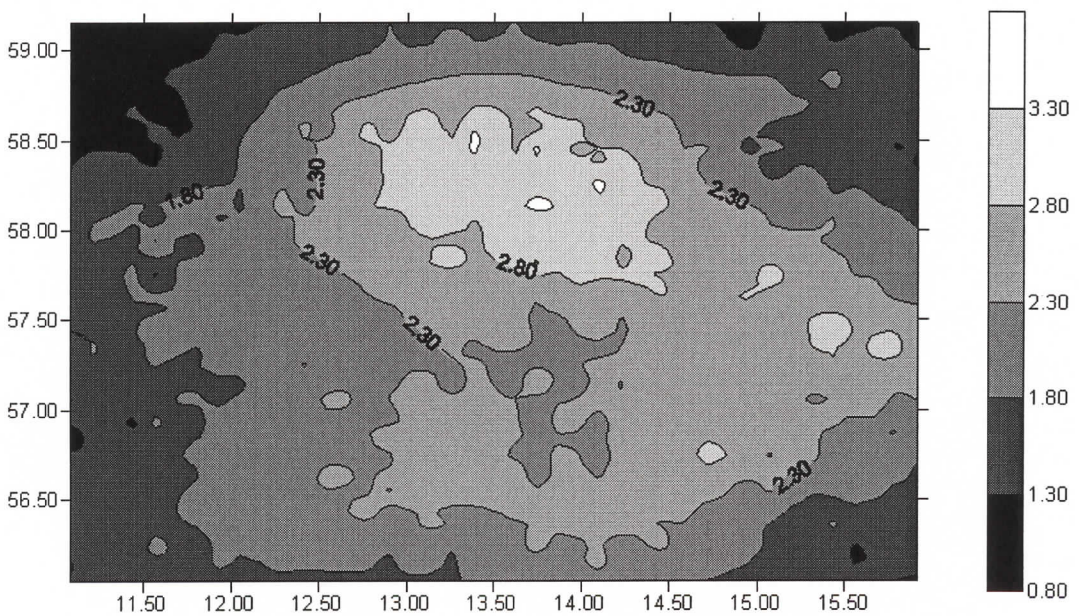

Figure 1: The correction due to the runcation error on geoid in the modified Poisson's integral. Contour interval is 0.5 mm.

the correction (δN^2_{dwc}) has a global nature and is evaluated from Eqs. (21). The main part of the correction (δN^1_{dwc}), described by Eq. (18), has to be integrated over the whole Earth, which is impractical. To investigate this, we have performed this effect in two integration areas 6° and 15°, and compared the results. The statistics of differences are presented in Table 1, which indicate the effect of the farzone contributions. This was obvious because of the shape of the Stokes's kernel. Hence, we decided to modify Stokes's kernel based on the minimization of the upper limit of the truncation error. The integration area is selected to be 6° around the computation point. The heights data used in this inner zone area are GETECH $2.5' \times 2.5'$ DTM (GETECH, 1995a). The long-wavelength part can be evaluated from a spectral form (Eq. 19). The harmonic coefficients of heights $(H^3)_{nm}$ and $(H^4)_{nm}$ are determined from Eq. (20). For this, a $30' \times 30'$ Digital Terrain Model (DTM) was generated using the GETECH $5' \times 5'$ DTM (GETECH, 1995b). This $30' \times 30'$ DTM is averaged using area weighting. Since the interest is in continental elevation coefficients, the heights below sea level are all set to zero. The coefficients were computed to degree and order 360. Finally, the low frequency part (δN^2_{dwc}) is added to the results from the innerzone area.

Table 1: The statistics of the differences of downward continuation correction on geoid by the method based on the topographic-isostatic potential in 6° and 15° integration area. Units in cm

	$\psi_0 = 6°$-$\psi_0 = 15°$
Min	0.21
Max	5.02
Mean	2.60
SD	0.95

The statistics of the results of downward continuation of mean free-air anomaly by different methods are shown in Table 2. It shows that the effect on geoid from downward continuation gravity anomaly to sea-level is everywhere positive. In the next step, the statistics of differences

Table 2: The statistics of downward continuation correction on geoid computed by different methods. Units in cm

	Poisson's integral	topographic-isostatic	Pellinen approximation	Simple method
Min	14.27	16.78	23.72	22.09
Max	19.87	18.50	17.65	24.15
Mean	17.06	17.63	20.72	23.30
SD	1.45	0.53	1.59	0.54

the iterative process from other methods for each point of interest are shown in Table 3. The results of Table 3 show that the downward continuation of mean free-air anomaly by the Poisson's integral and the method based on the topographic-isostatic potential have the smallest differences among the other methods. Maximum of differences has been computed to 3.51 cm. This

Table 3: The statistics of differences of downward continuation correction on geoid between the Poisson's integral and the other methods. Units in cm

	Poisson - topographic/isostatic potential	Poisson-Pellinen	Poisson -simple method
Min	-2.77	3.22	4.27
Max	3.51	4.28	8.01
Mean	0.97	3.66	6.24
SD	1.03	0.22	1.13

difference may be caused by the differences in the definition of these two methods. In the former method the downward continuation is only applied to the surface gravity anomalies, but in the latter, the direct gravity anomaly effect, caused by the reduction of the terrain

masses, has also been included in the solution. The topographic-isostatic model includes several approximations/assumptions which might be the second reason for the differences (see, Sjöberg, 1998). Also, the effect of the truncation error is considered in the iterative process, while it is not applied in the method based on the topographic-isostatic potential. Results of Table 3 also show that there are some differences between the iterative process, the simple formula and the method based on the Pellinen approximation. A maximum difference of 8.01 cm has been computed in the test area between the first two methods. This difference can be caused by the linear approximation made in the latter method. Also, in the simple formula, we have assumed that the vertical gradient of gravity is only dependent to the variation of gravity anomaly in the computation point, and the effect of the other points are neglected. They are considered in the former method.

The methods based on the Poisson's integral and the Pellinen approximation are mostly in good agreement with each other. A mean of differences 3.66 cm has been estimated in the test area. There are some reasons for these differences. Firstly, a linear approximation is used to evaluate the latter method. Also, in the method based on the Pellinen approximation, some long-wavelength contributions might be missing due to the limitation of integration area. The other reason is that free-air gravity anomalies may not simply change linearly with elevation according to the Bouguer plate using Pellinen approximation. Such a linear correlation with elevation was derived by Moritz (1968) based on a topographic-isostatic potential using a simplified Airy/Heiskanen compensation, with a density layer at an internal sphere. Sjöberg (1998) uses original Airy/Heiskanen compensation potential for the downward continuation of gravity anomaly to sea-level. This explains the differences between the methods based on the Pellinen approximation and the topographic-isostatic potential (see Table 2). It has to be mentioned that there are not any convergence problem in the iterative process in this study. By 5 iterations the results converge to an accuracy better than 0.01 mGal, which it makes sure that the downward continuation is accurate enough. However, these procedures have to be tested in other test areas with more rugged topography.

The question, if the cell size (in this study $6' \times 10'$) of the gravity anomalies is enough dense to guarantee the correctness of the iterative process, still remains. Subsequently, this question arises that, if we have treated the Poisson's integral correctly, by replacing it simply with the summations. Otherwise, it has to be treated more carefully (see e.g. Vaníček et al., 1996). To study this, the iterative process is recomputed with the gravity anomalies in $10' \times 12'$ cells in the same test area. The statistics of the differences between the results computed with $6' \times 10'$ and $10' \times 12'$ cells are shown in Table 4. Mean of differences are estimated to 0.60 cm with a maximum difference of 2.02 cm. It means that the $6' \times 10'$ free-air anomalies is enough dense in this test area. Therefore, Poisson's integral can safely be discretized by summations. The effect of the cell size in more rugged area has still to be tested. It has to be mentioned that the effect of downward continuation on gravity anomalies shows a very short-wavelength nature. Figure 2 shows this nature in the test area. However, convolving this effect with Stokes's integral and estimating the effect on geoid (which is our final goal), smooth the results. Contribution to the geoid from the downward continuation of mean free-air gravity anomalies by iterative procedure is shown in Figure 3.

Table 4: The statistics of differences between the effect of downward continuation on geoid by Poisson's integral in $6' \times 10'$ and $10' \times 12'$ cells. Units are in cm.

	$6' \times 10'$ -$10' \times 12'$
Min	-1.21
Max	2.02
Mean	0.60
SD	0.85

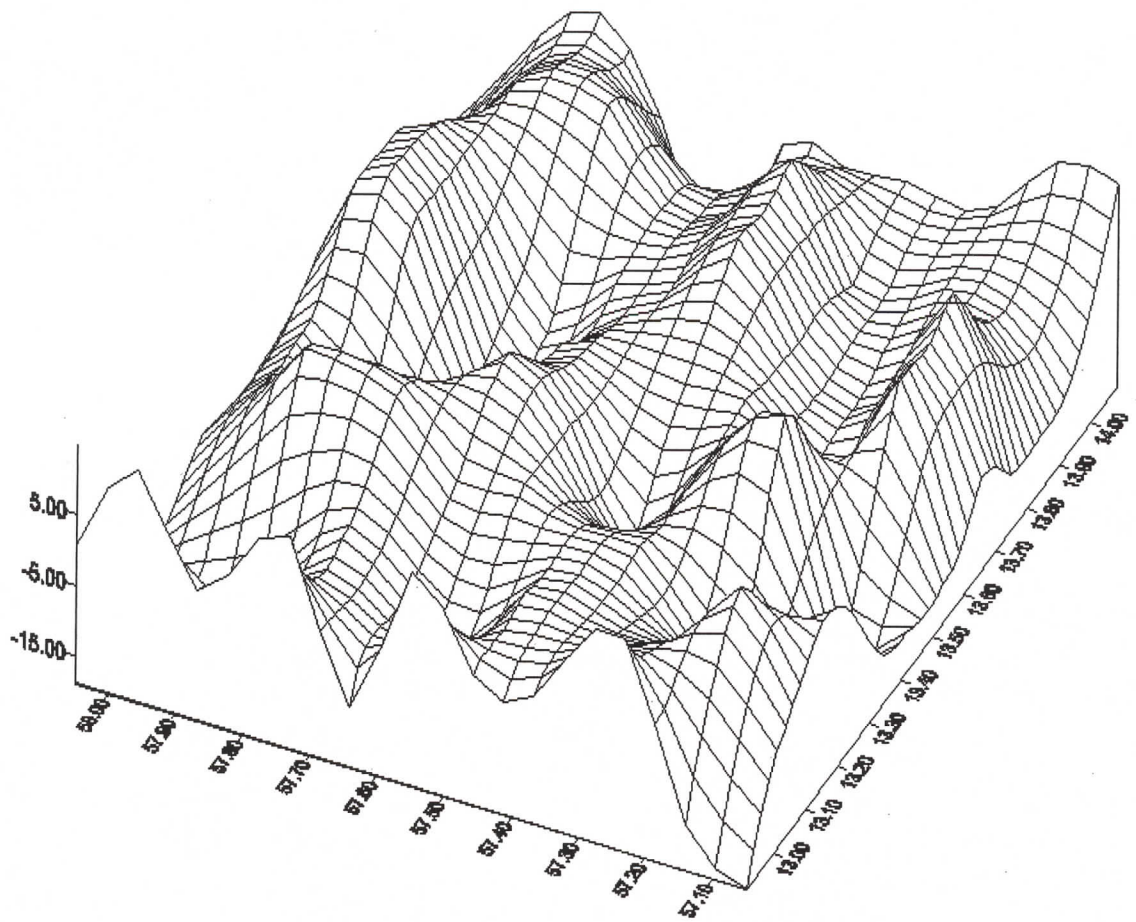

Figure 2: Downward continuation of free-air gravity anomalies by Poisson's integral in mGal.

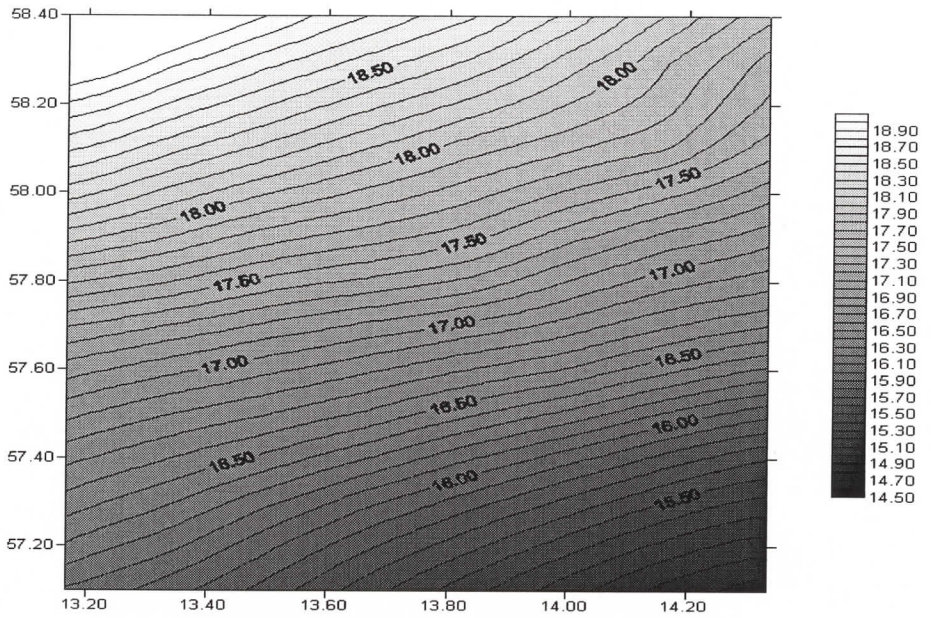

Figure 3: The effect on geoid from the downward continuation of free-air gravity anomalies. Contour interval is 0.1 cm.

The edge effect, which is due to the incompleteness of data used in the boundary of the area of interest, is the other problem which is here studied. We have performed the iterative process in a smaller area being immerged in the $13^\circ \times 13^\circ$ computing area. The results of downward continuation for these two areas are next subtracted. The differences are depicted in Figure 4. This figure presents clearly the boundary effect in the $6^\circ \times 5^\circ$ area. Figure 4 also shows that the area of integration could be safely chosen around 1° in each direction (see also Sun and Vaníček, 1998).

In another experiment to check the correctness of the solution by Poisson's integral, we have back substituted the downward continued values at sea-level to compute the values at the surface of the Earth. The results have been compared with the original values at the surface of the Earth. Statistics of the differences are shown in Table 5. The results of the iterative process agree with the original values at the surface of the Earth with an accurcay of better than 0.07 μGal.

6 Conclusions

We have numerically investigated four methods for the downward continuation of free-air anomalies to the sea-level. The first method is an iterative process based on the Poisson's integral. A simple formula based on linear approximation and a method based on the Pellinen approximation is the other two methods. The last one is based on the topographc-isostatic potential derived from Airy/Heiskanen model.

Numerical investigations have been done in a test area of size $1^\circ \times 1^\circ$. To reduce the effect of leakage of the data coverage in the edges of the test area, the integration area is increased

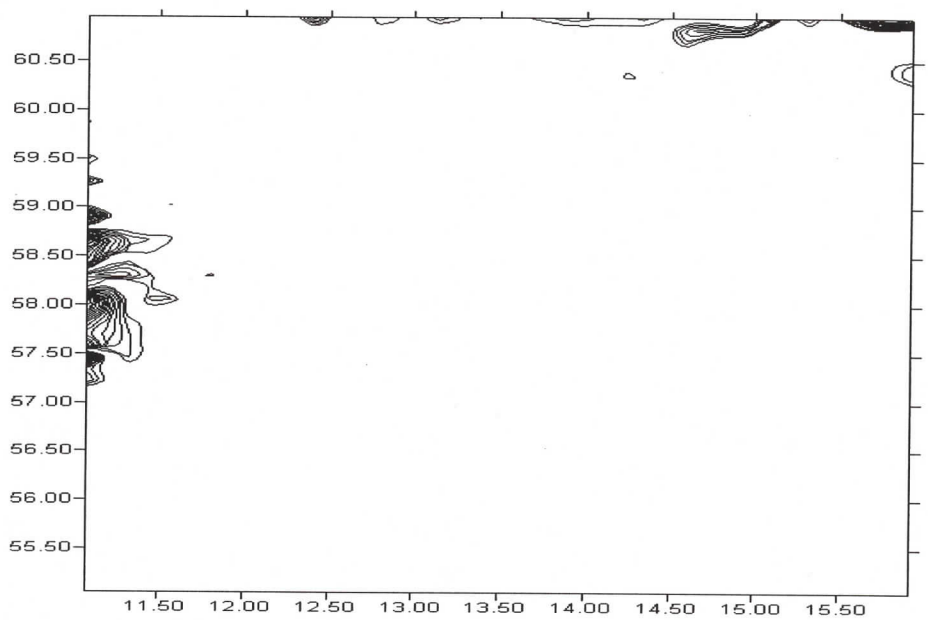

Figure 4: The boundary effect in $6° \times 5°$ ared due to the incompletness of the data. Contour interval is 0.1 mGal.

Table 5: The statistics of differences between back substituted values by the Poisson's integral with the original values at the surface of the Earth. Units are in μGals.

	back substituted values-original values
Min	0.002
Max	0.07
Mean	0.04
SD	0.002

with 6° in each direction. Finally, to escape from the edge effects, we have only used the original $1^\circ \times 1^\circ$ test area. Choosing 1° computation area around the point of interest guarantees that the edge effect does not cause any problem.

Using the Poisson's kernel in the iterative process may cause some problems due to this fact that it has to be integrated over the whole Earth, which is impractical. We have overcome this problem by using two integration areas, inner and outer zones. A 1° integration cap is appropriate for the inner zone area. The effect of the outer zone area (truncation error) has been found to be within 4 mm. This effect is evaluated from EGM96 gravity model. The correction due to the truncation error is finally added to the short-wavelength contributions coming from the iterative process. To minimize the effect of the outer zone, we have subtracted the low degree and order field (to degree and order L=20) from the observed mean free-air anomalies at surface of the Earth. This contribution is downward continued, separately, and added to the downward continuation of the short-wavelength contributions, carried out by the iterative process. It is demonstrated that mean free-air anomalies in $6' \times 10'$ cells (the cell size used in Sweden) can be successfully downward continued from the Earth's surface to the geoid. However, in the smaller cell sizes this might not have a unique solution. The smoothing induced by averaging also helps to the solvability of the downward continuation. This is the case in practice when the mean gravity anomalies are used instead of point gravity anomalies.

In the method based on the topographic-isostatic potential, the main part of the correction (δN^1_{dwc}) has to be evaluated over the whole Earth, by convolution with the Stokes's kernel. But, because of the behaviour of Stokes's kernel, we split the effect into two parts; low frequency part computed from the convolution with modified Stokes's kernel, and high frequency part computed from a spectral form. We have modified the Stokes's kernel according to the Molodenskii et al. (1962) procedure. The contribution of the rest of the world has been evaluated from a $30' \times 30'$ height data set in a spectral form. The results of the Poisson's integral and this method have the smallest differences among the methods computed. The method based on the topographic-isostatic potential considers the direct effect in downward continuation of gravity anomalies. However, this effect is not applied in the other methods. The other source of the the differences is several approximations made in the method based on the topographic-isostatic potential.

The short- and long-wavelength contributions are considered in the iterative process based on the Poisson's integral and the method based on the topographic-isostatic potential. This might be the reason for the better agreement of these two methods among the other methods. We have also shown that the effect of downward continuation on gravity anomaly has short-wavelength nature. However, this effect on geoid behaves smoother. The results also show that the density of $6' \times 10'$ for the mean gravity anomalies are enough in this study.

Disregarding the simple method which is not accurate enough, the topographic-isostatic model has the smallest computing labour, while it is the largest in the Poisson's integral.

Finally, for the check of the correctness of the iterative solution, we have back substituted the downward continued values at the sea-level, to compute them at the surface of the Earth. The results show that the accuracy of the solution is within 0.07 μGal.

Acknowledgement The author wishes to thank Prof. Lars E. Sjöberg for his valuable com-

ments and proof reading the manuscript. Special thanks go to Dr. Wenke Sun for very useful discussions on some parts of this study.

References

[1] Bjerhammar A (1962) Gravity reduction to a spherical surface. Report of the Royal Institute of Technology, Geodesy Division, Stockholm.

[2] Bjerhammar A (1963) A new theory of gravimetric geodesy. Report of the Royal Institute of Technology, Geodesy Division, Stockholm.

[3] GETECH (1995a) DTM2.5 of Europe. Geophysical Exploration Technology (GETECH), University of Leeds, Leeds, UK

[4] GETECH (1995b) Global DTM5. Geophysical Exploration Technology (GETECH), University of Leeds, Leeds, UK

[5] Heiskanen WA, Moritz H (1967) Physical Geodesy. W H Freeman and Company, San Francisco

[6] Kellogg OD (1929) Foundations of potential theory. Springer, Berlin (reprinted 1967).

[7] Lemoine F G, Smith D E, Kunz L, Smith R, Pavlis E C , Pavlis N K, Klosko S M, Chinn D S, Torrence M H, Williamson R G, Cox C M, Rachlin K E, Wang Y M, Kenyon S C, Salman R, Trimmer R, Rapp R H, Nerem R S (1997) The development of the NASA GSFC and NIMA Joint Geopotential Model. In: Gravity, geoid and marine geodesy, Vol. 117, IAG Sym, J. Segawa, H. Fujimoto, and S. Okubo (editors) pp. 461-469.

[8] MacMillan WD (1930) The theory of the potential. Dover reprint, 1958.

[9] Molodenskii MS, Eremeev VF, Yurkina MI (1960) Methods for study of the external gravitational field and figure of the Earth. Office of Technical Services, Department of Commerce, Washington D.C.

[10] Moritz H (1968) On the use of the terrain correction in solving Molodenskii's problem. Department of Geodetic Science, Report No. 79, Ohio State University, Columbus, Ohio, USA.

[11] Moritz H (1980) Advanced Physical Geodesy. Herbert Wichmann Verlag, Karlsruhe. and Company, San Francisco

[12] Sjöberg L E (1984) Least squares modification of Stokes's and Vening Meinez' formulas by accounting for truncation and potential coefficient errors. Manuscr Geod 9:209-229.

[13] Sjöberg L E (1998) The exterior Airy/Heiskanen topographic-isostatic gravity potential anomaly and the effect of analytical continuation in Stokes formula. J Geod:Submitted

[14] Sun W, Vaníček P (1996) On the discrete problem of downward continuation of Helmert's gravity. In Proc. EGS XXI general assembly, The Haugue, The netherlands, 6-10 May, 1996. (Ed:) Ilias N. Tziavos and Martin Vermeer.

[15] Sun W, Vaníček P (1998) On some problems of the downward continuation of $5' \times 5'$ Helmert gravity disturbance. J Geod 72:411-420.

[16] Vaníček P, Sjöberg LE (1991) Reformulation of Stokes theory for higher than second degree reference field and modification of integration kernels. J Geophys Res 96:6529-6539.

[17] Vaníček P, Martinec Z (1994) The Stokes-Helmert scheme for the evaluation of a precise geoid. Manuscr Geod 19:119-128.

[18] Vaníček P, Sun W, Ong P, Martinec Z, Najafi M, Vajda P, Ter Horst B (1996) Downward continuation of Helmert's gravity. J Geod 71:21-34.

There is no such thing as "The" EGM96 geoid: Subtle points on the use of a global geopotential model.

Dru Smith

NOAA/National Geodetic Survey, 1315 East-West Highway, Silver Spring Maryland, 20910
fax: 001-301-713-4172
phone: 001-301-713-3202
e-mail:dru@ngs.noaa.gov

Abstract

The Earth's gravity potential field contains infinitely many level surfaces, each parallel to the others. The geoid is one such surface with a particular potential value, W_0. Spherical harmonic models of the Earth's external gravitational potential ("geopotential models") contain no explicit information about which level surface, out of the infinitely many that may be generated from the potential coefficients, is "the" geoid. Therefore, computing geoid undulations from a geopotential model requires additional information which should be carefully understood. Computer programs which compute gravimetric quantities from geopotential coefficients should contain prompts for this additional information. Submitted to the International Geoid Service (IGeS) is a FORTRAN program, **geopot97** which accounts for all points in this paper except for the use of "correction coefficients" for topographic masses.

Introduction

At the recent joint meeting of the International Gravity Commission (IGC) and the International Geoid Commission (IGeC), numerous presenters did something which has occurred for years: they referred to such data sets as "The EGM96 geoid" and "The OSU91A geoid" (emphasis mine), among others, in a way that implied that "the geoid" is built into the spherical harmonic coefficients. The fact is, however, that no set of spherical harmonic coefficients of the Earth's external gravitational potential (which will be referred to as a "geopotential model") can be used by themselves to derive a model of geoid undulations. Four other pieces of information are required:

1) Choice of a normal gravitational potential field (encompassing the reference ellipsoid)
2) Choice of which level surface is "the" geoid
3) Knowledge of what permanent tide system the geopotential model refers
4) Knowledge of how the potential field acts inside topographic masses

Although well used for decades now, there still seems to be a general misunderstanding about how exactly geoid undulations are computed from a geopotential model. Very often, a program is run which is not fully documented and which is also missing one or more prompts for the information listed above. This paper hopes to briefly shed some light on what appears to be a frequently misunderstood issue. Finally, in an the spirit of "actions speak louder than words", a FORTRAN program, **geopot97**, has been submitted for testing to the International Geoid Service

(IGeS) which can be used for rigorously computing gravimetric quantities using a geopotential model *and* the necessary additional information.

Anatomy of a geopotential model

Most modern geopotential models will be made available with four components:

1) The set of coefficients (usually called "C_{nm}" and "S_{nm}") from degree 2 to degree N
2) The adopted gravity-mass constant (GM_1) value used when creating the model
3) An equatorial scale factor, "a_1"
4) The permanent tide system of the model

These four pieces of information are enough to compute gravitational potential outside a sphere of radius $r=a_1$, using equation 1. In fact, the formula can be used accurately inside the sphere, as long as the evaluation point remains outside the topographic masses.

$$V^{(1)}(r,\theta,\lambda)=\frac{GM_1}{r}\sum_{n=0}^{N}\left(\frac{a_1}{r}\right)^n\sum_{m=0}^{n}\left(\overline{C}_{nm}\cos(m\lambda)+\overline{S}_{nm}\sin(m\lambda)\right)\overline{P}_{nm}(\cos\theta) \qquad (1)$$

$V^{(1)}$ = gravitational potential to degree N from geopotential model (i.e. EGM96)
r,θ,λ = geocentric radius, spherical co-latitude, longitude of computation point
a_1 = equatorial scale factor of the geopotential model
GM_1 = gravity-mass constant of the geopotential model
$\overline{P}_{nm}$ = fully-normalized Legendre functions
$\overline{C}_{nm}, \overline{S}_{nm}$ = fully-normalized coefficients of geopotential model
($\overline{C}_{0,0}=1.0$; $\overline{S}_{n,0}$ *does not exist* ; $\overline{C}_{1,m}=0.0$; $\overline{S}_{1,m}=0.0$;
$\overline{C}_{2,0}$ must be defined in a specific permanent tide system)

One should not put too much emphasis on "a_1" in equation 1. It is little more than a scale factor and does not represent the semi-major axis of any ellipsoid of interest to this problem.

Equation 1 yields gravitational potential, which is not, of course, the geoid undulation. To compute the geoid undulation requires the use of equation 1, and additional information, combined in the generalized Bruns equation.

The generalized Bruns equation

The generalized Bruns equation (to first order terms), which can be used to compute geoid undulations, is written as follows:

$$N_{PQ} = \frac{T_P}{\gamma_Q} - \frac{W_P-U_Q}{\gamma_Q} \qquad (2)$$

where (see also Figure 1):

P = point on the geoid (r_P , θ_P , λ_P)
Q = point on the ellipsoid (r_Q , θ_Q , λ_Q)
N_{PQ} = geoid undulation, between P, and Q
T_P = disturbing potential at point P
γ_Q = normal gravity at point Q
W_P = gravity potential at point P
U_Q = normal gravity potential at point Q

To see how a geopotential model is used in conjunction with the generalized Bruns equation and with additional information, we must expand equation 2, as shown below:

$$
\begin{aligned}
N_{PQ} &= \frac{T_P}{\gamma_Q} - \frac{W_P - U_Q}{\gamma_Q} \\
&= \frac{W_P - U_P}{\gamma_Q} - \frac{W_P - U_Q}{\gamma_Q} \\
&= \frac{\left(V_P^{(1)} + \Phi_P\right) - \left(V_P^{(2)} + \Phi_P\right)}{\gamma_Q} - \frac{W_P - U_Q}{\gamma_Q} \\
&= \frac{V_P^{(1)} - V_P^{(2)}}{\gamma_Q} - \frac{W_P - U_Q}{\gamma_Q} \\
&= \frac{1}{\gamma_Q}\left(V_P^{(1)} - V_P^{(2)}\right) - \frac{1}{\gamma_Q}\left(W_P - U_Q\right)
\end{aligned}
\qquad (3)
$$

where Φ is the centrifugal potential (assumed identical for the true field and the normal field, thus the cancellation). $V_P^{(2)}$ is the normal gravitational potential at P. Note that to use equation 3, there must be a-priori knowledge of the gravity potential on the geoid (W_P). In addition, the location of P itself must be known to evaluate $V_P^{(1)}$ and $V_P^{(2)}$. That is, one must know the location of P, to use this formula to compute the location of P. As convoluted as that sounds, it is solved through a simple iterative computation in most programs which manipulate geopotential models (see Rapp, 1971).

It is seen in equation (3) that one must know the normal field ($V_P^{(2)}$), as well as the level surface which will be called the geoid (W_P). In addition, the difference between $V_P^{(1)}$ and $V_P^{(2)}$ contains the implicit assumption that both $V_P^{(1)}$ and $V_P^{(2)}$ refer to the same tide system. If the tide systems are different from each other (or if either is different than the tide system in which you desire the output quantities computed), a correction should be applied to one or both of $V_P^{(1)}$ and $V_P^{(2)}$. This is covered in a later section.

The Normal Potential Field

Equation 3 indicates a requirement for knowing the normal gravity potential, $V^{(2)}$. Because a geopotential model is used to evaluate $V^{(1)}$, it will be useful to set up the normal potential field, $V^{(2)}$, in a similar way, that is:

$$V^{(2)}(r,\theta,\lambda)=\frac{GM_2}{r}\sum_{n=0}^{N}\left(\frac{a_2}{r}\right)^n\sum_{m=0}^{n}\left(\overline{C}^*_{nm}\cos(m\lambda)+\overline{S}^*_{nm}\sin(m\lambda)\right)\overline{P}_{nm}(\cos\theta) \qquad (4)$$

$V^{(2)}$ = normal gravitational potential to degree N from reference field
r,θ,λ = geocentric radius, spherical co-latitude, longitude of computation point
a_2 = semi-major axis of reference ellipsoid
GM_2 = gravity-mass constant of normal field
$\overline{P}_{nm}$ = fully-normalized Legendre functions
$\overline{C}^*_{nm}$,$\overline{S}^*_{nm}$ = fully-normalized coefficients of normal field
($\overline{C}^*_{0,0}$=1.0 ; $\overline{S}^*_{0,0}$ *does not exist* ; $\overline{C}^*_{1,m}$=0.0 ; $\overline{S}^*_{1,m}$=0.0 ;
$\overline{C}^*_{2,0}$ must be defined in a specific permanent tide system)

Note that a normal potential field consists purely of even zonal harmonics, so that most of the C^* and S^* terms (except $C^*_{n,0}$, where n is even) in equation 4 are zero.

Using the previous equations, we may write the disturbing potential at a point ($T = V^{(1)}-V^{(2)}$) as:

$$T(r,\theta,\lambda)=\frac{GM_1}{r}\sum_{n=0}^{N}\left(\frac{a_1}{r}\right)^n\sum_{m=0}^{n}\left[\left(\overline{C}_{nm}-\left(\frac{GM_2}{GM_1}\right)\left(\frac{a_2}{a_1}\right)^n\overline{C}^*_{nm}\right)\cos(m\lambda)+\overline{S}_{nm}\sin(m\lambda)\right]\overline{P}_{nm}(\cos\theta) \qquad (5)$$

(Note here that we have made use of the fact that $S^*=0$ for all n and m). Often in practice, the ratios GM_2/GM_1 and $(a_2/a_1)^n$ are dropped except for the n=0 term. For terms where n>0, these ratios generally can affect the geoid computation by as much as 2 to 3 millimeters (effectively all in the n=2 term). Considering the miniscule computational burden of using the ratios, there is good reason for keeping the equation intact if one is interested in a truly "centimeter accuracy" geoid.

From the standpoint of geometry, the ellipsoid to which the geoid undulations will refer can be inferred from the normal potential field parameters. The semi-major axis of the reference ellipsoid is a_2. The flattening of the reference ellipsoid can be determined by the terms a_2, $C^*_{2,0}$, GM_2 and an adopted ω (rotational velocity) through an iterative procedure to any needed accuracy (Rapp, 1971).

Choice of W_0

Equation 3 shows that a value of W_P ($=W_0$) needs to be known, or adopted, as the gravity potential on the level surface which is to be called "the" geoid. This seems to be one of the most confusing aspects of geoid computation, and, hopefully, will be clarified below.

One approach is to just pick a "reasonable" W_0 value. Recent estimates of W_0 have been published by the IAG Special Commission SC3 (IAG 1995). This method is the one chosen by the EGM96 team (Lemoine et al 1998, section 11.2), though they also point out the consistency between the adopted W_0 and a set of "a" and "f" values for an ellipsoid. This leads to the next method of W_0 determination, below.

Another, more round-about method is through the adoption of a so-called "best fitting ellipsoid", which is not far from the methods used by the IAG SC3 for computing their estimates of W_0. The logic for this method is as follows.

Assume that measurements of mean sea level (MSL) can be made through altimetry. Define "the geoid" (G) as the *particular* level surface which best fits (in the least squares sense, globally[1])to mean sea level. By definition then, the mean dynamic topography (geoid/mean sea surface separation) should be zero, globally. Now define the "best fitting ellipsoid" (E_{bf}) as that ellipsoid which best fits to mean sea level (with semi major axis a_{bf} and flattening f_{bf}). By extension, therefore, the "best fitting ellipsoid" is also that *ellipsoid* which best fits to *the geoid*. As such, the "global" average separation between E_{bf} and G is zero. That is, if one were to average up, globally, the "geoid undulations, relative to the best fit ellipsoid" that average would be zero. For the global average geoid undulation to be zero, the following equations must be true (based on the generalized Bruns equation):

$$GM_1 - GM_2 = 0 \tag{6a}$$

$$-(W_0 - U_{0,bf}) = 0 \tag{6b}$$

Because this discussion has made no mention of either the true GM (GM_1) or the normal GM (GM_2), it may be adopted that the "best fitting ellipsoid" is part of a normal field where $GM_2 = GM_1$ (thus ensuring the validity of equation 6a). The real pay-off comes from equation 6b. Re-arranged, it reads:

$$W_0 = U_{0,bf} \tag{7}$$

Now, since the "best fitting ellipsoid" has been adopted, that means that the semi major axis, a_{bf}, and the flattening, f_{bf}, are known. If, as mentioned above, GM_2 is set equal to the best known

---

[1] A global fit is not truly possible, as altimetric measurements do not reach to the poles. For the purposes of this paper, "global" will be approximated by the range of the altimetry.

GM_1 value, and a value of ω is adopted, then U_0 may be computed by equation 8, and subsequently, from equation 7, W_0 is known! Equation 8 is a slightly re-arranged version of equation (2-61) in Heiskanen and Moritz (1967):

$$W_0 = U_{0,bf} = \frac{GM_2}{a_{bf}\sqrt{2f_{bf} - f_{bf}^2}} \arctan\left(\frac{\sqrt{2f_{bf} - f_{bf}^2}}{1 - f_{bf}}\right) + \frac{1}{3}\omega^2 a_{bf}^2 \qquad (8)$$

Both of the methods for choosing/calculating W_0 have the advantage that they are based on the most recent estimates about the size and shape of mean sea level and the geoid. There are other methods used, and these often have a critical mis-understanding of how to compute a geoid undulation.

Based on how rarely W_0 is explicitly stated in papers and presentations, there appears to be a lack of explicit knowledge about how to properly incorporate a choice of W_0, when using a geopotential model for computing geoid undulations. One misconception which occurs is that the GRS-80 ellipsoid is still a reasonable fit to the size and shape of the geoid. This is clearly not true, if centimeter accuracy is desirable. Recent estimates of the size of a best fitting ellipsoid differ in semi-major axis with GRS-80 by many decimeters (Rapp 1995, IAG 1995, Burša 1995). Additionally, recent estimates of the true GM for the Earth differ significantly from the GM of GRS-80 (McCarthy 1996, IAG 1995, Burša 1995). This does not make it impossible nor invalid to use GRS-80 as an ellipsoid to which geoid undulations refer -- it simply means that the degree zero terms arising from the differing GM values and the difference between U_0 and W_0 must be properly accounted for (errors of nearly a meter can occur through incorrect consideration of these terms -- see Smith and Small 1998). Other misconceptions are that the reference ellipsoid to which "the EGM96 geoid" can, or must, refer is somehow contained in the EGM96 information. For example, that the EGM96 "a_1" value is the semi-major axis of a reference ellipsoid, or that the flattening of the reference ellipsoid must be determined through the EGM96 $C_{2,0}$ term. These are both false. However, any software which does not explicitly prompt a user for information about *which* level surface is to be considered *the* geoid, must inherently be making some assumption about it. Most likely those assumptions will *not* match more recent estimates of the size and shape of the geoid.

Permanent Tide System

One subtle point, with a long history of study, but a short history implementation, is the permanent tide system. There are three systems in common use: Mean, Zero and Tide-free. In each system the contributions to the potential field, deformation of the crust, and best fitting ellipsoid to the geoid have their own definitions. And, while the shape of the geoid changes (from one tide system to another), the value of W_0 does not change from one system to another (IAG 1995). That is, the *shape* of the the level surface which best fits mean sea level in each of the three systems changes, but the *potential* of that level surface has an unchanged W_0 value.

Because both the potential field, and the normal potential field can be defined under three different permanent tide systems, it is mandatory that they refer to the same permanent tide system to in order to compute geoid undulations through the generalized Bruns equation. Thankfully this is fairly simple. The effect of changing a permanent tide system is seen only in the $C_{2,0}$ term. This goes for both the geopotential model ($C_{2,0}$) as well as the normal potential field ($C^*_{2,0}$). The change in the $C_{2,0}$ term is identical to the change in $C^*_{2,0}$, meaning that the change in shape of the geoid, between tide systems is identical to the change in shape of the ellipsoid. As such (and this is also seen through the Bruns equation) there is no difference between geoid undulations in any of the three permanent tide systems. This *seems* to be (but is *not*) in conflict with published formulas for transforming geoid undulations between tide systems (Lemoine, et al 1998, section 11.1; Rapp 1989). In those formulas, there is no change allowed to the reference ellipsoid. It is treated as a purely geometric quantity, unchanged by permanent tide systems, and only the geoid itself is allowed to change due to the permanent tide systems. Under these circumstances, the geoid undulation obviously changes from one tide system to another, but only represents the geometric change in the shape of the geoid ($W=W_0$) relative to an *unchanging* ellipsoid.

If the permanent tide system of $V_p^{(1)}$ differs from that of $V_p^{(2)}$, then the two values should be brought into the same permanent tide system before proceeding with the generalized Bruns equation. This may be done by applying one, or both, of the following corrections to the $C_{2,0}$ term in the computation of $V_p^{(1)}$:

$$\overline{C}_{2,0}^{(mean\ tide)} - \overline{C}_{2,0}^{(zero\ tide)} = 1 \times \frac{(-0.198m)r^3\gamma}{a^2GM\sqrt{5}} \approx -1.39\times10^{-8} \tag{9}$$

$$\overline{C}_{2,0}^{(zero\ tide)} - \overline{C}_{2,0}^{(tide-free)} = k \times \frac{(-0.198m)r^3\gamma}{a^2GM\sqrt{5}} \approx k \times (-1.39\times10^{-8}) \tag{10}$$

where k is the (fundamentally unknowable) zero frequency Love number, which must be adopted. (For EGM96, k=0.3 was adopted). Although r and γ have latitude dependence, this does not alter the effectively constant values computed in equations 9 and 10. These equations were derived from equations 1,3 and 4 combined with the following equations (for a change in geoid undulation relative to a fixed ellipsoid, Rapp, 1989):

$$N^{(mean\ tide)} - N^{(zero\ tide)} = 1 \times (-0.198m) \times \left(\frac{3}{2}\sin^2\varphi - \frac{1}{2}\right) \tag{11}$$

$$N^{(zero\ tide)} - N^{(tide-free)} = k \times (-0.198m) \times \left(\frac{3}{2}\sin^2\varphi - \frac{1}{2}\right) \tag{12}$$

Equations 9 and 10 also agree with the results found in (Melbourne et al, 1983).

Topographic Masses

It has been pointed out (Rapp 1997, Rapp 1992) that the potential computed from a geopotential model is inaccurate (over and above omission and commission errors) when the evaluation point lies inside the Earth's masses. These inaccuracies lead to incorrect geoid undulation computations which can be erroneous by up to 3 meters (Himalayas). Smith and Milbert (1998) show the error can exceed 1.5 meters in the Rocky Mountains. To compute more accurate geoid undulations, various methods have evolved, which all generally refer back to the same source -- Heiskanen and Moritz (1967, page 327, equation 8-102). The basic philosophy is that height anomalies (ζ) can be accurately computed at the surface of the Earth using the geopotential model, and then a correction (based on Bouguer anomalies, to first order) can be applied which yields the geoid undulation. When EGM96 was released, "correction coefficients" were also generated which would simulate this "Bouguer correction", for the express purpose of generating geoid undulations from the geopotential. Unfortunately there has been no published research on how to generate other gravimetric quantities (such as gravity anomalies) "in the masses" from geopotential models.

Although methods for applying the Bouguer correction are not encoded in program **geopot97**, there is one related "trick" which is coded in there, and that is for the fast evaluation of height anomalies at the surface of the Earth. As pointed out in Rapp (1997), if the radial distance (r) is unchanged then equation 5 (and any gravimetric quantities related to equation 5) may be quickly evaluated in latitude rows. This is an effect of using Clenshaw summation (Tscherning, Rapp and Goad 1983). When computing values at the geoid, the shallow gradients of the geoid allow a program to keep "r" constant for long stretches of latitude rows (while this is strictly untrue the evaluation point may be kept at a constant radius "r", which may deviate from the 'true' geoid position by as much as 10 meters without affecting the geoid or gravity anomaly computations in any significant way). The nature of quickly-changing topography, however, means that r must change quickly, and this significantly slows down the evaluation of equation 5. To get around this problem, one can evaluate disturbing potential (T), as well as the first and second upward derivatives of T, *at the surface of the ellipsoid.* Then, one can upward continue the disturbing potential to the surface of the Earth using the ellipsoid height, h. In computing the upward derivatives, the derivative with respect to h (not r) must be used to avoid centimeter level errors in the final height anomaly at the surface of the Earth. The derivatives of T with respect to r,θ and λ are simple to compute as part of the Clenshaw summation subroutine (ibid), and should be used to compute the derivative of T with respect to h through the following equation:

$$\frac{\partial T}{\partial h} = \frac{\partial T}{\partial r}\frac{\partial r}{\partial h} + \frac{\partial T}{\partial \theta}\frac{\partial \theta}{\partial h} \approx \frac{\partial T}{\partial r}\frac{\partial r}{\partial h} \qquad (13)$$

where:

$$\frac{\partial r}{\partial h} = \frac{1}{r}[(N_\varphi + h) - N_\varphi e^2 \sin^2\varphi] \qquad (14)$$

and N_ϕ is the radius of curvature of the ellipsoid in the prime vertical, and e is the first eccentricity of the ellipsoid.

This method is detailed in Rapp (1997). Note that this method works, even though the values of T and its derivatives on the ellipsoid are "in the masses". This is due to the fact that equation 5 (and related equations for the derivatives) are continuous and smooth. Equation 5 may be evaluated anywhere (such as on the ellipsoid) without regard for whether it matches the "true" values. Because they are smooth and continuous, the use of T and its derivatives on the ellipsoid may be used in a Taylor expansion to reveal the value of T elsewhere (such as the surface of the Earth). As pointed out earlier, as long as the evaluation point is at or exterior to the Earth's surface, the potential computed from a geopotential model can be considered reliable. In effect, we use mathematics (without regard for the topographic mass issue) to implement:

$$T_e + \frac{\partial T}{\partial h}\Big|_e h + \frac{1}{2}\frac{\partial^2 T}{\partial h^2}\Big|_e h^2 = T_s \qquad (15)$$

where the subscript "e" indicates the function evaluated at the ellipsoid, and "s" indicates the function at the surface of the Earth.

Running geopot97

A FORTRAN 77 program, **geopot97**, has been submitted to the IGeS for the computation of potential, and related quantities, from a geopotential model. Appropriate prompts for the normal field, the choice of W_0, and the permanent tide system are incorporated into that program. It is built around a Clenshaw summation routine (Tscherning, Rapp, Goad, 1983). Currently (version 0.4c) it will perform 11 different functions:

#1 - Given a spherical ϕ/λ and a value of gravity potential, find the radial distance to the surface of that potential

#2 - Given a geometric ellipsoid, an ellipsoidal ϕ/λ and a value of gravity potential, find the ellipsoidal height to the surface of that potential

#3 - Same as #1 but done on a grid of ϕ/λ values

#4 - Same as #2 but done on a grid of ϕ/λ values

#5 - Given a spherical $\phi/\lambda/r$ coordinate, compute gravity potential and gravitational potential at that point

#6 - Given an ellipsoidal $\phi/\lambda/h$ coordinate, compute gravity potential and gravitational potential at that point

#7 - Given a normal gravity field and an ellipsoidal $\phi/\lambda/h$ coordinate, compute gravity potential, gravitational potential, gravity, gravity anomaly, height anomaly, gravity disturbance, deflections of the vertical, and 3-D gradients of gravity at that coordinate

#8 - Given a normal gravity field and an ellipsoidal ϕ/λ coordinate and a defined W_0 value for the geoid, compute the geoid undulation and gravity anomaly for that location

#9 - Given a normal gravity field and a grid of ellipsoidal ϕ/λ coordinates and a defined

W_0 value for the geoid, compute a grid of geoid undulations and/or gravity anomalies

#10 - Given a normal gravity field and a grid of ellipsoidal ϕ/λ coordinates, compute the height anomaly, and its first and second order upward derivatives, at the surface of the ellipsoid at the grid points

#11 - Given a gridded digital elevation model, compute a grid of gravity values at the surface of the Earth on that grid

Summary

Geopotential models have a long and important history in the geodetic community, specifically as a tool for computing geoid undulations. Often, the experience of using such models has been through provided programs -- sort of a "black box" approach (coefficients in, "geoid undulations" out). This approach is not generally valid due to the assumptions that such black box programs must make. This paper has argued that four important questions must be posed to properly *compute* geoid undulations, and fully *document* exactly what was computed. Those questions are:

1) What reference ellipsoid/normal potential field is used?
2) Which level surface, of the infinitely many, will be adopted as "the" geoid?
3) To what permanent tide system does the geopotential model refer?
4) How will I properly account for the topography?

In an attempt to answer the first three questions (which are inherently different than the fourth), a program **geopot97** has been submitted to the IGeS for testing. It is hoped that future consistency in geoid computations may be achieved through this effort.

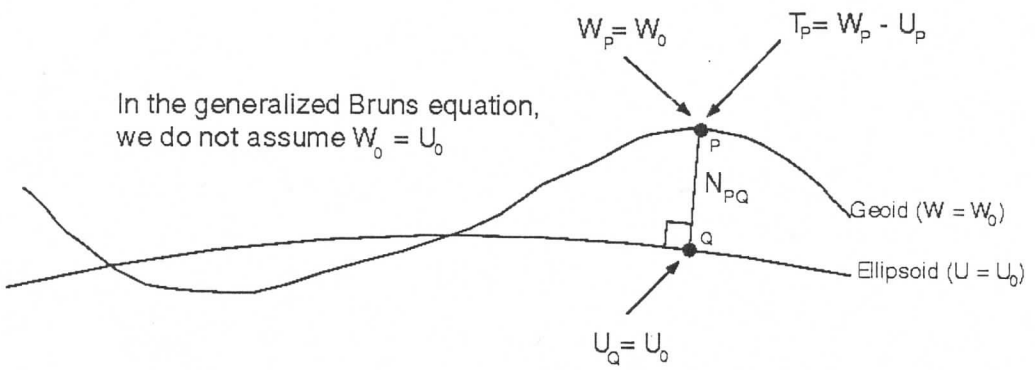

Figure 1: Paying attention to the "P's and Q's" of the generalized Bruns equation

References

Burša, M, 1995: Primary and derived parameters of common relevance of astronomy, geodesy, and geodynamics. *Earth, Moon and Planets,* 69, pp. 51-63

Heiskanen, W.A. and H. Moritz, 1967: *Physical Geodesy*. W.H. Freeman, San Francisco, 364 pp

IAG, 1995: report of Special Commission SC3, Fundamental constants, International Association of Geodesy, Paris

Lemoine, F.G., et al, 1998: The Development of the Joint NASA GSFC and the National Imagery and Mapping Agency (NIMA) Geopotential Model EGM96, NASA Technical Report NASA/TP-1996\8-206861

McCarthy, D., 1996: IERS Technical Note 21, Observatoire de Paris

Melbourne, W, 1983: Project Merit Standards, U.S. Naval Observatory Circular. Report 167, Washington, D.C.

Rapp, R.H., 1971: Methods for the computation of geoid undulations from potential coefficients. *Bulletin Géodésique*, 101, p. 283-297

Rapp, R.H., 1989: The treatment of permanent tidal effects in the analysis of satellite altimeter data for sea surface topography. *manuscripta geodaetica*, 14(6), 368-372

Rapp, R.H., 1992: Global Geoid Solutions, in Geophysical interpretations of the geoid, ed. By Vaní_ek and Christou, CRC Press, Boca Raton, FL, pp. 57-76

Rapp, R.H., 1995: Equatorial radius estimates from TOPEX altimeter data, in Festschrift Erwin Groten, Institute of Geodesy and Navigation, Univ.

Rapp, R.H., 1997: Use of potential coefficient models for geoid undulation determinations using a spherical harmonic representation of the height anomaly/geoid undulation difference. *Journal of Geodesy*, 71(5), 282-289

Smith, D.A., and D.G. Milbert, 1998: The GEOID96 high resolution geoid height model for the United States, *Journal of Geodesy*, in press

Smith, D.A., and H.J. Small, 1998: The CARIB97 high resolution geoid height model for the Caribbean Sea, *Journal of Geodesy*, in press

Tscherning, C.C., Rapp, R.H. and C. Goad, 1983: A comparison of methods for computing gravimetric quantities from high degree spherical harmonic expansions. *Manuscripta geodaetica*, 8, pp. 249-272

Documentation for the GPS Benchmark Data Set of 23-July-98

Dennis G. Milbert

National Geodetic Survey, NOAA, SSMC-3, 1315 East-West Hwy., Silver Spring, MD, 20910

Introduction

The GPS benchmark data set was obtained from a synoptic data base retrieval on July 23, 1998. The general retrieval parameters were that each point must be in the conterminous United States, must have an orthometric height in the NAVD 88 datum established by geodetic leveling, and must have an ellipsoidal height in the NAD 83 datum established by GPS surveys of 10 ppm horizontal accuracy (or better). Both the NAVD 88 and the NAD 83 datums are tide-free. After retrieval, the data were cleansed of outliers that could not be ascribed to gravimetric geoid model error. The result is a data set suitable for testing of geoid and global geopotential models. Details on the data components, the datums, retrieval parameters, and the data cleansing process can be found below. The data are located at `www.ngs.noaa.gov/GEOID/GPSBMS/gpsbms.html`

The GPS Ellipsoidal Heights

The National Geodetic Survey (NGS) has recently completed a major project: establishment of a high accuracy Federal Base Network (FBN), and an associated Cooperative Base Network (CBN), through nationwide measurement of GPS baselines of 1 ppm accuracy or better. The FBN stations are located at a nominal 1° x 1° spacing, are surveyed to 1 ppm accuracy, and are maintained at the expense of NGS. A portion of the FBN is set at a nominal 3° x 3° spacing, and is surveyed to 0.1 ppm accuracy. NGS encourages individual states to establish additional 1 ppm stations at about 15' x 15' spacing. These additional stations are designated CBN. The FBN and CBN stations are often observed in a single cooperative GPS survey, frequently known as a High Accuracy Reference Network (HARN). These surveys are typically performed on a state-by-state basis (Milbert and Milbert 1994, Bodnar 1990).

One of the objectives of the FBN/CBN effort is to upgrade the accuracy of the geodetic control within a state. This is done by occupation of existing high order control points, connected by classical, terrestrial measurements, with subsequent readjustment. It is clear that those FBN/CBN points which are on NAVD 88 leveled benchmarks provide a powerful data set for accuracy assessment and improvement of geoid and global geopotential models. Figure 1 displays the locations of 5168 points that are leveled benchmarks with NAVD 88 Helmert orthometric heights, and which have GPS measured ellipsoidal heights in the NAD 83 reference system as of July 23, 1998. The irregular distribution illustrates the state-by-state approach to the surveying, and the differing levels of state participation.

The FBN/CBN (HARN) survey effort began with Tennessee in 1990, and fieldwork on the project was completed in Illinois in 1997. Over this period major advances were made in

GPS receivers, processing models, vector reduction software, orbit accuracy, and in the GPS constellation itself. In addition, the surveys were designed to provide accurate *horizontal* control. Data reduction and analysis procedures focused on horizontal accuracies. Typical observing procedures are static, and involve occupation of a point for about 6 hours on two different days (three days for 0.1 ppm). Orbit relaxation was used for the 0.1 ppm coordinates until 1994, when improved orbit accuracies removed the need for that particular process. Meteorological data were not always taken on site. Only recently has the influence of antenna phase center variation (Schluper et al. 1994) been incorporated into processing software. For these reasons, the FBN/CBN surveys can not be considered as a homogenous set. And, one must expect a level of error in the GPS ellipsoidal heights greater than that associated with continuously operating GPS receivers.

In addition to the heterogenous character of the FBN/CBN, an additional category of GPS surveys is designated the User Densification Network (UDN). The UDN consists of GPS or conventional horizontal surveys of 10 ppm relative accuracy or better and/or second-order, class II geodetic leveling. These surveys were performed by (or for) national, state, or local governments or other entities, and are deemed as providing significant contribution to the public good. NGS acts as a depository and dissemination point for these data. Since UDN surveys are frequently performed for horizontal control requirements, one can see a wide variation in the ellipsoid height accuracies. Sometimes, UDN height accuracy is very good, due to the shorter line spacing of the survey points. The UDN GPS benchmarks were retrieved due to the information they may provide on fine scale geoid model error. One should note that the character of UDN surveys, plus the issues discussed above regarding the FBN/CBN surveys, cause the GPS benchmark ellipsoid heights to have heterogenous accuracy.

High accuracy GPS surveys (1 ppm or better) were processed through either OMNI or PAGE4 reduction software. These programs do a complete computational removal of the solid Earth tide, including the permanent part of the solid Earth tide. While solid Earth tide corrections are not required for lower accuracy (10 ppm) GPS surveys, these data are constrained to fit the FBN/CBN. Thus, the GPS ellipsoidal heights are in a tide free system.

The NAD 83 / ITRF94(1996.0) Transformation

The coordinates of the GPS benchmarks stored in the NGS database are in the NAD 83 datum. While most of the points in that datum are from a horizontal, classical network, the NAD 83 was controlled by VLBI and Doppler data sets, and can be considered three-dimensional. Over the years, as GPS surveys were incorporated into the network, they were connected into the three-dimensional framework. The NAD 83 reference system differs from modern ITRF systems, primarily due to a non-geocentricity. Richard Snay, National Geodetic Survey, has computed the seven parameter Helmert transformation from NAD 83 to ITRF94(1996.0) with 8 points common to both reference systems. The RMS of fit was 13 millimeters (mm).

Transformation from NAD 83 to ITRF94(1996.0):

```
Delta X      -0.9738  +/- 0.0261 m
Delta Y      +1.9453  +/- 0.0215 m
Delta Z      +0.5486  +/- 0.0221 m
Rotation X   -0.02755 +/- 0.00087 arc sec
Rotation Y   -0.01005 +/- 0.00081 arc sec
Rotation Z   -0.01136 +/- 0.00066 arc sec
Scale        -0.00778 +/- 0.00264 ppm        (0.0 scale difference applied)
```

Note that in the application of the transformation, the scale difference is not applied. The reason is historical. After the NAD 83 readjustment, GPS surveys were performed. It was felt that the scale of these GPS surveys was superior to that of the existing network. So, while the GPS vectors were rotated into the NAD 83 frame prior to adjustment, no scale difference was ever applied. For this reason, when one considers the set of GPS coordinates in the NAD 83 reference system, the scale should be essentially identical to that of the ITRF94(1996.0).

The transformation above was applied to the set of GPS benchmarks in the NAD 83 reference system to obtain the file of GPS benchmarks in the ITRF94(1996.0) system. All points, whether flagged as outliers or not, were transformed. Note that the transformation has no influence whatsoever on the NAVD 88 orthometric heights.

The Benchmark Orthometric Heights

The NAVD 88 datum is expressed in Helmert orthometric heights, and was computed in 1991. The network contains over 1 million kilometers (km) of leveling at precisions ranging from 0.7 to 3.0 mm/$\sqrt{}$km, and incorporates corrections for rod scale, temperature, level collimation, astronomic, refraction, and magnetic effects (Zilkoski et al. 1992). For geoid analysis in a local region, leveling can be considered nearly error free. Accuracy assessment of leveling at a national scale is problematic. An interesting result is that shown in Figure 8 of Zilkoski et al. (1992). Two independent leveling data sets, that of Canada and that of the United States, match at the 11 cm level or better at 14 points along the Canadian-U.S. border. While repeatability is not a measure of accuracy, the agreement is remarkable.

The NAVD 88 datum was realized by a single datum point, Father Point/Rimouski, in Quebec, Canada. The strategy and the value of the constraint were based on a number of factors. But, the foremost requirement was to minimize recompilation of national mapping products. Thus, there is no guarantee that the NAVD 88 datum coincides with the normal potential, U_0, defined by the GRS80 system, nor with the level of global mean sea level. Smith and Milbert (1998) estimate that the NAVD 88 vertical datum is 31.1 cm below the current best estimate of the Earth's best-fit global geopotential. Tests show the vertical datum bias to be nearly constant throughout the conterminous United States.

In addition to the general requirement of having an NAVD 88 Helmert height in the conterminous United States, the leveled benchmarks were also selected according to a number of categories:

```
A - Adjusted.
B - Hand Keyed but not Verified.
C - Computed from nearby Bench Marks.
R - Reset.
M - Readjusted due to earth movement.
H - From Horizontal Branch.
```

Benchmarks in other categories were not retrieved:

```
P - POSTED - Force Fix to NAVD88.
N - Determined by Single Spur.
O - From Horizontal Branch but Other Agency.
```

Briefly, "adjusted" benchmarks form the bulk of NGS data. Using more recent software, these level surveys were checked and adjusted into the network. "Hand keyed" benchmarks refer to historical data (typically associated with the NGVD 29 datum) that have been adjusted and keyed manually, but have not been processed through the full set of more recent data checking and adjustment software. "Computed from nearby bench marks" refers to the same historical data as "hand keyed", but are incomplete in some respect, most likely due to superseded and/or missing adjusted heights. "Reset" benchmarks denote geodetic leveling over short distances to establish a replacement mark for a benchmark, and usually have only one network point connection. "Readjusted due to earth movement" benchmarks have elevations computed from the most recent leveling measurements in areas of known vertical motion. "From horizontal branch" benchmarks represent short level tie data measured by NGS in the course of performing horizontal control surveys.

For the categories that were not retrieved: "Posted" benchmarks were withheld from the NAVD 88 general readjustment due to excessive misclosures. After the readjustment, the troublesome survey lines were fit to the network, and the points were flagged. "Determined by single spur" benchmarks are established from only one network point, and are not considered sufficiently reliable for this data set. "From horizontal branch but other agency" benchmarks are short level ties performed by other agencies when conducting horizontal control surveys. Due to issues of data reduction, this category was not retrieved. In addition, control points obtained from standard trigonometric leveling were not considered to be of sufficient accuracy. And, benchmarks established from GPS surveys were not used. While such orthometric heights can be accurate, a data set independent of any underlying geoid model was desired.

Note that no retrieval criterion was placed on the accuracy of the leveling surveys for the benchmarks. Instead, the data set format (Appendix 1) contains codes for the relative accuracy of the orthometric heights. It was felt that, given the high relative accuracy of geodetic leveling, that even lower order leveling could provide valuable checks.

The NAVD 88 vertical datum (while subject to a constant offset) should be considered as a tide free system. The leveling reduction program does a complete computational removal of both the direct and indirect components of the Earth tide, including the permanent part, as part of the "astronomic" correction (Balazs and Young 1982).

In closing this section one must recall that a Helmert orthometric height is not a true orthometric height. This difference lies in the error in the estimate of the mean value of gravity along the plumb line between the surface and the geoid. The Helmert height is based on a model of an infinite Bouguer plate with a uniform density of 2.67 gm/cm^3. Variations in density and topographic relief will cause departures of Helmert heights from true orthometric heights. As a gauge on the influence of rock density variation, Heiskanen and Moritz (1967, pp.169) show a 4 mm error in Helmert height for a point at 1000 m elevation and with a constant 0.1 gm/cm^3 surficial density departure from 2.67 gm/cm^3. Such error is proportional, so that if one assumes an average density of 2.87 gm/cm^3 (e.g., diorite/gabbro combination or an alkaline basalt as found in the Rocky Mountains) distributed as a Bouguer plate with an elevation of 3000 m, then one would obtain a Helmert height error of 2.4 cm. Terrain variations also influence the mean value of gravity along the plumb line. Heiskanen and Moritz (1967, pp.169) quote a comparison of a Niethammer height and a Helmert height for a point at 2504 m elevation in the Alps. The error in estimating the mean gravity (23 mGal) causes a height error of 6 cm. Thus, one can expect a certain level of GPS benchmark/geoid model misclosure in the mountains solely due to the character of Helmert orthometric heights.

Data Set Cleansing

The objective in cleaning the gravity data set was to flag those points whose error could not be ascribed to a high resolution geoid height model. The basic approach entails locating misclosures between a point's ellipsoid height, h, orthometric height, H, and geoid height, N, where these heights are expected to obey the theoretical relationship:

$$h = H + N \ .$$

Since the geoid is formed by integration of gravity data, one can expect geoid error to be correlated over distance. Thus, the appearance of a large (e.g., 20 cm) misclosure in close proximity to a number of small misclosures (e.g., 3 cm) leads one to suspect the GPS or the leveled heights as the probable source. Such outliers are flagged in the data set (see data set formats, Appendix 1), the data record is never deleted.

A geoid model was created by applying the NAD 83/ITRF94(1996.0) datum transformation in reverse to the G96SSS geoid height model. The result is a gravimetric geoid model in the NAD 83 system, which is denoted G96S83. This model is used to compute misclosures in the sense of:

e = G96S83 geoid height - (NAD 83 ellipsoid height - NAVD 88 orthometric height).

A mean offset of 47.2 cm was computed and removed from the misclosures. This mean offset is a combination of the 12.0 cm offset in the underlying G96SSS model and a 35.2 cm offset in the NAVD 88 vertical datum (when both are referred to global mean sea level). A fit of a tilted plane to the misclosures indicates the possibility of a 0.01 ppm trend in the North-South

direction. The lack of an East-West tilt indicates that there is no strong height dependence in the NAVD 88 datum bias, as heights in the conterminous U.S. have a strong East-West correlation.

The simple Gaussian covariance function of Smith and Milbert (1998) (where $L = 400$ km and $C_0 = (0.095)^2$ m^2) was used to predict the expected misclosure by using least-squares collocation with noise (Moritz 1980, p.102-106). The collocation was not used to establish an optimal height conversion or geoid improvement. Rather, collocation was used to model the general trends of the misclosures and easily highlight local departures (outliers) from the trend.

The residuals from the collocation fits were examined over a progressively tighter set of tolerances, where a new collocation computation was performed after a given set of outliers were flagged for rejection. The first round of rejections were made with a +/- 50 cm tolerance. And, in subsequent rounds, the tolerances were eventually lowered to +/- 10 cm. In no circumstance was a point automatically rejected for exceeding a tolerance. Each large misclosure was graphically displayed to show its relationship to its neighbors in a 1° x 1° degree block before a judgement was made. In addition, when outliers were found in mountainous regions, such as the Rocky Mountains or the Appalachians, those points were typically not flagged for rejection. This is due to certain theoretical and computational inaccuracies related to terrain corrections and gravity reductions in the G96SSS geoid model computation (Smith and Milbert 1998). While it is likely that a number of GPS benchmark outliers in the mountains are due to GPS or leveling error, the points are not rejected unless the error source is unequivocal. In addition, an outlier was not rejected if it did not have sufficient neighbors to verify that it was a localized error.

211 GPS benchmark points were flagged for rejection. The misclosures range from a maximum of +/- 4 meters to +/- 10 cm. It was found that one could not reliably identify outliers below a 10 cm level, although this varied with the region of the country. The RMS of 5168 collocation residuals, after cleansing, was 5.25 cm. This RMS value was assigned as the random error component in the last round of the collocation with noise computation.

In two circumstances, all GPS benchmark points were rejected in an area, irrespective of their misclosures. These cases were regions of known subsidence due to the pumping of underground water. One region was the Houston-Galveston area in Texas, and the other region was the Casa Grande area in Arizona. While it is true that the leveling and the GPS work can be considered correct for those points, the absence of vertical motion models makes these points useless for geoid studies.

Certain patterns were seen in the process of outlier examination. For example, it was necessary to flag a disproportionate number of "reset" benchmarks. As discussed earlier, these points are established through short level ties to replace existing or destroyed marks. However, these surveys are typically only single mark ties, and are less reliable. It is seen that the reset GPS benchmarks, as a category, provide useful information on the geoid. However, the number of rejections demonstrate that reset benchmarks must be used with caution.

Another pattern seen in outlier examination was the presence of isolated misclosures along the coast. In some cases these points contain the word "TIDAL" in their name. On

occasion, a series of nearly identical, sizable misclosures can be found for points on islands. These sets of GPS benchmark outliers are most likely due to the fact that the orthometric heights are not in the NAVD 88 datum. Rather, the elevations are on some local vertical datum derived from a tide gage.

Other patterns seen are of a regional character. For example, the GPS benchmark misclosures in South Carolina are remarkably small. This HARN survey was one of the most recent GPS surveys, and was performed with short station spacing. The GPS ellipsoid heights are extremely accurate in this state. In addition, recent, extensive leveling was performed. These data show very small misclosures (2.6 cm RMS), and demonstrate the high accuracy of the geoid model in low elevation areas.

By contrast, the GPS benchmark misclosures in Florida show systematic patterns of approximately +10 cm and - 10 cm. The misclosures are so prevalent that it is essentially impossible to distinguish points as outliers. Many points share systematic offsets in the ellipsoid heights. These problems are also seen in network adjustments of GPS vectors (which do not involve the geoid or leveled benchmarks). The GPS network in Florida was only the second HARN ever performed. And, the adjusted ellipsoid heights were subject to all the systematic effects discussed at the beginning of this paper. While newer GPS surveys have been performed, they often tie into the old, erroneous control, and propagate these systematic errors. For an example of the situation in Florida, one can inspect the misclosures in the vicinity of 30.5° N, 278.3° E. One can find misclosures of -12.6 cm and +9.1 cm for two points only 10 km apart. The troublesome GPS benchmarks are not flagged for rejection because it is not clear which points, irrespective of the size of misclosure, can be considered correct.

Problems in the GPS ellipsoid height network are not confined to Florida. For example, one may find a set of systematic outliers along the coast of New Jersey (34.9° N, 285.5° E). These are GPS ellipsoid height problems, since numerous problems have been found in GPS adjustments in that state due to inconsistent network adjustment constraints (Maralyn Vorhauer, personal communication, 1998).

It must be repeated that GPS benchmarks were only flagged if the misclosure was clearly due to a GPS or a level network source. Patterns of misclosures can be found, for example, in the Rocky Mountains. But, such misclosures may be due to the geoid model and are retained. One notable pattern of misclosures, found in a low elevation area, is on the Eastern shore of Lake Michigan (43.4-44° N, 273.5-273.7° E). It is believed that these misclosures are of gravimetric origin, probably related to marine data taken on the Lake itself. These misclosures are not flagged for rejection.

Finally, a cautionary note must be made regarding the possibility of long scale (200-400+ km) systematic error in the GPS heights. A number of HARN surveys were controlled by 0.1 ppm stations established with orbit relaxation procedures. Intercomparisons with newer GPS ellipsoid height control, derived from CORS (continuously operating reference stations), show systematic height errors can reach the 8-10 cm level. It is believed that the collocation residual

RMS of 5.25 cm may reflect a portion of this error. Despite these instances of GPS network problems, the GPS benchmark data set has been found to be very useful in geoid and geopotential model tests.

Tests Using GPS Benchmarks

A brief sketch is now made of geoid and global geopotential tests that have been performed with the growing NGS GPS benchmark data set. This section illustrates the utility of GPS benchmarks in the evaluation and improvement of geoid and global geopotential models.

Milbert (1991a) reported one of the first evaluations of the GEOID90 model using data in the Commonwealth of Virginia. Even at this early time of GPS surveying, it was possible to isolate a 13 cm discrepancy at benchmark TOANO 2. This discrepancy was traced to the fact that TOANO 2 was on a local mean sea level datum, and not part of NGVD 29. A portion of that report can be found in Milbert (1992). Some results from one of the first studies of a statewide HARN (Oregon) can be found in Milbert (1991b).

Milbert (1995) first used a nationwide GPS benchmark data set for geoid improvement in computing the G9501C geoid model by collocation of 1889 geoid/GPS benchmark misclosures. The empirical covariance function was extremely smooth, having a correlation length of 500 km (and power of $(18.5)^2$ cm^2). The residual statistics for G9501 had a variance of $(6.5)^2$ cm^2 which dropped to a covariance of $(2.6)^2$ cm^2 for points spaced only 5 km apart. This 6.5 cm figure was an independent measure of the random noise in the GPS ellipsoid heights.

Rapp (1997) discusses the problem of computing a geoid undulation from a set of geopotential coefficients, and uses GPS benchmarks to illustrate the need to apply an appropriate correction. This study lead to the computation of the correction coefficients available at the NIMA EGM96 WWW page (`http://164.214.2.59/GandG/wgs-84/egm96.html`).

The global geopotential model, EGM96, was computed after the "beta" test of 5 models (Lemoine el al., 1997). Smith and Milbert (1997a) analyzed the beta models with 2497 GPS benchmarks in the conterminous United States. Through analysis of misclosure statistics gathered into elevation cohorts, the X02 and X05 models were found to be best. In addition, commission error was identified in the Northwest United States. When the EGM96 model was released, Smith and Milbert (1997b) found a quasi-periodic error around spherical harmonic degree 40 that was confirmed with GPS benchmarks in Oklahoma. One can also find tests of these models by Bursa, et al. (1997) and Bursa, et al. (1998) using a 1835 point GPS benchmark data set.

The experiment in combining GPS benchmarks with a gravimetric geoid by Milbert (1995) led to the development of an operational product, GEOID96, which is described in Milbert and Smith (1996), Milbert and Smith (1997), and Smith and Milbert (1998). This latter study illustrates cases where the GPS benchmarks remove long-wavelength commission error in the underlying gravimetric geoid model, G96SSS, while retaining the high relative accuracy over

shorter length scales. Smith and Milbert (ibid) also point out that systematic errors in the GPS or the leveling networks, that extend over long distances (e.g., 400 km), will be absorbed into the geoid in this approach.

Numerous studies have been performed of the GEOID96 model, typically using new GPS survey data on benchmarks. One test, by Milbert (1997) explored the GEOID96 model in Ohio. Milbert attempted to develop a local covariance function for geoid improvement, but was hampered by the current distribution and accuracy of the GPS benchmarks in the state. An abridged version of this study is available (Milbert 1998).

Although not within the conterminous United States, Smith and Small (1998) used an NGS GPS benchmark data set of 31 points to evaluate the CARIB97 geoid model. They found local leveling errors and inter-island discrepancies caused by use of local mean sea level datums for the islands. They recommend future studies that would incorporate models of permanent ocean dynamic topography.

Future Developments

This GPS benchmark data set is a milestone, since it incorporates the completion of the HARN projects. However, the NGS GPS benchmark data set will evolve as the GPS network of the United States continues to grow and improve. The NGS is currently engaged in a new nationwide GPS survey effort for height modernization. The objective of this project is to obtain a set of GPS ellipsoid heights accurate to +/- 2 cm (two-sigma). Associated with this new effort will be the analysis of existing GPS control, and the eventual readjustment of the network in 2002. This project will represent an approximate fivefold increase over the current ellipsoidal height accuracy of the nationwide GPS network.

As the new surveys for height modernization proceed, it will be necessary to make format changes to this file to better characterize vertical accuracy in ellipsoidal and orthometric height. Note that in this document, vertical accuracies relative to the coordinate system origin are not stated. They are only inferred, in a qualitative sense, from various codes in the format. It is anticipated that realistic height accuracies in a network or datum sense will be assigned in the course of analysis of the national spatial reference system. The result will be future data sets that are not only more accurate, but will also have better defined accuracies, and will support more sophisticated statistical analysis.

(The July 23, 1998 data set is located at `www.ngs.noaa.gov/GEOID/GPSBMS/gpsbms.html`)

Acknowledgments

This study incorporates the contributions of numerous NGS employees involved in the creation and evaluation of the gravity, NAVD 88, and GPS data sets. In particular, Dr. Dru Smith is the co-author of the G96SSS and GEOID96 models. Mr. Craig Larrimore wrote the

data base retrieval applications for the GPS benchmarks. The National Imagery and Mapping Agency (NIMA, formerly DMA) provided a major portion of the NGS land gravity data, and was instrumental in the creation of various 3" and 30" digital elevation data grids in use today. Dr. Walter Smith, NOAA, provided altimeter-derived gravity anomalies used in the G96SSS and GEOID96 models. Ms. Katherine Koepsell provided much needed insight on the coding system for leveled benchmarks.

References

Balazs, E. I, and G. M. Young, 1982: Corrections applied by the National Geodetic Survey to precise leveling observations. *NOAA Technical Memorandum NOS NGS 34*, June 1982, Information Services Branch, National Geodetic Survey, NOAA, Silver Spring, MD., 12 pp.

Bodnar, A. N., 1990: National geodetic reference system statewide upgrade policy. *Technical Papers of ACSM-ASPRS Fall Convention*, Nov. 5-10, 1990, pp. A71-82.

Bursa, M., K. Radej, Z. Sima, S. A. True, and V. Vatrt, 1997: Tests for accuracy of recent geopotential models. *IGeS Bulletin N.6, "The Earth Gravity Model EGM96: Testing Procedures at IGeS"*, International Geoid Service, Milan, 1997, 167-188.

Bursa, M., J. Kouba, K. Radej, S. A. True, V. Vatrt, and M. Vojtiskova, 1998: Final report on testing accuracy of geopotential models EGMX01-X05, EGM 96. *IGeS Bulletin N.7*, International Geoid Service, Milan, 1998, 14-23.

Heiskanen, W. A. and H. Moritz, 1967: *Physical Geodesy*. W.H. Freeman, San Francisco.

Lemoine, F. G., D. E. Smith, L. Kunz, R. Smith, E. C. Pavlis, N. K. Pavlis, S. M. Klosko, D. S. Chinn, M. H. Torrence, R. G. Williamson, C. M. Cox, K. E. Rachlin, Y. M. Wang, S. C. Kenyon, R. Salman, R. Trimmer, R. H. Rapp, and R. S. Nerem, 1997: The development of the NASA GSFC and NIMA joint geopotential model. In: *Gravity, Geoid, and Marine Geodesy, International Association of Geodesy Symposium Vol. 117*, Tokyo, Japan, Sept. 30 to October 5, 1996, Edited: J. Segawa, H. Fujimoto, and S. Okubo, Springer-Verlag, Berlin, 461-469.

Milbert, D. G., 1991a: An accuracy assessment of the GEOID90 geoid height model for the Commonwealth of Virginia. *National Geodetic Survey Report (unnumbered series)*, June 1991, 52 pp.

Milbert, D. G., 1991b: GEOID90: A high-resolution geoid for the United States. *Eos*, 72(49), pp. 545-554.

Milbert, D. G., 1992: GPS and GEOID90 -- The new level rod. *GPS World*, 3(2), pp. 38-43.

Milbert, K. O. and D. G. Milbert, 1994: State readjustments at the National Geodetic Survey. *Surv. and Land Info. Sys.*, 54(4), 219-230.

Milbert, D. G., 1995: Improvement of a high resolution geoid height model in the U.S. by GPS height on NAVD88 benchmarks. *IGeS Bulletin N.4, "New Geoids in the World"*, International Geoid Service, Milan, 1995, 13-36.

Milbert, D. G. and D. A. Smith, 1996: Converting GPS height into NAVD88 elevation with the GEOID96 geoid height model. *Proceedings of the GIS/LIS'96 Annual Conference*, Denver, Colorado, November 19-21, pp. 681-692.

Milbert, D. G. and D. A. Smith, 1997: Converting GPS height into local elevation: the GEOID96 height model for the United States. *Geomatics Info Magazine*, 11(9), pp. 60-63.

Milbert, D. G., 1997: An accuracy assessment of the GEOID96 geoid height model for the State of Ohio. Unnumbered Report, February 1997, Information Services Branch, National Geodetic Survey, NOAA, Silver Spring, MD., 51pp.

Milbert, D. G., 1998: An accuracy assessment of the GEOID96 geoid height model for the State of Ohio. *Surv. and Land Info. Sys.*, 58(2), 83-96.

Rapp, R. H., 1997: Use of potential coefficient models for geoid undulation determinations using a spherical harmonic representation of the height anomaly/geoid undulation difference. *Journal of Geodesy*, 71(5), 282-289.

Schupler, B. R., R. L. Allshouse, and T. A. Clark, 1994: Signal characteristics of GPS user antennas. *Navigation*, 41(3), 277-295.

Smith, D. A. and D. G. Milbert, 1997a: Evaluation of preliminary models of the geopotential in the United States. *IGeS Bulletin N.6, "The Earth Gravity Model EGM96: Testing Procedures at IGeS"*, International Geoid Service, Milan, 1997, 7-32.

Smith, D. A., and D. G. Milbert, 1997b: Evaluation of the EGM96 model of the Geopotential in the United States. *IGeS Bulletin N.6, "The Earth Gravity Model EGM96: Testing Procedures at IGeS"*, International Geoid Service, Milan, 1997, 33-46.

Smith, D. A. and D. G. Milbert, 1998: The GEOID96 high resolution geoid height model for the United States. *Journal of Geodesy*, in press.

Smith, D. A. and H. J. Small, 1998: The CARIB97 high resolution geoid height model for the Caribbean Sea. *Journal of Geodesy*, in press.

Zilkoski, D. B., J. H. Richards, and G. M. Young, 1992: Results of the general adjustment of the North American Vertical Datum of 1988. *Surv. and Land Info. Sys.*, 52(3), 133-149.

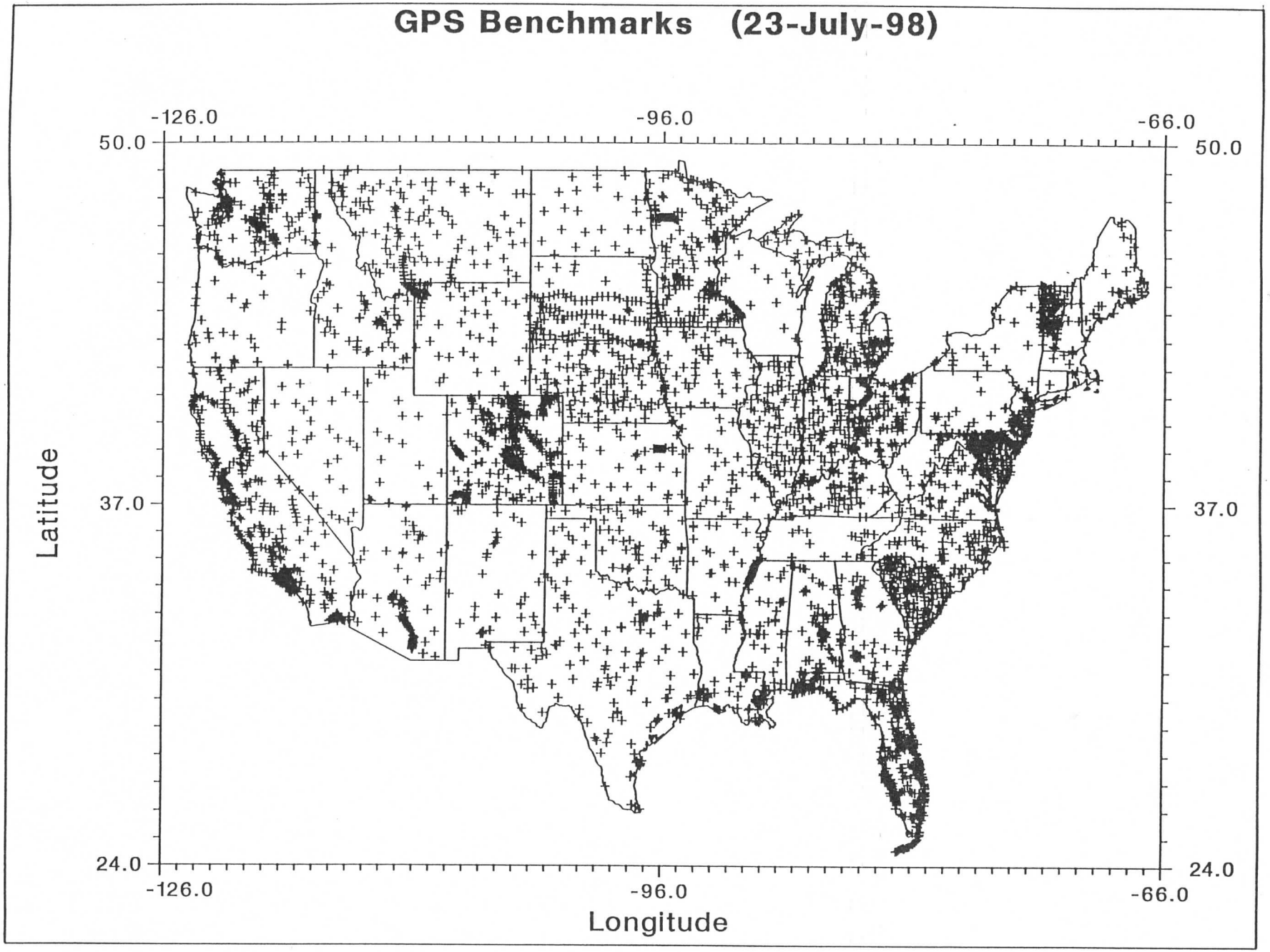
GPS Benchmarks (23-July-98)
-126.0
-96.0
-66.0
50.0
37.0
24.0
Latitude
Longitude

Appendix 1 — Formats for GPS on Leveled Benchmarks

Format of the "GPS/Leveling" file (code: eval2 26-feb-92 dgm)

01-04	Station Serial Number	integer, right justified
05-34	Station Name	character, left justified
35-36	Geodetic Lat., deg.	integer, right justified
37-38	Geodetic Lat., min.	integer, right justified
39-45	Geodetic Lat., sec.	integer, right justified, units 0.00001"
46-46	Code (N/S)	character, upper case
47-49	Geodetic Lon., deg.	integer, right justified
50-51	Geodetic Lon., min.	integer, right justified
52-58	Geodetic Lon., sec.	integer, right justified, units 0.00001"
59-59	Code (E/W)	character, upper case
60-66	Ellipsoidal Height	integer, right justified, units of 1 mm
67-67	blank	
68-74	Orthometric Height	integer, right justified, units of 1 mm
75-75	blank	
76-76	GPS Order (Hztl)	character, upper case
77-77	Ortho Elevation Code	character, upper case
78-78	Ortho Order	character, upper case
79-79	Ortho Datum Code	character, upper case
80-80	Reject Code	character, upper case

COMMENTS

Station Serial Number

Arbitrary positive index number. Not to be repeated within a given file.

GPS Order (Hztl)

Code	Explanation
A	Length Relative Accuracy (2 sigma) better than 1:10,000,000
B	Length Relative Accuracy (2 sigma) better than 1: 1,000,000
1	Length Relative Accuracy (2 sigma) better than 1: 100,000
2	Length Relative Accuracy (2 sigma) better than 1: 20,000
3	Length Relative Accuracy (2 sigma) better than 1: 5,000

Ortho Elevation Code

Code	Explanation
A	OHT established using FGCS leveling specifications and procedures, adjusted height determined using NGS Vertical Network Branch procedures, leveling data is in the NGSIDB.
B	OHT established using FGCS leveling specifications and procedures, adjusted height determined using NGS Vertical Network Branch procedures, leveling data is not in the NGSIDB. (USGS, COE, some state DOT data.)
C	OHT established using FGCS leveling specifications and procedures, adjusted height is 'posted'. See explanation in the footnote (*) below.
H	OHT established using FGCS leveling specifications and procedures except for the two-mark leveling tie requirement. (Horizontal field party level ties, some state DOTs, some GPS level ties.)
L	OHT established using leveling RESET specifications and procedures.

F	OHT established by fly-leveling.
T	OHT established by leveling between control points which are not Bench Marks.
R	OHT established by reciprocal vertical angles.
V	OHT established by non-reciprocal vertical angles.
P	OHT established by photogrammetry.
M	OHT established by scaling from a contoured map.
G	OHT established by GPS observations.
D	OHT established by datum transformations.

* Data for level lines containing 'posted' BMs were purposely not included in the NAVD88 general adjustment. Subsequently, these data were adjusted to NAVD88 by forcing them to fit the existing NAVD88 general adjustment heights.

Ortho Order

Code	Explanation
1	Relative Accuracy (2 sigma) better than 0.7 mm x sqrt(Km)
2	Relative Accuracy (2 sigma) better than 1.3 mm x sqrt(Km)
3	Relative Accuracy (2 sigma) better than 2.0 mm x sqrt(Km)

Ortho Datum Code

Code	Explanation
blank	North American Vertical Datum of 1988
9	National Geodetic Vertical Datum of 1929

Reject Code

An asterisk ("*") indicates a rejection (for various experiments) Blank indicates no rejection.

Report on the Second Continental Workshop on the Geoid in Europe Budapest, March 10 – 13, 1998

József Ádám and Martin Vermeer

August 28, 1998

The Second Continental Workshop on the Geoid in Europe was organized by the **IAG - Subcommission for the Geoid in Europe** in co-operation with the **Department of Geodesy, Technical University of Budapest**, under the Sponsorship of

- the International Union of Geodesy and Geophysics (IUGG),
- the International Association of Geodesy (IAG) and its
  - Section III ("Determination of the Gravity Field"),
  - Section IV ("General Theory and Methodology"),
  - Special Commission 1 ("Mathematical and Physical Foundation of Geodesy"), and
  - Subcommission for Europe (EUREF European Reference Frame).

The workshop was co-sponsored by

- the Hungarian Academy of Sciences (MTA),
- the Hungarian National Committee of IUGG,
- the Hungarian Scientific Research Fund (OTKA),
- the National Committee for Technological Development (OMFB) and
- the Technical University of Budapest (BME).

The **Finnish Geodetic Institute** (FGI) has committed itself to produce the Proceedings of the Workshop.

Now that the meeting is over, we may say that indeed the successful format and atmosphere established by the previous meeting in Prague in 1992 continued in Budapest. The European geoid scientists have really grown into a community in the years that have elapsed since Prague.

Participants: 77 from 30 countries. The following countries were represented (number of participants): Austria (3), Belgium (1), Bulgaria (3), Croatia (3), Czech Republic (3), Denmark (2), Egypt (1), Finland (4), France (3), Germany (8), Greece (4), Hungary (12), Italy (3), Israel (1), Latvia (1), The Netherlands (2), Norway (1), Poland (2), Portugal (2), Romania (3), Russia (1), Slovenia (1), Slovakia (1), Spain (1), Sweden (1), Switzerland (3), Turkey (1), U.K. (3), The Ukraine (1) and the U.S.A. (2).

Papers: 54 (9 invited, 44 contributed and 1 cancelled).

Workshop scientific programme and timetable as realized

March 10 (Tuesday)

Official Opening

- Martin Vermeer
  President of IAG Subcomission for the Geoid in Europe, Convenor of the Workshop
- Ákos Detrekõi
  Rector Magnificus of the Technical University of Budapest
- Rene Forsberg
  President of Section III ("Determination of the Gravity Field")
- Petr Holota
  President of Section IV ("General Theory and Methodology")
- Erik W. Grafarend
  President of Special Commission 1 ("Mathematical and Physical Foundations of Geodesy")
- Erich Gubler
  President of Subcommission for Europe (EUREF)
- József Ádám
  Chairman of the LOC, Co-Convenor of the Workshop

Invited Presentations (1)

Session: "The EUREF Connection", **Chairman :** Martin Vermeer

H. Seeger (Germany) : Ten Years of EUREF.

C. Boucher (France) : ITRS, ETRS89 and WGS84: Definitions and Realizations.

E.C. Pavlis (USA) : On the Reference Frames Inherent in the Recent Geopotential Models.

Chairman : Erich Gubler

W. Augath (Germany) : UELN95/EUVN97 and EVS2000 – Recent Activities toward an Unified European Vertical System.

J. Kakkuri (Finland) : Discussion on Geodetic Measuring Techniques to Determine the Sea Surface Topography for Unification of European Vertical Datums.

T. Baker (United Kingdom) : Sea Level and Height Variations in Europe.

March 11 (Wednesday)

Invited presentations (2)

Session: "The Geoid in Society" , **Chairman :** Péter Biró

Torge, W. - Denker, H. (Germany) : The European Geoid – Development over More Than 100 Years and Present Status.

H. Denker (Germany) : Evaluation and Improvement of the EGG97 Quasigeoid Model for Europe by GPS and Levelling Data.

F. Sansò (Italy) : Activities at the International Geoid Service (IGeS).

M. Vermeer (Finland) : The Geoid as a Product.

Contributed presentations

Session : "Global and Regional Models", **Chairman:** Heiner Denker

Sansò, F. - Venuti, G. (Italy) : What is a Local Solution for a Gravimetric Geoid?

H.G. Wenzel (Germany) : Ultra High Degree Geopotential Model GPM3E97A to Degree and Order 1800 Tailored to Europe.

Bursa, M. (Czech Republic) - Kouba, J. (Canada) - Mueller, A. (Germany) - Radej, K. (Czech Republic) - True, S.A. (USA) - Vatrt, V. - Vojtísková, M. (Czech Republic) : Accuracy Estimates of EGM96 Geoid With Emphasis on Central Europe, Scandinavia and Baltic Region. [Poster only]

Kumar, M. - Burke, K.J. (USA) : Realizing a Global Vertical Datum with the Use of a Geoid.

Reinhart, E. - Richter, B. - Wilmes, H. (Germany) - Erker, E. - Ruess, D. (Austria) - Kakkuri, J. - Mäkinen, J. (Finland) - Marson, I. (Italy) - Sledzinski, J. (Poland) : UNIGRACE - A Project for the Unification of Gravity Systems in Central Europe.

March 12 (Thursday)

Session: "Geoid Innovations" , **Chairman:** Lars E. Sjöberg

E.W. Grafarend (Germany) : High Resolution Regional Geoid Computation (Case Study : Baden-Würtenberg) from Geopotential and Gravity Data.

P. Holota (Czech Republic) : Variational Methods and Subsidiary Conditions for Geoid Determination.

Petrovskaya, M.S. (Russia) - Zielinski, J.B. (Poland) : Application of Spatial Gradiometry for Constructing Geoid/Quasigeoid Models.

Strykowski, G. (Denmark) - Dahl, O.Ch. (Norway) : Geoid as an Equipotential Surface in a Sense of Newton's Integral - Ideas and Examples.

Kr. Pichtoukhina-Skhodorova (Bulgaria) : On the Geoid Height Determination by Combining Integral Formulas and a Set of Geopotential Coefficients.

Gy. Tóth (Hungary) : Topographic-isostatic Models Fitted to the Geopotential.

Session: "Geoid Innovations and Variations", **Chairman:** Hans-Georg Wenzel

E.W. Grafarend (Germany) : The Time Variation of the Geoid Due to the Deformation of Geometry and Gravity Space.

P. Varga (Hungary) : Temporal Variations of the Figure of the Earth.

Ivan, M. (Romania) - Sevilla, M.J. (Spain) : Local Quasi-Geoid and Downward Continuation by Integrated Harmonic Series. Application to Dobrudja Area - Romania.

K. Zhang (U.K.) : Altimetric Gravity Anomalies, Their Assessment and Combination with Local Gravity Field.

L. Völgyesi: Geoid Computations Based on Torsion Balance Measurements. [Not presented]

Papp G. (Hungary) - Wang, Z.T. (Finland) : Comparison of Planar and Spherical Approximations Used in Forward Local Gravitational Field Modelling.

Doufexopoulou, M. - Pagounis, V.N. (Greece) : Investigation of Tectonic Traces upon the Regional Geoid without the Use of Gravity.

Session: " Corrections" , **Chairman:** Erik W. Grafarend

L.E. Sjöberg (Sweden) : The Atmospheric Geoid and Gravity Corrections.

Seitz, K. - Heck, B. (Germany) : Ellipsoidal and Topographical Effects in the Scalar Free Geodetic Boundary Value Problem.

B. Heck (Germany) : Ellipsoidal Corrections to Gravity Anomalies Derived from Satellite Altimeter Data.

Tziavos, I.N. - Andritsanos, V.D. (Greece) : Recent Advances in Terrain Correction Computations.

H. Abd-Elmotaal (Egypt) : Gravity Reduction Techniques and their Comparisons Applied to the Gravity Field in Egypt.

Rózsa Sz. (Hungary) : Determination of Terrain Correction in Hungary and the Surrounding Area.

Session: "GPS/Levelling", **Chairman:** Juhani Kakkuri

R. Forsberg (Denmark) : Geoid Tayloring to GPS - with Example of a 1-cm Geoid of Denmark.

Ihde, J. - Schirmer, U. - Stefani, F. - Töppe, F. (Germany) : Geoid Modelling with Point Masses.

M. Ollikainen, (Finland) : GPS Levelling Results Obtained in Finland.

A. Kenyeres (Hungary) : GPS-Heighting in the Hungarian National Network : Final Results.

Ihde, J. - Franke, P. - Lang, H. - Sacher, M. - Schoch, H. - Weber, G. (Germany) : Combination of Repeated Levellings and GPS Permanent Observations for the Realization of a Kinematic Height Reference System.

Paunescu, C. - Dina, C. (Romania) : The Fitting of Romanian Airports to the ETRF89 Network on the WGS-84 Ellipsoid.

Kenyeres A. - Virág G. (Hungary) : Testing of Recent Geoid Models with GPS/Levelling in Hungary. [Poster only]

March 13 (Friday)

Session: "National Geoid Solutions, I", **Chairman:** René Forsberg

Zhang, K. (U.K.) - Featherstone, W. - Stewart, M. (Australia) : A New Gravimetric Geoid of Australia.

Heiland, R. - Hoffmann-Wellenhof, B. - Kienast, G. - Kühtreiber, N. (Austria) : Recomputation of the Austrian Astrogeodetic Geoid.

Kühtreiber, N. (Austria) : Comparing Different Geoid Computations for Austria.

Minchev, M. (Bulgaria) : A Note on the Contemporary Geoid Investigations in Bulgaria.

Colic, K. - Pribicevic, B. - Svehla, D. (Croatia) : First cm-geoid in Republic of Croatia.

Duquenne, H. (France) : QGF98, a New Solution for the Gravimetric Quasi-Geoid in France

Session: "National Geoid Solutions, II", **Chairman:** Petr Holota

Tziavos, I.N. (Greece) - Ádám J. - Tóth Gy. (Hungary) - Andritsanos, V.D. (Greece) - Rózsa Sz. (Hungary) : Recent Geoid Computations in Hungary and the Surrounding Area.

Sharni, D. - Papo, H. - Forrai, J. (Israel) : The Geoid in Israel : Haifa Pilot.

Kaminskis, J. - Zagars, Y. (Latvia) : The Analysis of Different Geoid Solutions in Latvia and Practical Ways of their Improvement.

Łyszkowicz, A. (Poland) : The Polish Gravimetric Quasigeoid QGEOID97 Versus Vertical Reference System Kronsztad 82.

Ioane, D. (Romania) - Featherstone, W.E. (Australia) : Gravimetric Geoids for Geophysics in Romania.

Mojzes, M. - Janák, J. (Slovakia) : Gravimetric Model of Slovak Quasigeoid.

Marti, U. (Switzerland) : The New Geoid CHGEO97 of Switzerland.

Panel Discussion: "The Future Direction of the Geoid in Europe"

Chairman: Martin Vermeer

The panel discussion was taped, and a transcript will be published in the Proceedings. You may be asked to assist in checking the transcript, if you participated in the discussion.

Business Session: Resolutions, Chairman: Martin Vermeer

Official Closure

Resolutions adopted

The participants of the Second Continental Workshop on the Geoid in Europe, Budapest, Hungary, March 10-14, 1998:

1. (unanimous)

recognizing the high resolution and high precision demonstrated in European geoid determination projects, like the recently completed Gravimetric Geoid EGG97, and

realizing

1. that long-wavelength systematic discrepancies exist between the gravimetric geoids and GPS/levelling derived height anomalies,
2. the importance to reduce such errors by international cooperation

recommend that the national agencies release GPS/levelling derived geoid or height anomalies to the International Geoid Service for scientific purposes, along with the necessary documentation for the used reference systems.

2. (unanimous)

recognizing the deficiencies in the existing gravity data in Europe at medium to longer wavelengths, and

realizing the difficulties in improving the situation by terrestrial means only,

recommend that dedicated space gravity field missions be realized for the purpose of obtaining a uniformly accurate European geoid and vertical reference system.

3. (unanimous)

recommend that in computing precise geoid in Europe and its national segments various solution strategies are explored with emphasis on

1. merging such solutions like global geopotential models or the recently completed Gravimetric Geoid EGG97 with detailed gravimetry information and constraints of local nature;
2. their theory and methodology reflecting driving impulses coming from new technologies and contemporary developments in geodesy and other geosciences.

4. (acclamation)

wish to extend their most sincere thanks to the Local Organizing Committee under the leadership of József Ádám for its very competent and conscientious organization of this workshop being essential for its success. This includes organizing an excursion into the beautiful city of Budapest and the gala dinner, and wish for the more to sincerely thank the Department of Geodesy, Technical University of Budapest for its generosity in supporting the organization of this workshop.

Conclusion

We wish to thank everybody that has contributed in one way or another to the success of this workshop: Of course the participants; the organizations that have in various ways sponsored this event; the numerous – often anonymous – local organizers, the people volunteering to chair session or to participate in the panel discussion; and the people that are or will be reviewing the papers submitted. To all our most sincere thanks!

Technical University of Budapest

Second Continental Workshop on the Geoid in Europe

Budapest, Hungary **March 10-14, 1998**

A classification of reproducing kernels according to their functional and physical significance [a)]

by A. Marchenko and D. Lelgemann

„Forse altri cantera con miglior plettro !"

As well-known all the reproducing kernels $K^q(P,Q)$ used for collocation in physical geodesy can be expressed in form of an infinite sum

$$K^q(P,Q)=\sum_{n=0}^{\infty} k_n^q \cdot \left(\frac{R_B^2}{r_P r_{\tilde{Q}}}\right)^{n+1} P_n\left(\cos\psi_{PQ}\right)=\sum_{n=0}^{\infty} k_n^q \cdot \left(\frac{r_Q}{r_P}\right)^{n+1} P_n\left(\cos\psi_{PQ}\right) \quad , \qquad (1)$$

where Q is a point obtained by a Kelvin transformation $r_Q = R_B^2 / r_{\tilde{Q}}$ of the position $\tilde{Q}$ of a measurement with respect to the Bjerhammar sphere (Hauck and Lelgemann, 1984). The asymptotic k_n^q describing the asymptotic behaviour of different kernels for $\sigma = R_B^2 / r_P r_{\tilde{Q}} = r_Q / r_P = \text{const}$, that is

$$k_n^q = c_q / n^{2(q-1)} \sim 1/n^{2(q-1)} \quad , \qquad c_q=\text{const} \quad , \qquad (2)$$

provides the index q of the corresponding Sobolev space H_2^q. Sobolev spaces are complete subspaces of the general Hilbert space and therefore Hilbert spaces by themselves, namely Hilbert spaces with reproducing kernels.

Suitable for practical applications are kernels in case the degree coefficients are chosen such, that the infinite summation can be performed and a closed function for the kernel can be obtained.

It will be shown that the set of all those suitable kernel functions can be obtained from finite linear combinations of

- only two point singularities, that are a pole (point mass) and a dipole;
- radial straight line singularities with density function of the form $\nu = r^{A-1}$, forming two classes according whether $(A \le 0)$ or $(A > 0)$.

Regarding the potential of point harmonics (multipoles) by the application of Kelvin transformation to the potential of multipoles (Marchenko, 1987) expressions for the corresponding kernel functions can be obtained in the form

$$K_m(\sigma,\psi)=\sum_{n=m}^{\infty}\binom{n}{m}\cdot\sigma^{n+1}P_n\left(\cos\psi_{PQ}\right) \quad , \qquad (3)$$

where the degree coefficients are given by the binomial coefficients.

For m = 0 we get the set of the degree variances $k_n^q = 1$ (Krarup's kernel; potential of a simple pole or point mass, respectively)

$$K_0(\sigma,\psi)=\sigma\sum_{n=0}^{\infty}\sigma^n P_n\left(\cos\psi_{PQ}\right)=\sigma/L, \qquad L=\sqrt{1+\sigma^2-2\sigma\cos\psi_{PQ}} \quad , \qquad (4)$$

and for m = 1 the set $k_n^q = n\,(n > 0)$ (Poisson's kernel without term of the degree zero; potential of a dipole)

$$K_1(\sigma,\psi)=\sigma\sum_{n=1}^{\infty}\sigma^n P_n\left(\cos\psi_{PQ}\right)=(1/2)\cdot\left[\sigma\left(1-\sigma^2\right)/L^3-\sigma/L\right] \quad . \qquad (5)$$

Closed expressions for all other point harmonic kernels K_m (kernels corresponding to radial

---

[a)] Paper presented at the „Geodetic Week", Berlin, October, 1997.

multipoles) can be obtained by the recursion formula

$$mK_m(\sigma,\psi)=(2m-1)\frac{K_1(\sigma,\psi)}{K_0(\sigma,\psi)}K_{m-1}(\sigma,\psi)-(m-1)\cdot K_0(\sigma,\psi)\cdot K_0(\sigma,\psi)\cdot K_{m-2}(\sigma,\psi). \quad (6)$$

Regarding the line harmonic kernels (corresponding to potentials of radial straight lines) we have to consider two classes according to the two expressions (regard the summation indices)

$$K_{+A}(\sigma,\psi)=\sum_{n=0}^{\infty}\frac{1}{n+A}\left(\frac{R_B^2}{r_P r_{\tilde{Q}}}\right)^{n+1}P_n(\cos\psi)=\sum_{n=0}^{\infty}\frac{1}{n+A}\left(\frac{r_Q}{r_P}\right)^{n+1}P_n(\cos\psi), \qquad A>0 \quad , \quad (7)$$

$$K_{-A}(\sigma,\psi)=\sum_{n=l-A}^{\infty}\frac{1}{n+A}\left(\frac{R_B^2}{r_P r_{\tilde{Q}}}\right)^{n+1}P_n(\cos\psi)=\sum_{n=l-A}^{\infty}\frac{1}{n+A}\left(\frac{r_Q}{r_P}\right)^{n+1}P_n(\cos\psi), \quad A\le 0 \ . \quad (8)$$

Closed expressions of the first type (A > 0) can be obtained from the general expression

$$K_{+A}(\sigma,\psi)=\frac{r_Q^{l-A}}{r_P}\left[r_P\int_0^{r_Q}\frac{r^{A-l}}{\ell}dr\right], \quad (9)$$

where ℓ is the distance between Q and P.
We will get immediately (see also Hauck and Lelgemann, 1984) for A = 1

$$K_1(\sigma,\psi)=\ell n\frac{\ell+r_Q+r_P}{\ell-r_Q+r_P}=\ell n\left(1+\frac{2\sigma}{L-\sigma+1}\right), \quad (10)$$

that is the potential of the radial line from the origin to the point Q with the line density $\nu=\nu_1=1$.
We can get further for A=2

$$K_2(\sigma,\psi)=\frac{r_P}{r_Q}\left(\frac{\ell}{r_P}-1+\cos\psi\cdot K_1(\sigma,\psi)\right)=\sigma^{-1}\left[L-1+\cos\psi\cdot K_1(\sigma,\psi)\right], \quad (11)$$

that is the potential of the radial line from the origin to the point Q with a line density $\nu=\nu_2=\ell$.
Furthermore, the kernel for A = 3 may be obtained too, namely

$$K_3(\sigma,\psi)=\frac{1}{3\cdot\sigma}\left[L+5\cos\psi K_2(\sigma,\psi)-2\sigma^{-1}\cdot K_1(\sigma,\psi)\right]. \quad (12)$$

The last kernel as well as closed expressions for all (A > 2) can be obtained using the general expression (Moritz, 1980, p. 188)

$$K_{A+1}(\sigma,\psi)=\frac{1}{A\cdot\sigma}\left[L+(2A-1)\cos\psi K_A(\sigma,\psi)-(A-1)\cdot\sigma^{-1}\cdot K_{A-1}(\sigma,\psi)\right]. \quad (13)$$

Closed functions of the second type $(A\le 0)$ can be obtained using the general expression

$$F_{-A}(\sigma,\psi)=\frac{r_Q^{l-A}}{r_P}\left[r_P\int\frac{r^{A-l}}{\ell}dr-\sum_{n=0}^{-l-A}\frac{1}{n+A}\frac{r_Q^{n+A}}{r_P^k}P_n(\cos\psi)-\ell n r_Q\cdot r_P^A\cdot P_{-A}(\cos\psi)+k_A\right], \quad (14)$$

where k_A is an integration constant.

We get for (A = 0) with $k_0=\ln(4r_P^2)$ the closed expression

$$K_0(\sigma,\psi)=\frac{r_Q}{r_P}\ell n\frac{2r_P}{r_P-r_Q\cos\psi+\ell}=\sigma\cdot\ell n\frac{2}{N} \quad , \quad (15)$$

where

$$N=1+L-\sigma\cdot\cos\psi=\frac{r_P-r_Q\cos\psi+\ell}{r_P} \quad , \quad (16)$$

that is the potential of the radial line (without a term of degree n = 0) from the origin to the point Q with a line density $\nu = r^{-1}$.

Further, we may get for (A = -1) with the integration constant $k_{-1} = -\cos\psi / r_P$

$$K_{-1}(\sigma,\psi) = \frac{r_Q}{r_P}\left[M + \frac{r_Q \cdot \cos\psi}{r_P}\ell n\frac{2}{N}\right] = \frac{r_Q^2}{r_P}\left[\frac{M}{r_Q} + \frac{\cos\psi}{r_P}\ell n\frac{2}{N}\right] \quad , \tag{17}$$

where

$$M = \frac{r_P - \ell - r_Q\cos\psi}{r_P} = 1 - L - \sigma\cdot\cos\psi \quad , \tag{18}$$

that is the potential of the radial line (without terms of degree 0 and 1) from the origin to the point Q with a line density $\nu = r^{-2}$.

Furthermore, we get for (A = -2) the relationship

$$K_{-2}(\sigma,\psi) = \frac{r_Q}{r_P}\left[\frac{1}{2}\left(1 + 3\frac{r_Q}{r_P}\cos\psi\right)M + \left(\frac{r_Q}{r_P}\right)^2 P_2(\cos\psi)\cdot\ell n\frac{2}{N} + \frac{1}{4}\left(\frac{r_Q}{r_P}\right)^2\left(1 - t^2\right)\right] , \tag{19}$$

that is the potential of the radial line (without terms of degree 0, 1 and 2) from the origin to the point Q with a line density $\nu = r^{-3}$.

Kernels of the second type or of certain linear combinations of this type are well-known in geodesy (see Tabl.1). All of these kernels can be expressed by a linear combination of line harmonics. In regarding the Tscherning-Rapp kernel, remember that

$$k_n^{2.5} = \frac{\alpha}{(n-1)(n-2)(n+B)} = \frac{\alpha}{(B+1)(B+2)}\left[\frac{B+1}{n-2} - \frac{B+2}{n-1} + \frac{1}{n+B}\right] \quad . \tag{20}$$

The reader is invited to create his own kernel forming another linear combination.

Line harmonics may be used to get an approximation of the gravity field which can be interpreted as an approximation of a density distribution in vertical spherical columns, whose line density ν and volume density ρ are related to each other by

Table 1. Various kernels used in geodetic applications.

Class (Type of the singularity)	Author	k_n^q	Index q of the Hilbert space H_2^q
Radial multipoles			
Radial quadrupole	Marchenko, 1987	$k_n^q = \binom{n}{2}$	q=0
Radial dipole	Hauck and Lelgemann, 1984	$k_n^q = n$	q=0.5
Pole (point mass)	Krarup, 1969	$k_n^q = 1$	q=1
Finite radial straight lines with the density $\nu = r^{A-1}$			
A=0	Moritz, 1980	$k_n^q = 1/n$	q=1.5
A=1	Hauck and Lelgemann, 1984	$k_n^q = 1/(n+1)$	q=1.5
A=0, A=-1	Tscherning, 1972	$k_n^q = 1/n(n-1)$	q=2
A=-1, A=-2	Lauritzen, 1973	$k_n^q = 1/(n-1)(n-2)$	q=2
A=-1, A=-2, A=+B	Tscherning and Rapp, 1974	$k_n^q = 1/(n-1)(n-2)(n+B)$	q=2.5

$$\nu(r) = \rho(r) \cdot 4\pi \cdot r^2 \quad . \tag{21}$$

For a constant volume density contrast $\rho = \text{const}$, we have to use as corresponding line density distribution

$$\nu(r) = C \cdot r^2 \qquad \text{with} \qquad C = 4 \cdot \pi \cdot \rho \quad . \tag{22}$$

that is, a reproducing kernel of the form (A = +2) and a kernel depending on the length of the vertical column, that is

$$K(\psi, \sigma_1, \sigma_2) = K(\psi, \sigma_2) - K(\psi, \sigma_1) = K(\psi, (r_2 / r_P)) - K(\psi, (r_1 / r_P)) \quad , \tag{23}$$

where r_2 and r_1 are the radii of the upper and lower end of the columns, respectively.

There is a close connection to Darwin's density law (1884)

$$\rho(r) = \rho_0 \cdot \left(\frac{R}{r}\right)^n , \tag{24}$$

if such a kind of density law will be used for describing a hydrostatic Earth model to provide the necessary „normal potential". Finally comparison of (24) with (21) leads to a relation between Darwin's value **n** and the parameter **A** of the „line" reproducing kernels:

$$A = 3 - n \quad . \tag{25}$$

Conclusion.

Reproducing kernels for the solution of the problems of physical geodesy can be described by singularity harmonic functions and have the remarkable division onto two parts.

1. If $(0 \le q \le 1)$ the reproducing kernels are described by singular point harmonic functions from zero up to second degree.
2. If $(1.5 \le q \le 2.5)$ the kernel function of can be interpreted by special combinations of line harmonic functions with different laws of line density distribution for the finite segment.

The asymptotic, which corresponds to the reproducing kernel $K^q(P,Q)$ with $q \ge 3 / 2$ (well-known in the physical geodesy), is in agreement with G. Darwin's law of density.

References

Darwin, G. (1884) On the figure of equilibrium of a planet of heterogeneous density. *Proceeding of the Royal Society*, Vol. XXXVI, 158-166.

Hauck, H., and Lelgemann, D. (1984) Regional Gravity Field Approximation with Buried Masses Using Least-Norm Collocation. *Manuscripta Geodaetica*, Vol. 10, 50-58.

Krarup, T. (1969) A Contribution to the Mathematical Foundation of Physical Geodesy. *Danish Geod. Inst. Public.*, No 44, Copenhagen.

Lauritzen, S. (1973) The Probabilistic Background of some Statistical Methods in Physical Geodesy. *Danish Geod. Inst. Public.*, No 48, Copenhagen.

Marchenko, A. (1987) Description of the Earth's gravity field by the system of potentials of non-central multipoles. I. Theoretical backgrounds; II. Preliminary multipole analysis. *Kinematics and Physics of Celestial Bodies*, Kiev, Vol.3, No 2, 54-62; Vol.3, No 3, 38-44 (in Russian).

Moritz, H. (1980) *Advanced Physical Geodesy*, Wichmann, Karlsruhe, 1980.

Tscherning, C. C. (1972) Representation of covariance function related to the anomalous potential of the Earth's using reproducing kernels. *Danish Geod. Institute Internal Report*, No 3, Copenhagen.

Tscherning, C.C., and Rapp, R. (1974) Closed covariance expressions for gravity anomalies, geoid undulations, and deflections of vertical implied by anomaly degree variance models. *Dep. of Geod. Sci., Ohio State Univ.*, Rep. No 208, Columbus.

ON THE DIFFERENCE BETWEEN QUASI-GEOID HEIGHT AND GEOID UNDULATION*)

Marian Ivan

University of Bucharest, Geophysical Department, 6 Traian VUIA str.,

70138 Bucharest o.p.37, Romania

phone/fax: 40 1 211 31 20, e-mail: ivam@gg.unibuc.ro

---

*) Partially presented at the 2^{nd} *Joint Symposium of IGC and IGeC*, Trieste, Italy, 7-12 September 1998

Abstract

The difference between the quasi-geoid heights and geoid undulations is analyzed in detail with respect to the classical formula, an application along a meridian crossing the Romanian Carpathian Mountains being presented.

A geometrical surface which is closer to the geoid than the quasi-geoid is defined.

Key words: quasi-geoid, geoid, difference, topographic potential

Introduction

The difference between quasi-geoid height and geoid undulation (Heiskanen and Moritz 1967) presents a particular interest for most East-European countries. Here, quasi-geoids rather then geoids have been computed in the last decades, basically following the Molodenski's approach (e.g. Pick, Picha and Vyskočil 1973). A particular case is represented by the Romanian territory, where an astro-gravimetric quasi-geoid has been derived (Dragomir et al 1977). In this paper, the difference between quasi-

geoid height and geoid undulation is discussed, by considering a general model of the Earth. An application to the area of the Romanian Carpathian Mountains, involving variations of elevations up to $1600m$ and an amplitude of the Bouguer anomaly up to $-130mGals$ is presented.

Theoretical background

General remarks.—

In the most general case, the Earth can be regarded as a superposition of the reference equipotential ellipsoid, of the homogeneous relief and of the mass inhomogeneities (sources of the Bouguer anomalies)(Fig.1), the potential at a certain point being consequently the sum of three terms. By using a Bruns'like formula (e.g. Ivan and Sevilla 1998), the quasi-geoid height has the explicit equation

$$N(S_0) = \frac{V_B(S) + V_T(S)}{\gamma_0} \tag{1}$$

The implicit equation of the geoid undulation (e.g. Hipkin 1988; Ivan 1996) is

$$\zeta(S_0) = \frac{V_B(P) + V_T(P)}{\gamma_0}. \tag{2}$$

Here, S is the observation point located on the topographic surface, having the projection on the reference ellipsoid denoted by S_0, and P is located on the geoid. The term denoted by V_B in eqs.(1) and (2) is the Bouguer anomalous potential, corresponding to density inhomogeneities placed inside the relief or into the reference ellipsoid. The term denoted by V_T is the potential of the homogeneous relief of the whole Earth (see Appendix B), having the lower bound represented by the reference ellipsoid (sphere). The upper bound is the topography. Its (Bouguer, normal) density is denoted by δ^*, usually $\delta^* = 2670kg/m^3$. The normal gravity at S_0 is γ_0. Using eqs.(1) and (2), it

follows that

$$N(S_0) - \zeta(S_0) = \frac{V_B(S) - V_B(P)}{\gamma_0} + \frac{V_T(S) - V_T(P)}{\gamma_0}. \tag{3}$$

The difference between the plumb line and the ellipsoidal normal is assumed to be a second order effect (e.g. Hipkin 1988). Consequently, it will be ignored here. Also, the spherical approximation of the reference ellipsoid will be used for simplicity. Hence the difference between the quasi-geoid height and the geoid undulation is represented by the sum of two terms. The first one represents the effect of the density inhomogeneities (Bouguer anomalous sources) placed inside the reference ellipsoid or inside the relief . It can be evaluated as

$$\Delta_B = \frac{V_B(S) - V_B(P)}{\gamma_0} = -\frac{\Delta g(M)}{\gamma_0} H, \tag{4}$$

where H is the orthometric height of the point S and M is a mean point somewhere located between S and P. Following Heiskanen and Moritz (1967), that term is approximated by

$$\Delta_B \approx -\frac{\Delta g(S)}{\gamma_0} H. \tag{5}$$

It should be outlined that Δg in (4) or (5) is a theoretical Bouguer anomaly (Naudy and Neumann 1965). Hence

$$\Delta g(S) = g - \left[\gamma_0 - \frac{\partial \gamma_0}{\partial h}(H + \zeta) + g^T_{H+\zeta}\right], \tag{6}$$

where g is the observed value, $\partial\gamma_0/\partial h$ is the vertical gradient of the normal gravity and $g^T_{H+\zeta}$ is the vertical component of the gravitational attraction due to the homogeneous relief bounded by the exact topographical surface of the whole Earth and by the reference ellipsoid. However, in real life the approximation of the ellipsoidal height $H + \zeta$ by the orthometric height H ("elevation") is used to obtain the Bouguer anomaly. It follows that the quantity

$$\Delta g''_0(S) = g - \left[\gamma_0 - \frac{\partial \gamma_0}{\partial h} H + g^T_H\right], \tag{7}$$

is evaluated and regarded as "Bouguer anomaly". The usual truncation of the last term to a certain radius around the station (e.g. Talwani 1998) will be not considered here. From eqs.(6) and (7) it follows that

$$\Delta g(S) - \Delta g_0''(S) = \frac{\partial \gamma_0}{\partial h}\zeta - \left(g^T_{H+\zeta} - g^T_H\right), \tag{8}$$

i.e. the approximative value is obtained by ignoring the spherical effect

$$\Delta g(S) \approx \Delta g_0''(S) + \left(\frac{\partial \gamma_0}{\partial h} - 2\pi G\delta^*\right)\zeta, \tag{9}$$

where G is the gravitational constant.

Concluding, it follows the exact difference $N(S_0)-\zeta(S_0)$ between quasi-geoid height and geoid undulation is related to the same value $[N(S_0) - \zeta(S_0)]^{H-M}$predicted by Heiskanen and Moritz (1967) by

$$N(S_0) - \zeta(S_0) = [N(S_0) - \zeta(S_0)]^{H-M} + \Delta_T + \varepsilon_B, \tag{10}$$

where

$$\Delta_T = \frac{V_T(S) - V_T(P)}{\gamma_0} \tag{11}$$

is a term related to the potential of the homogeneous relief and

$$\varepsilon_B = \frac{V_B(S) - V_B(P)}{\gamma_0} + \frac{\Delta g(S)}{\gamma_0}H \tag{12}$$

is a correction related to the mass inhomogeneities inside Earth.

A theoretical bound on the relief term.—

Consider now the term defined by (11). Let h_M and h_m be the maximum, respectively the minimum ellipsoidal heights for the relief of the whole Earth (Fig.1). At a certain point (S or P), the volume integral representing the topographic potential can be divided in two parts

$$V_T = U + I \tag{13}$$

Using the results from Appendix A, the first term in (13) is evaluated on a spherical slab having the inner radius equal to $R_1 = R$, i.e. the radius of the reference ellipsoid (sphere). The outer radius of the slab is $R_2 = R + h_m$. It follows

$$U(S) - U(P) = u(R; R + h_m; R + H + \zeta) - u(R; R + h_m; R + \zeta), \tag{14}$$

where the function u is defined by eq.(28). The second term in (13) is evaluated on a domain D bounded by the spherical surface of radius equal to $R + h_m$ and by the topography. In absolute value, it follows

$$|I(S) - I(P)| = G\delta^* \left| \iiint_D \left(\frac{1}{QS} - \frac{1}{QP} \right) dv \right|, \tag{15}$$

where dv is the volume element at the current point denoted by Q. But

$$|QS - QP| \leq H, \tag{16}$$

and

$$\frac{1}{QS}\frac{1}{QP} \leq \frac{1}{2}\left(\frac{1}{QS^2} + \frac{1}{QP^2} \right) \tag{17}$$

It follows that

$$|I(S) - I(P)| \leq \frac{G\delta^* H}{2} \iiint_D \left(\frac{dv}{QS^2} + \frac{dv}{QP^2} \right) \leq \frac{G\delta^* H}{2} \iiint_{\sum} \left(\frac{dv}{QS^2} + \frac{dv}{QP^2} \right), \tag{18}$$

where $\sum$ is the spherical slab having the inner/outer radii equal to $R_1 = R + h_m$ and $R_2 = R + h_M$ respectively. The volume integrals at the right hand of (18) are evaluated in Appendix A. Hence

$$|I(S) - I(P)| \leq \frac{G\delta^* H}{2} \left[i(R + h_m; R + h_M; R + H + \zeta) + i(R + h_m; R + h_M; R + \zeta) \right], \tag{19}$$

where the function i is defined by eq.(31). From (3), (5), (9), (13), (14) and (19) the next bound is obtained for the difference between the quasi-geoid height and the geoid undulation

$$|N(S_0) - \zeta(S_0) + A| \leq C, \tag{20}$$

where

$$A = \left[\Delta g_0''(S) + \left(\frac{\partial \gamma_0}{\partial h} - 2\pi G\delta^*\right)\zeta\right]\frac{H}{\gamma_0} - B, \tag{21}$$

$$B = \frac{1}{\gamma_0}\left[u(R; R+h_m; R+H+\zeta) - u(R; R+h_m; R+\zeta)\right], \tag{22}$$

and

$$C = \frac{G\delta^* H}{2\gamma_0}\left[i(R+h_m; R+h_M; R+H+\zeta) + i(R+h_m; R+h_M; R+\zeta)\right]. \tag{23}$$

Application to a part of the Romanian territory

The difference

$$\Delta_T \approx \frac{V_T(S) - V_T(S_0)}{\gamma_0} \tag{24}$$

has been evaluated for 31 points placed along the meridian of longitude equal to $24°33'45"E$, between the latitudes $43°47'30"N$ and $46°17'30"N$, the sampling interval being of approximate $10km$. The $4 \times 4km$ DTM produced by University of Leeds in the trapezoid of longitudes $18.55° \div 30.55°E$ and latitudes $40.30° \div 49.30°N$ has been used with a polyhedral approximation of the relief (Ivan 1996). The results are plotted in Fig.2. They show a maximum error of $-18mm$ corresponding to the point having the maximum (mean) elevation of $1664m$. The density of the homogeneous relief is $2670kg/m^3$ and the normal gravity is $\gamma_0 = 9.80708m/s^2$. By approximating the orthometric heights by the corresponding elevations, the results of Heiskanen and Moritz (1967) eq.(5)along the same profile show a maximum value of $103mm$, located at $20km$ South with respect to the point of maximum elevation.

By using the same approximation, the correction

$$\varepsilon_B \approx \frac{V_B(S) - V_B(S_0)}{\gamma_0} + \frac{\Delta g(S)}{\gamma_0} H(S) \tag{25}$$

has been also evaluated by using a $2.5D$ forward modelling of the geological structure above Moho discontinuity. If the pairs of the computed gravity field values at the ends

of the profile are ignored, a rms error of $3.55mGals$ is obtained. Details are presented by Ivan (1997). The values of the correction represented by (25) are plotted too in Fig.2, showing values between $-17 \div 20mm$. In this case, the sum of (24) and (25) has a maximum amplitude of $-18mm$.

Conclusions

The difference between the quasi-geoid height and the geoid undulation at a certain point is both the result of the density inhomogeneities placed inside the Earth (i.e. sources of the Bouguer anomalies) (Heiskanen and Moritz 1967) and of the topographic relief. The effect of the relief can be theoretically bounded, or evaluated by using a DTM. A further correction can be added to the formula of Heiskanen and Moritz (1967), but it asks a forward modelling of the sources of the Bouguer anomalies. In the case of a rough relief, like the Carpathian area, these corrections are important with respect to a centimeter geoid.

It should be outlined too that the above presented approach, which is based on the Bouguer anomaly rather than on the free-air one, allows one to define a geometrical surface ("peri-geoid")which is closer to the geoid than the quasi-geoid, by the equation

$$\mu(S_0) = \frac{V_B(S) + V_T(S_0)}{\gamma_0} \tag{26}$$

In the usual spherical approximation, eq.(2) becomes

$$\zeta(S_0) = \frac{V_B(S_0) + V_T(S_0)}{\gamma_0}, \tag{27}$$

Clear, in real cases, eq.(26) is closer to eq.(27) than eq.(1).

Appendix A. Potential of a spherical slab. A volume integral.

Consider a spherical slab having the inner radius equal to R_1. The outer radius is R_2, with $R_1 < R_2$. The gravitational potential of the slab at a certain point placed

at a distance r from its centre is (e.g.Kittel et al 1973)

$$u(R_1;R_2;r)=\begin{cases} 2\pi G\delta^*\left(R_2^2-R_1^2\right)\,,\ for \quad 0\le r<R_1 \\ 4\pi/3G\delta^*\left(3R_2^2/2-r^2/2-R_1^3/r\right)\,,\ for \quad R_1\le r<R_2 \\ 4\pi/3G\delta^*\left(R_2^3-R_1^3\right)/r\,,\ for \quad R_2\le r \end{cases} \tag{28}$$

The next integral follows to be evaluated on the volume represented by the above spherical slab at a point placed at a distance $d>0$ from the centre of the sphere

$$i(R_1;R_2;d)=\iiint\limits_{\Sigma}\frac{dv}{QS^2}=\int\limits_0^{2\pi}\int\limits_0^{\pi}\int\limits_{R_1}^{R_2}\frac{r^2\sin\theta d\varphi d\theta dr}{r^2-2rd\cos\theta+d^2}. \tag{29}$$

Hence

$$i(R_1;R_2;d)=\frac{\pi}{d}\left[\int\limits_{R_1}^{R_2}r\ln\left(r+d\right)^2dr-\int\limits_{R_1}^{R_2}r\ln\left(r-d\right)^2dr\right] \tag{30}$$

By using some elementary integrals (e.g. Smoleanski 1967), it follows for $d>0$ that

$$\begin{aligned} i(R_1;R_2;d) \;=\; & 2\pi(R_2-R_1)+\frac{\pi}{d}\left[(R_2-d)L(R_2+d)-(R_2+d)L(R_2-d)\right. \\ & \left.+(R_1+d)L(R_1-d)-(R_1-d)L(R_1+d)\right], \end{aligned} \tag{31}$$

where

$$L(x)=\begin{cases} x\ln|x| \quad ,for \quad x\neq 0 \\ 0 \quad ,for \quad x=0 \end{cases}. \tag{32}$$

Appendix B. The topographic potential.

The potential due to a homogeneous relief can be obtained by numeric integration over the vertical coordinate (Hipkin 1988). A formula approximating the relief by a polyhedral surface is presented by Ivan (1996). It is especially useful at short distances from the computation point. If eq.(3) is to be used, a formula is necessary too in order to obtain the effect due to the topography placed at great distances. For such cases, an approximation of the relief by a spherical prism is useful. Consider

the spherical coordinate system (r, θ, λ). Here, θ is the geocentric colatitude and λ is the longitude. The computation point S is placed at the Northern pole, having the spherical coordinates equal to $(D, 0, 0)$. A spherical prism is the volume defined here by

$$\begin{aligned} R &\leq r \leq R+h, \\ \theta_N &\leq \theta \leq \theta_S, \\ \lambda_W &\leq \lambda \leq \lambda_E \end{aligned} \tag{33}$$

It follows the potential is

$$V(S) = G\delta^* \int_R^{R+h} \int_{\theta_N}^{\theta_S} \int_{\lambda_W}^{\lambda_E} \frac{r^2 \sin\theta dr d\theta d\lambda}{\sqrt{r^2 - 2rD\cos\theta + D^2}} \tag{34}$$

Hence

$$V(S) = G\delta^* \frac{\lambda_E - \lambda_W}{D} \int_R^{R+h} r \left[\sqrt{(r - D\cos\theta)^2 + (D\sin\theta)^2}\right]\Big|_{\theta_N}^{\theta_S} dr \tag{35}$$

Using (Smoleanski 1967) it follows that

$$\begin{aligned} V(S) \;=\; & G\delta^* (\lambda_E - \lambda_W) \Big\{ (r^2 - 2rD\cos\theta + D^2)^{3/2}/(3D) \\ & + \cos\theta \left[D^2 \sin^2\theta \ln\left(r - D\cos\theta + \sqrt{r^2 - 2rD\cos\theta + D^2}\right) \right. \\ & \left. + (r - D\cos\theta)\sqrt{r^2 - 2rD\cos\theta + D^2} \right] /2 \Big\} \Big|_{\theta_N}^{\theta_S} \Big|_R^{R+h} \end{aligned} \tag{36}$$

The logarithm in (36) presents a singularity when θ_S, θ_N have the values 0 or π and D is equal to R or to $R+h$. Because of the sine function multiplying the logarithm, that weak singularity can be removed in a similar way to (32). No rounding errors (Holstein and Ketteridge 1996) have been observed in (36) for spherical prisms of various dimensions placed at arbitrary locations with respect to the computation point.

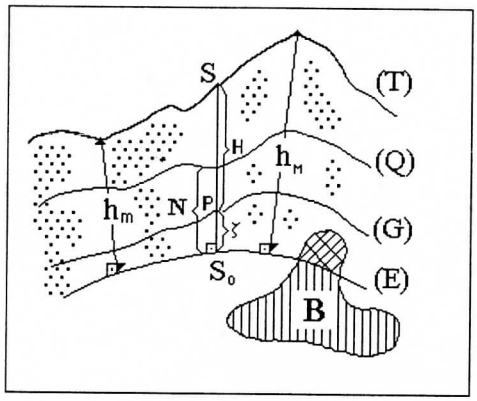

FIG. 1.

Fig.1. A model of the Earth, regarded as the superposition of the reference ellipsoid (E), of the homogenous relief and of the mass inhomogeneities (B). The topographic surface is denoted by (T), (Q) is the quasi-geoid and (G) is the geoid. A station S has the projection on (E) denoted by S_0. Its orthometric height is H, the undulation of the geoid is ζ and the quasi-geoid height is N. The maximum and minimum ellipsoidal heights for the relief of the whole Earth are h_M and h_m respectively.

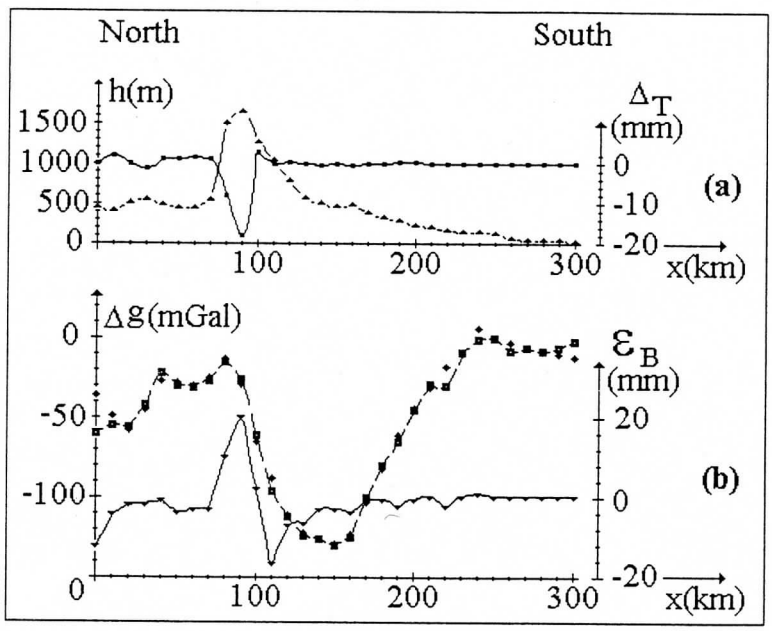

FIG. 2.

Fig.2. A profile crossing the Southern Carpathians. (a) The dashed line (with triangular points) shows the elevations. The solid line represents the effect due to the homogeneous topographic relief Δ_T. (b) The dashed line (with square points) represents the observed Bouguer anomaly. The diamonds are the computed values corresponding to a model of the geological structure above Moho discontinuity. The solid line shows the correction ε_B to the effect due to the mass inhomogeneities.

References

Dragomir V, Ghitău D, Mihăilescu M, Rotaru M (1977) The Theory of Earth's Shape (in Romanian), Technical Publishing House, Bucharest

Heiskanen WA, Moritz H (1967) Physical Geodesy, Freeman, San Francisco

Hipkin RG (1988) Bouguer anomalies and the geoid: a reassessment of Stokes' method. Geophysical J 92:53-66

Holstein H, Ketteridge B (1996) Gravimetric analysis of uniform polyhedra. Geophysics 61:357-364

Ivan M (1996) Polyhedral approximations in physical geodesy. J Geodesy 70:755-767

Ivan M (1997) Algorithm for computing the flexure of the crust, Rev. roum. GEOPHYSIQUE, in press

Ivan M, Sevilla MJ (1998) Local quasi-geoid and downward continuation by integrating harmonic series. Application to Dobrudja area - Romania, presented at the Second Continental Workshop on the geoid in Europe, Budapest, Hungary, March 10-14, 1998

Kittel C, Knight WD, Ruderman MA (1973) Berkeley Physics Course, v.1, Mechanics, Mc Graw-Hill, Inc., N.Y.

Naudy H, Neumann R (1965) Sur la definition de l'anomalie de Bouguer et ses consequences pratiques. Geophysical Prospecting 13:1-11

Pick M, Picha J, Vyskočil V (1973) Theory of the Earth's Gravity Field, Academia, Prague

Smoleanski ML (1967) Tables of indefinite integrals (in Russian). Nauka, Moscow

Talwani M, (1998) Errors in the total Bouguer reduction. Geophysics 63:1125-1130

African Regional Gravimetric Geoid 1997: Stokesian Approach

Hassan. H. Fashir* , A. Majid. A. Kadir
Centre For Geodetic and Geodynamics Studies, Faculty of Geoinformation Science and Engineering,
University of Technology Malaysia, Locked Bag 791, 80990 Johor Bahru
Johor, Malaysia
e-mail fashir@mailcity.com

Abstract

A new regional co-geoid has been computed for the whole of Africa, ranging from 35^0 S to 40^0 N in Latitude and 20^0 W to 50^0 E in Longitude. The EGM96 geopotential model truncated to degree and order 70 was combined with surface gravity data and modified Stokes's Kernel to generate the geoid file. The surface data consists of 1^0 x 1^0, 30' x 30' mean gravity anomalies and 30'x 30' topographic information. Comparison of the gravimetric geoid with the Doppler/ levelling derived geoidal heights of 92 stations all over Africa shows that the absolute agreement with respect to the Doppler/ levelling datum is generally better than 1.85m RMS. Other geoids, such as OSU91A and EGM96 complete to degree and order 360 were also included in the comparison, showing that the new gravimetric geoid achieves the best agreement with the Doppler/ levelling data.

1. Introduction

The determination of the geoid has been one of the prime objectives of geodesy. The knowledge of the geoid with respect to some reference ellipsoid, either on a global or local scale is valuable to geodesy, surveying and geophysics for a number of purposes such as the reduction of measured distances to a reference surface and the processing of satellite observations. The geoid represents the datum to which height differences and the gravity potentials are referred. Also its knowledge is useful for verification of global vertical datum.

The lack of gravity measurement over much of the earth surface is still the major problem in gravimetric geodesy. Many well known algorithms exist to compute geoid undulation from surface gravity data, namely, Stokes's integration, Fast-Fourier Transform (FFT) and Least Squares Collocation (LSC). The combination of spherical harmonics potential coefficient set with terrestrial gravity data in order to reduce the latter requirement to a localised region for geoid height computation has been considered in this investigation. A modified spheroidal Stokes's Kernel $S_{70}(\psi)$ is used in the computation instead of the conventional ellipsoidal Stokes's Kernel $S(\psi)$. It is found that spheroidal function tapers off more rapidly than the ellipsoidal function for increasing spherical distances. Thus we can expect that a truncation of the spheroidal (modified) integration at a certain spherical

* On Sabbatical leave, Dept. of Surveying Engineering, Faculty of Engineering, University of Khartoum, Sudan

distance leads to smaller truncation errors compared to the truncation of the ellipsoidal (original) Stokes's integration.

2. Mathematical Models

As is well known, the geoidal height N, at any point of geographical co-ordinates (ϕ,λ) can be computed from a surface integral derived by Stokes in 1949 as:

$$N(\phi,\lambda) = \frac{R}{4\pi\gamma}\iint_{\sigma}\Delta g S(\psi)\,d\sigma \qquad (1)$$

where:

R : mean radius of the earth;

γ : mean value of gravity over the earth;

Δg : free air gravity anomaly;

$S(\psi)$: original Stokes's Kernel

$d\sigma$: surface element

In this paper a procedure to obtain the geoid over the whole African continent is based on the combination of spherical harmonics potential coefficient set with terrestrial gravity data. The final formulae to compute gravimetric geoid heights were given in [1] as follows:

$$N = N^S + N^C + \Delta N \qquad (2)$$

Where,

N^S : long wavelength component

N^C : short wavelength component

ΔN : is the Truncation error

$$N^S = R\sum_{n=2}^{L}\sum_{m=0}^{N}\left[\overline{C}^*_{nm}\cos m\lambda + \overline{S}^*_{nm}\sin m\lambda\right]\overline{P}_{nm}(\sin\overline{\phi}) \qquad (3)$$

$$N^C = \frac{R}{4\pi\gamma}\iint_{\sigma_c} S_L^m(\psi)\Delta g^L\,d\sigma \qquad (4)$$

$$\Delta N = \frac{R}{2\gamma}\sum_{N=2}^{L}\Delta g_N \overset{m}{Q}_n^{l}(\psi_o) \qquad (5)$$

where;

$S_L^m(\psi)$: the modified Stokes's kernel

$\overset{m\ L}{Q}_n(\psi_0)$: truncation coefficient associated with the modified stokes's kernel

L : the degree of the spheroid

$\overline{C}^*_{n,m}, \overline{S}^*_{n,m}$: are the fully normalised potential coefficients

$\bar{\phi}$: geocentric latitude

λ : geocentric longitude

$\overline{P}_{nm}(\sin\bar{\phi})$: associated Legendre function

Δg^L : residual gravity anomaly

Δg_n : Laplace's surface harmonic of degree n

with:

$$\Delta g^L = \Delta g - \Delta g^S \qquad (6)$$

$$\Delta g^S = \gamma\sum_{n=2}^{L}(n-1)\sum_{m=0}^{N}\left[\overline{C}^*_{nm}\cos m\lambda + \overline{S}^*_{nm}\sin m\lambda\right]\overline{P}_{nm}(\sin\bar{\phi}) \qquad (7)$$

$$S_L^m(\psi) = s(\psi) - \sum_{n=2}^{L}\frac{2n-1}{n-1}P_n(\cos\psi) - \sum\frac{2k+1}{2}T_k(\psi_0)P_k(\cos\psi) \qquad (8)$$

$$S(\psi) = \cos ec\frac{\psi}{2} - 6\sin\frac{\psi}{2} + 1 - 5\cos\psi - 3\cos\psi Log_e(\sin\frac{\psi}{2} + \sin^2\frac{\psi}{2}) \qquad (9)$$

where,

Δg : the gravity anomaly

Δg^s : the long wavelength gravity component from spherical harmonics

$P_n(\cos\psi)$: Legendre polynomial of degree n

$T_k(\psi)$: modifying truncation coefficients

The coefficients $T_K(\psi_0)$ are solved for from the system of linear equations:

$$\sum_{k=0}^{L} \frac{2k+1}{2} e_{nk}(\psi_0) T_k(\psi_0) = Q_n^L(\psi_0) \qquad (10)$$

with:

$$e_{nk}(\psi_0) = \int_{\psi=\psi_0}^{\Pi} P_n(\cos\psi) P_k(\cos\psi) \sin\psi d\psi \qquad (11)$$

$$Q_n^L(\psi_0) = Q_n(\psi_0) - \sum_{k=2}^{L} \frac{2k+1}{k-1} e_{nk}(\psi_0) \qquad (12)$$

$$Q_n^{mL}(\psi_0) = Q_n^L(\psi_0) - \sum_{k=0}^{L} \frac{2k+1}{2} T_k(\psi_0) \qquad (13)$$

$$Q_n(\psi_0) = \int_{\psi=\psi_0}^{\Pi} s(\psi) P_n(\cos\psi) \sin\psi d\psi \qquad (14)$$

where,

$Q_n(\cos\psi)$: original Molodenskii truncation coefficients

$Q_n^L(\cos\psi)$: spheroidal Molodenskii type truncation coefficients

σ_C : spherical cap from the computation point

3. Data Used In The Computations

3.1 The 1^0 x 1^0 (NIMA) Terrestrial Gravity Anomaly Data

The original mean gravity anomaly data were provided by the National Imagery and Mapping Agency (NIMA), the former Defense Mapping Agency (DMA). This data set is termed 1^0 x 1^0 mean anomalies from surface and airborne data [2]. In this study only data from the region 45^0 S to 50^0 N, and from 30^0 W to 60^0 E are used. The original data file contains 5401 records in that region and has 3335 1^0 x 1^0, cells with no information. Each record contains 11 pieces of information, namely, Latitude (centre of cells), Longitude (centre of cell), mean elevation , number of points used to estimate mean gravity anomaly, mean free-air gravity anomaly, standard deviation of mean free-air gravity anomaly, code of method of evaluation, code of source, code of type, number of (NIMA) 30' gravity anomalies used to estimate 1^0 mean gravity anomaly and number of Ohio State University (OSU) 30' mean gravity anomalies used to estimate mean 1^0 gravity anomaly. The anomalies refer to WGS-84 horizontal datum. Anomalies are corrected for the effect of atmosphere. The orthometric heights used for the compilation of the gravity anomaly database are derived from the JGP95E global topographic database.

3.2 The 30' x 30' (NIMA) Terrestrial Mean Free-Air Gravity Anomaly Data

These data originate from NIMA. This data set is termed the 30' mean terrestrial gravity anomalies from surface and airborne data [2]. In this study only data from the region 37^0 S to 43^0 N, and from 22^0 W to 58^0 E are used. The original data set contains 12344 records in that region. Each record contains 9 pieces of information. This information is identical to the first 9 pieces of the information of the 1^0 x 1^0 mean anomaly data set. Also the anomalies are referred to WGS-84 horizontal datum. The anomalies are corrected for the effect of atmosphere. The orthometric heights used for the compilation of gravity anomaly database are derived from JGP95E global topographic database.

30' x 30' (NIMA) Altimetric Mean Free-Air Gravity Anomaly Data

This data set originates from NIMA. This data set is termed the 30' mean gravity anomalies derived from satellite altimeter data [2]. In this study only data from the region 37^0 S to 43^0 N, and from 22^0 W to 58^0 E are used. The original data set contains 12257 records in that region. Each record contains 9 pieces of information identical to that of the 30' x 30' (NIMA) terrestrial mean free-air gravity anomaly data. Anomalies are referred to WGS-84 horizontal datum and corrected for atmospheric effect. The orthometric heights used for the compilation of gravity anomaly database are derived from JGP95E global topographic database.

3.4 30' x 30' (OSU) Terrestrial Mean Anomalies

These data set originate from Ohio State University. This data set is termed the 30' x 30' terrestrial mean free-air anomaly database [3]. The original data set contains 7497 records in the area of interest 37^0 S to 43^0 N and 22^0 W to 58^0 E. Each records contains 9 pieces of information identical to those of the 30' x 30' terrestrial mean anomaly data. Gravity anomalies are referred to WGS-84 datum. These anomalies were corrected for atmospheric effect.

3.5 Spherical Harmonics Quasi-Geoid to Geoid Correction Coefficient Set

These data set were provided in terms of correction coefficients [4]. Using OSU91A potential coefficient set together with 30' elevation data a degree 360 representation of the correction terms were computed in [4].The corrections are used to convert height anomaly(ζ) into geoid height (N). The magnitude of (N-ζ) reached -3.4 m in the Himalaya Mountains with smaller but still significant, magnitudes in other mountainous regions [4]. The conversion of the height anomaly to a geoid undulation is described in Heiskanen and Moritz [5] as:

$$N(\phi,\lambda) = \zeta(\phi,\lambda,r) + \frac{\Delta g_B}{\bar{\gamma}} H \qquad (15)$$

where;

Δg_B : Bouguer anomaly

$\bar{\gamma}$: average value of normal gravity

H : orthometric height

ζ : the height anomaly

Equation (15) was developed further by [4] to read:

$$N(\phi,\lambda) = \zeta(\phi,\lambda,r) + C_1(\phi,\lambda) + C_2(\phi,\lambda) \qquad (16)$$

with;

$$C_1(\phi,\lambda) = \frac{d\xi}{dr} H + \frac{d\xi}{dr}\frac{d\gamma}{dh} H \qquad (17)$$

$$C_2(\phi,\lambda) = \frac{\Delta g}{\bar{\gamma}} H \qquad (18)$$

The C_1 and C_2 terms were expanded [4] in spherical harmonics using OSU 91A model and the 30' x 30' topographic data. Finally the sum of C_1 and C_2 of equation (16) is computed. As it seems from equations (17) and (18) , the C_1 terms represents a height anomaly gradient term, that computes the difference between a height anomaly like value on the station.The C_2 term represents the difference between the geoid undulation and height anomaly, this term depends on the Bouguer anomaly and the elevation of the station.

3.6 EGM96 Geopotential Model Coefficients

The NASA Goddard Space Flight Centre, The National Imagery and Mapping Agency (NIMA; formally the Defense Mapping Agency or DMA) and the Ohio Sate University (OSU) have collaborated to produce EGM96, an improved degree 360 spherical harmonic model representing the earth gravitational potential. This model was developed using terrestrial, airborne and altimetry data together with satellite tracking data from more than 20 satellites, including new data from GPS and TDRSS, as well as altimeter data from TOPEX, GEOSAT and ERS-1. The final model, EGM 96, is a composite solution, It consists of a combination solution to degree and order 70, a block diagonal solution from degree 71 to 359, and a quadrature solution at degree 360.

The truncated EGM96 (70,70) coefficient set has been chosen out of the variety of potential field models published so far to compute the long wavelength geoid component. The truncated EGM96 model is complete to degree and order 70. This implies that the smallest gravity fields features represented in the truncated model have a spatial extent of 2.6^0 spherical distance or 288 km.

3.7 Gravity Anomaly Data for Computation

For the 1^0 x 1^0 anomaly data file, in our case we are interested in the area 45^0 S to 50^0 N and 30^0 W to 60^0 E, with a total of 8736 1^0 x 1^0 blocks. Almost 30% of these blocks were empty. Hence using the 30' x 30' files of sections,3.2,3.3 and 3.4,we predicted 24% of the missing data by simple averaging. For the remaining 6% of the empty cells, EGM96 complete to degree and order 360 was used to fill in the empty blocks. For the 30' x 30' anomaly data, the required area lies between 37^0 S to 43^0 N and 22^0 W to 58^0 E. Merging the data set of sections 3.2, 3.3 and 3.4, we have created our 30' x 30' file. Also some empty cells were filled using EGM96 potential coefficient set complete to degree and order 360. One direct access file has been created for the 30' x 30' mean gravity anomaly data. The file is divided conceptually into nine 40^0 x40^0 blocks. Their boundaries are shown in Table 1.

Longitude Interval	Latitude Interval
22^0 W - 18^0 E	37^0 S - 3^0 N
2^0 W - 38^0 E	17^0 S - 23^0 N
18^0 E - 58^0 E	3^0 N - 43^0 N

Table 1. Boundaries of the 30' x 30' Mean Gravity Anomaly Files

Each block overlaps with the right and upper adjacent blocks by twenty degree. The records in each block are stored in the order of increasing Longitude for points of equal Latitude. Given the computation point (ϕ, λ), a specific subroutine can obtain the appropriate 40^0 x 40^0 block for the integration in the inner zone, and the south-western position of this block. As a result one can easily figure out the co-ordinates of each record from its position in the file.

All the 1^0 x 1^0 and 30' x 30' anomaly data refer to WGS-84 horizontal datum. Corresponding gravity anomalies implied by the Truncated EGM96 model up to degree and order 70 have been subtracted from the gravity anomaly data files to compute the gravimetric geoid.

4. Computation of The Gravimetric Geoid

4.1 Selection of optimal integration Cap Size (Ψ_0)

Before the final computations of the geoid heights, we had to decide upon the optimal integration spherical cap beyond which gravity contribution is negligible. To decide upon the selection of Ψ_0, the gravimetric geoid was computed for the whole of African continent on a grid of 2^0 in decimate rate. The integration cap size was varied from 2^o up to 8^o and the geoid heights at the above mentioned grid points were computed and it was found that geoid contribution from gravity data beyond cap size 8^0 is negligible(of the order of 1cm).

4.2 The Long wavelength Component of The Geoid (N^S)

A major step forward in geodesy and geophysics is the rapid progress in the determination of the shape of the earth and its gravity field from the satellite orbit analysis combined with terrestrial data to the global solutions expanded in the spherical harmonics up to degree 360. Better knowledge of the geopotential models has created dramatic advances in point positioning, in the study of the earth's kinematics and tectonics, in understanding the earth's rheology and interior and in the study of global oceanic process with space- borne instrumentations. These high degree expansions can be used to evaluate quantities such as geoid undulations, height anomalies, gravity anomalies, gravity disturbances and deflections of the vertical.

The long wavelength geoid component (N^S) was computed using equation (3) from the truncated EGM96 potential coefficient set complete to degree and order 70 and the parameters of the WGS-84 ellipsoid. Also together with these model coefficients are the associated quasi – geoid to geoid corrections developed in terms of spherical harmonics. Hence using these corrections the quasi-geoid was converted to the geoid. The geoid heights were computed on a grid defined by 35° S to 40° N and 20° W to 50° E. The grid decimation rate is 0.5°. A total of 21291 grid points were considered in the computation. The contoured geoid on WGS-84 ellipsoid is shown in fig 1. The contour interval is 2 m. From fig 1. The geoid slopes from a high of about 52 m in north Morocco to a low of about -46 m in Somalia. In general there is a south-easterly down slope of undulations.

4.3 The Residual (Short & Medium) Wavelength Component of The Geoid (N^c).

The residual geoid was recovered from the numerical integration of the modified Stokes's function using surface gravity data. Stokes's Integral of equation (1) is certainly one of the most famous formulae in physical geodesy. This formula requires integration of the gravity anomaly over whole earth. The lack of gravity coverage has led to a natural approximation, whereby the integration is limited to spherical cap (Truncation of the integral). In this investigation the residual geoid was computed from the numerical evaluation of the spheroidal Stokes's integration using modified Stokes's function. This function differs from the ellipsoidal Stokes's function of equation (1) by the fact that it lacks the low frequency part and it tapers off more rapidly. The original Stokes's kernel $S(\psi)$, the spheroidal Stokes's kernel of degree 70 $S_{70}(\psi)$ and the modified spheroidal Stokes's kernel $S_{70}(\psi)$ are shown in Fig. 2.

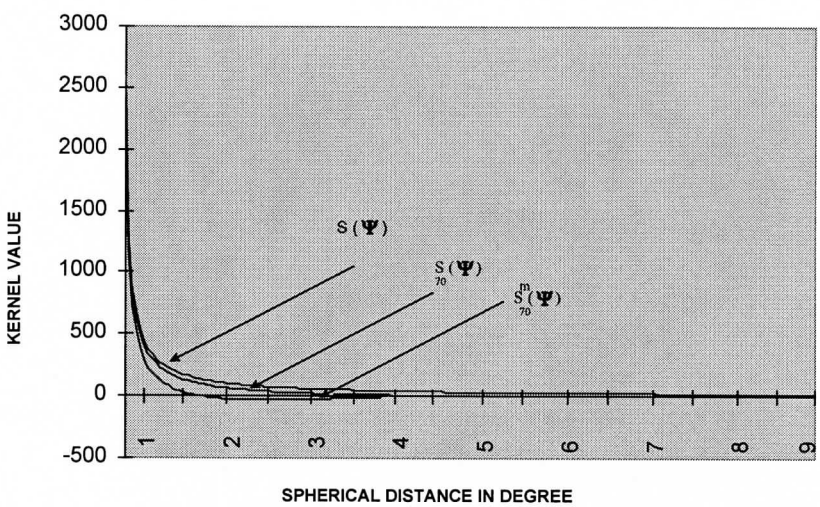

Fig 2. Different Stokes's Function

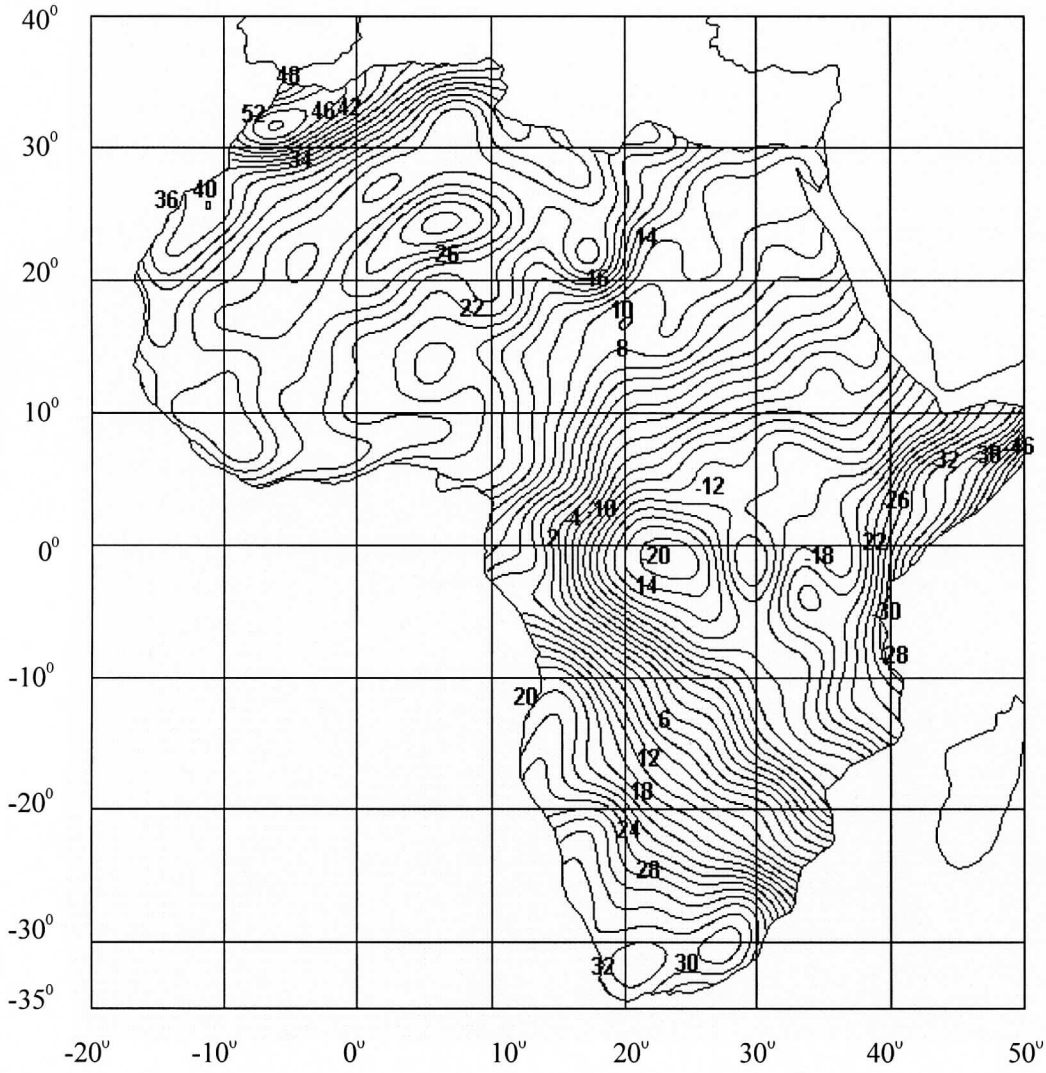

Fig. 1 The long wavelength geoid component(Nmax=70). Contour interval 2 m.

The spherical integration cap $\psi \leq \psi_0$ is approximated by one-degree square of ellipsoid co-ordinates ϕ, λ. The complete integration area, delineated by bold lines in Fig. 3 is divided into three main zones:

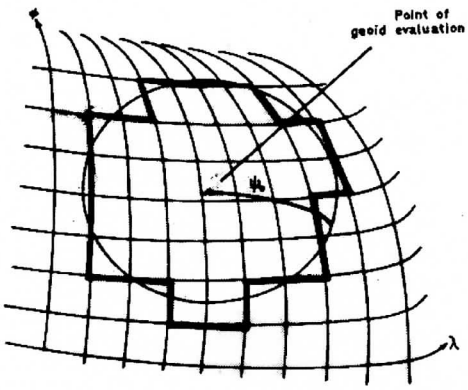

Fig 3. Approximation of spherical cap (ψ_0)

- **The innermost zone**

This covers the immediate neighbourhood of the point of geoid evaluation. The size of the innermost zone is 1^0 x 1^0. The boundaries of the innermost zone coincide with the grid division of the 30' x 30' gravity anomaly data file. The geoid contribution in this zone is computed from:

$$N_1 = \frac{R}{4\pi\gamma} \int_{x1}^{x2} \int_{y1}^{y2} S_L^m(\psi)\Delta g^L(x,y)dxdy \qquad (19)$$

with;

$$\psi = \sqrt{(x^2 + y^2)} \qquad (20)$$

$$\Delta g^L(x,y) = c_0 + c_1 x + c_2 y \qquad (21)$$

$$S_l^m(\psi) = 2/\psi - 3\ln(\psi/2) + M_L(\psi_O) \qquad (22)$$

$$M_L(\psi_O) = -\left[4 + \sum_{n=2}^{L} \frac{2n-1}{n-1} + \sum_{k=0}^{l} \frac{2k+1}{2} T_k(\psi_o)\right] \qquad (23)$$

At every time the four (30' x 30') gravity anomaly data around the computation point were considered in the integration, due to the fact that no point gravity anomalies were available in this investigation.

- **The Inner Zone**

This zone extends over an area of 2^0 x 2^0 minus the innermost zone. The boundaries of the innerzone coincide with the grid division of the 1^0 x 1^0 gravity anomaly data file. In this zone the geoid is computed using the twelve (30' x 30') gravity anomaly data in the inner zone. This is carried out as :

$$N_2 = \frac{a^2 R}{4\pi\gamma} \sum_{i=1}^{n} S_L^m(\psi_i) \cos\phi_i \Delta g_i^L \qquad (24)$$

where;

n : is the number of cells in the inner zone

a : is the cell size (10') in radians.

- **The Outer Zone**

This is the area between the boundaries of the inner zone and the integration area (8^0 spherical distance from the computation point). Also the geoid contribution in this zone is recovered as:

$$N_3 = \frac{b^2 R}{4\pi\gamma} \sum_{i=1}^{k} S_L^m(\psi_i) \cos\phi_i \Delta g_i^L \qquad (25)$$

with:

K : is the number of cells in the outer zone

b : is the cell size (30') in radians.

The subdivision of the integration area into three zones is a matter of convenience to allow for different integration technique and different data input in the integration. The summation of the integration results in the three zones resulted in the residual geoid. This residual geoid is contoured and shown in Fig. 4. The contour interval is 1.25 m. From Fig. 4 it is evident that the residual attains a maximum of 5 m. Finally, the co- geoid, the summation of the residual geoid , the long wavelength component and the truncation error is contoured in Fig. 5. The shape of the geoid with respect to WGS-84 ellipsoid are coincident approximately along a line joining latitude 16^0 N on the Sudanes Red Sea Coast. There is a general south-easterly slope of the geoid. The geoid slopes from a high of about 50 m in north Morocco to a low of -43 m in Somalia.

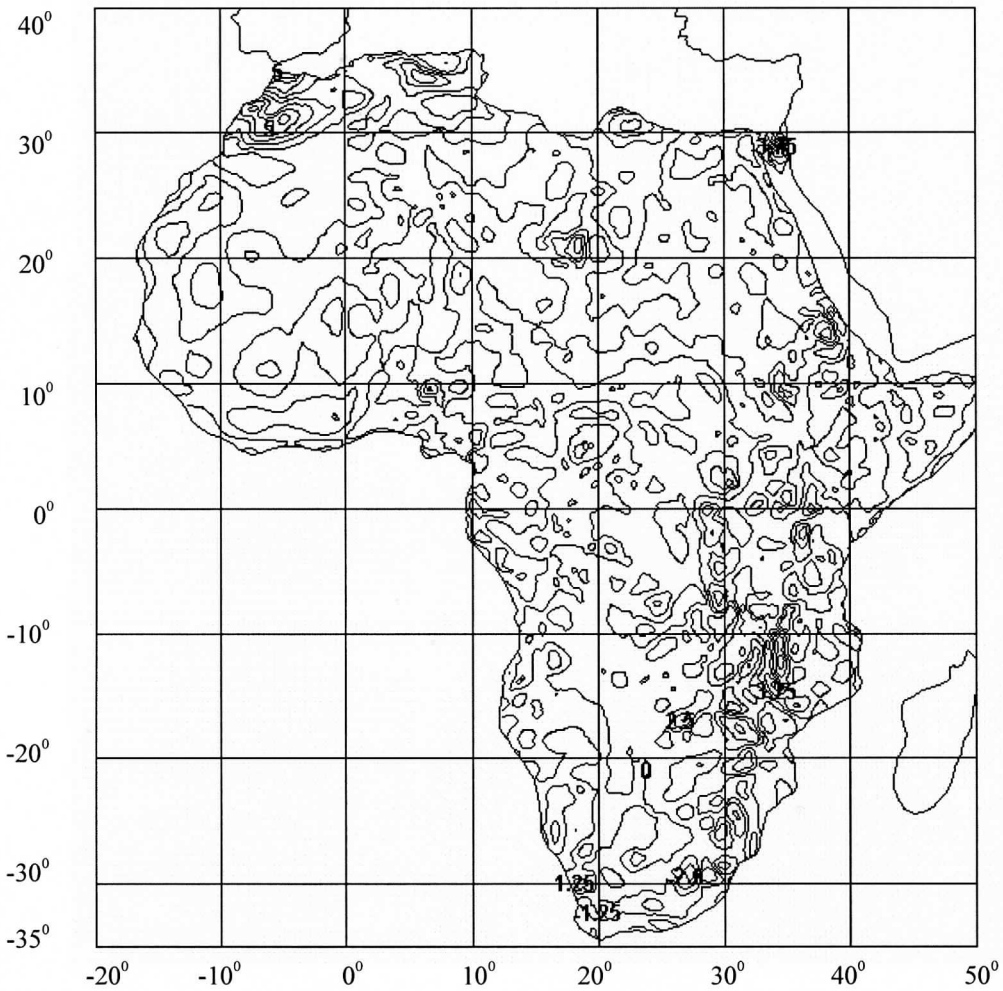

Fig. 4 The residual gravimetric geoid component. Contour interval 1.25 m

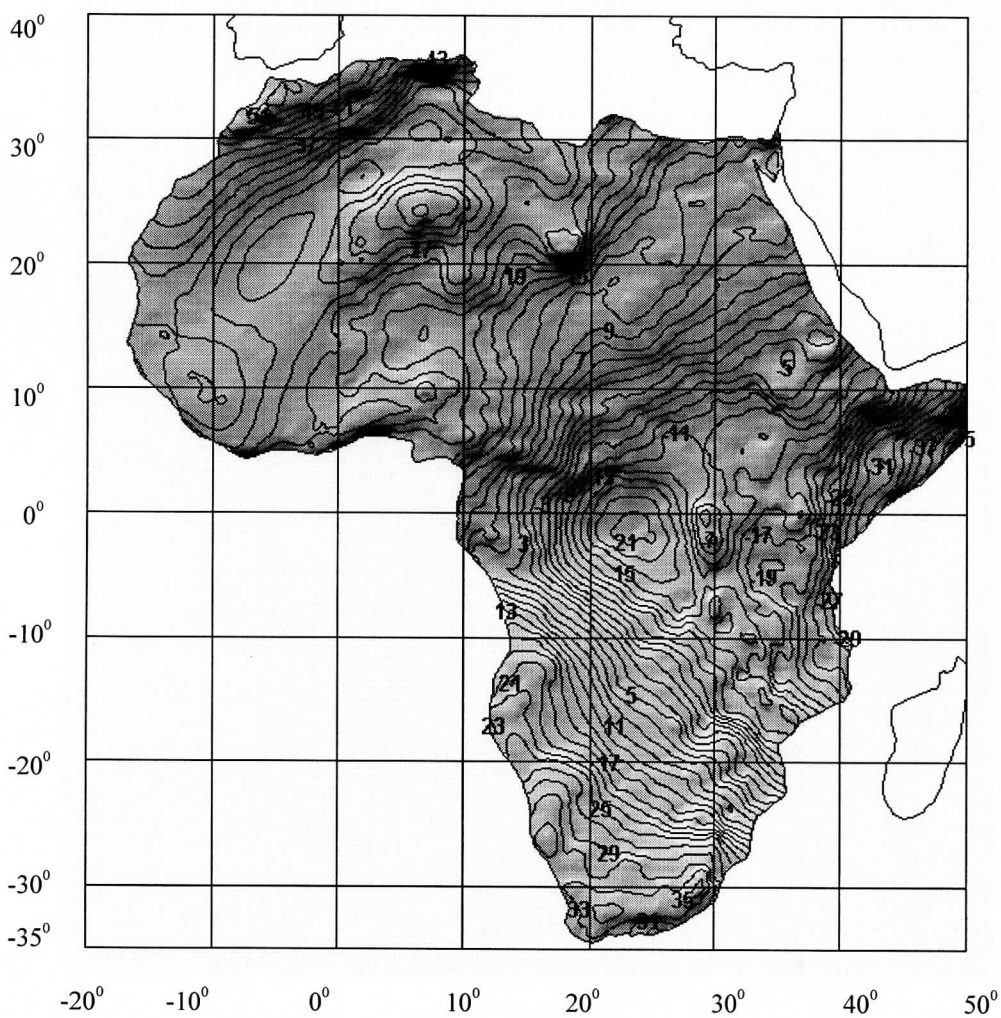

Fig. 5 The free-air co-geoid. Contour interval 2 m.

4.4 Point Testing Against Doppler Derived Undulations

As far as the geoid undulations are concerned, any two solutions from different techniques can be compared after reducing the two solutions to a common datum. The African Doppler Survey (A.D.O.S) project was initiated in 1982 and the project was completed in 1986. Out of the 52 countries in Africa at that time, 46 of them participated in this project. The total number of accepted A.D.O.S stations were 307 distributed throughout Africa. The final result was given in [6].

The data used in this investigation consisted of 92 A.D.O.S stations associated with levelling. The Doppler data was carried out by point positioning using precise ephemeris. The A.D.O.S data were given on the absolute figure NWL-9D. The geoid heights at the 92 A.D.O.S station were computed on NWL-9D and transformed to WGS-84 Datum [7].The gravimetric geoid height N_G, the EGM96 and OSU91A both complete to degree and order 360, geoid heights were computed at 92 stations. These stations were shown in (Fig.6) against a relief background. Also Doppler derived geoidal heights N_D were computed at these statations.The differences between the co-geoid and Doppler geoid heights at these stations, have then been analysed statistically, regarding the 92 values as a statistical sample. The results are shown in Table 2. Since we considered N_D as an external standard of comparison then the RMS differences provide a measure of accuracy of the gravimetric, the OSU 91A and the EGM 96 geoids.

Statistics	**N_G - N_D**	**N (OSU91A) - N_D**	**N (EGM96) - N_D**
Minimum difference (m)	-3.52	-7.72	-8.43
Maximum difference (m)	3.95	5.83	4.60
Mean difference (m)	1.66	1.80	1.70
RMS difference (m)	1.85	2.25	2.22
Standard deviation (m)	1.86	2.27	2.24

Table 2. Comparison of Doppler / levelling Data To Different Geoid Solutions

To our best of knowledge all Doppler stations have been connected to different national levelling networks in Africa. The vertical datum inconsistency there may reach up to 2 m [8] due to the fact that mean sea level at different locations does not lie on the same equipotential surface. Hence the expected accuracy of the residual geoid ΔN, is computed from:

$$\Delta N = N_G - N_D \qquad (26)$$

$$= N^S + N^C - h - H \qquad (27)$$

where;

N_G : gravimetric geoid

N^S : long wavelength component

N^C : short wave length component

h : ellipsoidal height

H : orthometric height

From the law of error propagation of (Eq.27), assuming no correlation between the above parameters,we obtain:

$$\sigma^2_{\Delta N} = \sigma^2_{N^S} + \sigma^2_{N^C} + \sigma^2_h + \sigma^2_H \qquad (28)$$

Assuming σ_h = 0.3m, σ^S_N = 0.5 m, σ_H = 2.0 m and σ^c_N = 0.5 m. The Law of error propagation yield $\sigma_{\Delta N}$ = 2.1 m. From Table 2 , we can conclude that the accuracy of gravimetric geoid is well in agreement with expected accuracy of (ΔN).This co-geoid could be used for all regional purposes such as datum connections, adoption of a unified vertical datum, engineering works, national and regional planning maps for the country, as well as to contribute needed geophysical data to the other branches of earth sciences.

5. **Conclusions**

The outcome of the investigation is a regional gravimetric co-geoid of Africa. The geoid is recovered using 1^0 x 1^0, 30' x 30' mean surface gravity anomaly data combined with truncated EGM 96 (70, 70) spherical harmonics potential coefficient set. To compute the gravimetric geoid in Africa, the modified Stokes's Kernel is being used instead of the original ellipsoidal Stokes's Kernel, to reduce truncation errors as the former tapers of more rapidly than the latter (the influence of distant gravity anomalies on local geoid heights is reduced). The reduction is proportional to the degree L of the satellite model being used to recover the long wavelength component of the geoid.

To recover the long wavelength contribution of the co- geoid, the EGM (70,70) model coefficient set complete to degree and order 70 has been chosen. This implies that the smallest gravity field features represented in EGM96 (70,70) model have spatial extension of 2.6^0 spherical distance or 288 km. Also the truncation error term of (Eq.5) was computed. The short wavelength component of the geoid was recovered by means of mean gravity anomalies after subtracting the corresponding EGM96 (70,70) model values from gravity anomalies. The optimal integration cap size in this case was found to be 8^0 from the computation point.

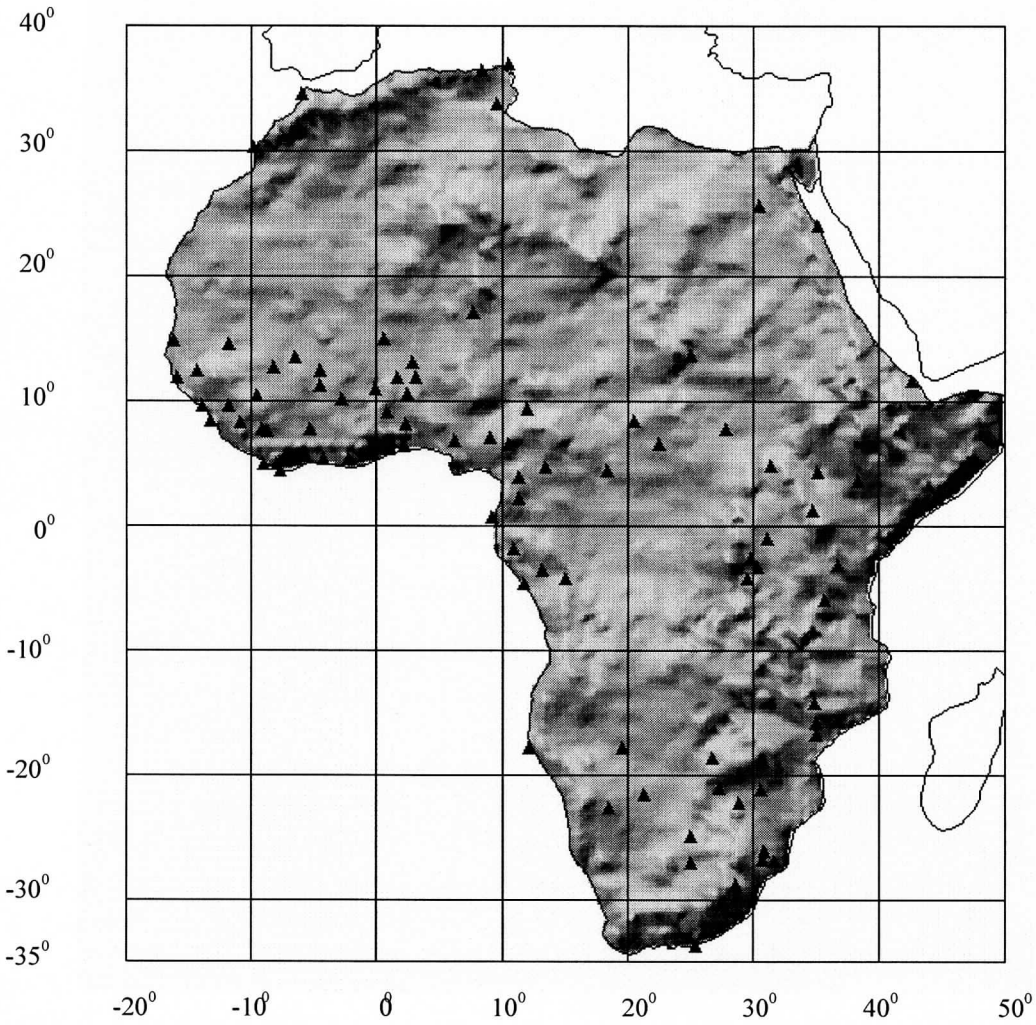

Fig. 6 Distribution of Doppler Data

The free-air co-geoid was obtained from the summation of the long wavelength component, the truncation error term of (Eq.5) and the short wavelength component. This solution was referred to the WGS-84. The comparison of Doppler geoid heights with corresponding gravimetric values showed quite a good agreement with an RMS of 1.85 m.

Also, comparing our geoid (Fig. 5) with that of [9], Fig. 8, shows that the shape of the geoid remain about the same. There is however, one important difference: there is an average change in value of about (10-30 m), except for points in the north-western and southern corners of the continent. These differences are mainly due to the poor quality and the distribution of gravity data within Africa 20 years ago. The comparison of our geoid Fig. 5 with that of [10], Fig. 2, shows the shape of the geoid remains the same, with an average change in value of about (5-8 m) in some parts of the continent.

Finally, to meet the 1 cm geoid which has been the goal of geodesists and geophysicists, we suggest it is very important to densify the regional gravity data to an average spacing of 5' (9 km), that is to say at least 144 point values in an area of 1^0 x 1^0 . The suggestion can not be met unless a mutual co-operation between geodetic communities in Africa, oil-exploring companies in Africa and the bonafide potential users of the gravity data is established. Also computation of the gravimetric geoid using Stokes's integral is based upon the following assumption:

- The attraction of the atmosphere is disregarded,
- The formulae is applied to the geoid, that is the topography is neglected;
- The reference ellipsoid is treated formally as a sphere, that is, the effect of the ellipticity of the reference ellipsoid is neglected.

Hence, if a determination of the geoid to an accuracy of the order of 1 cm is attempted, then the above assumptions will be no longer be valid. The effect of the atmosphere, the topography and the ellipticity of the reference surface on the gravity field must be taken into account. In this investigation only the atmospheric effect was accounted for. Due to enormous computation time and the fact that the resolution of our gravity data set was limited to 30' x 30' and 1^O X 1^O, we have not considered the topographic and the ellipticity effect on the computed co-geoid in this investigation.

To verify our gravimetric solution, an independent geoid should be derived from Global Positioning System (GPS) network established throughout the continent with its station located at known benchmark heights.

Acknowledgement

Free computer time for the enormous computations done here was provided through Centre For Geodetic and Geodynamic Studies (CGGS), Faculty of Geoinformation Science and Engineering, Universiti Teknologi Malaysia. We are also greatful to

Professor RAPP of the Ohio State University, for his valuable comments. We are indebted to Mr. Abdullah Hisam Omar for typing the paper and Zahidah Omar for producing the drawings.

References

1. Fashir, H.H., (1991). Determination of the shape of the geoid in sudan using heterogeneous data,unpublished ph.D thesis,University of Khartoum,Sudan

2. Lemoine,F.G.,Smith,D.E.,Kunz,L.,Smith,R.,Pavlis,E.C.,Pavlis,N.K.,Klosko,S.M., Chin,D.S.,Torrence,M.H.,williamson,R.G.,Cox,C.M.,Rachlin,K.E.,Wang,Y.M.,Kenyo n,S.C.,Salman,R.,Trimmer,R.,Rapp,R.H. and Nerem,R.S.,(1996). The Development of the NASA GSFC and NIMA joint Geopotential Model. *Proceedings of the International Symposium on gravity, geoid and marine geodesy*, The University of Tokyo, Japan.

3. Kim, J. and Rapp, R.H., (1990).The development of the July 1989 1^0 x 1^0 and 30' x 30' terrestrial mean free-air anomaly data bases, Dept. of Geodetic Science and Surveying, Rep.403, The Ohio State University, Columbus, Ohio.

4. Rapp, R.H., (1997). Use of potential coefficient models for geoid undulation determinations using spherical harmonic representation of the height anomaly/geoid undulation difference. Journal of geodesy, pp. 282-289.

5. Heiskanen, W. and Moritz, H., (1967). Physical geodesy, W.H. Freeman,and Co., San Francisco.

6. Chodata, M.W. L., (1990). Post A.DO.S. Strategy for unified networks for Africa. Proceedings of the 4th symposium on geodesy in Africa, Tunis.

7. Fashir, H.H., (1991). Doppler geoid in Africa. Survey Review, Vol 31, No. 241.

8. Rapp, R.H., and Nagarajan, B., (1992). A conceptual formulation of a world height system. Report No. 421. Dept of Geodetic science. Ohio State University, Columbus, Ohio.

9. Obenson, G., (1974). A 1973 gravimetric geoid of Africa. Geophys.J.R.astr.Soc.

10. Obenson, G., (1985). Geoidal heights for Africa from GEM9 potential coefficients and degree gravity anomalies. Survey Review, Vol 28, No. 218.

11. Rapp, R.H., (1997). Private communication.

A GIS based strategy for quality control of gravimetry

Thomas Knudsen Arne V. Olesen

{thk,avo}@kms.dk, National Survey and Cadastre—Denmark, Rentemestervej 8,
DK-2400 Copenhagen NV, Denmark,
1998-10-27

Abstract

We present a semi-automated procedure for detection and removal of residual erratic observations from a gravimetry database. The procedure is based on geographic information system (GIS) technology, provided by the *Busstop* system, a spatio-temporal information system prototype. The procedure is described through the presentation of a case study showing its use (and usefulness) in a limited area centered on the Skagerrak strait between Norway and Denmark. The entire process is compact enough to be implemeted in the form of a brief script, which is presented in extenso.

1 Introduction

Due to the labour-intensive nature of the data capture process, a gravimetry data set covering a given geographical area will typically consist of a relatively small number of observations. Despite this sparsity, detecting suspicious observations in a gravimetry database can be a remarkably tricky task. To reduce the necessity of that, new observations must be put through extensive screening procedures prior to inclusion in existing gravimetry databases.

Some erratic observations do, however, survive the trip through the sieve of the screening procedures and make their way into the database. Once included there, they may show up in derived data sets as features with no physical basis. In this paper, we present an example of such features, and describe a GIS based, semi-automated strategy for the picking and elimination of the remaining erratic data.

2 A manifestation of erratic data

The National Survey and Cadastre—Denmark (*KMS*) maintains an extensive gravimetry database covering North European and Greenlandic areas. As a part of the operation, customized grids of gravity anomalies are routinely generated for smaller areas in support for field work campaigns, research etc. This task is usually carried out using components from the *Gravsoft* package for gravity field modelling [Tscherning et al., 1992]. Gravsoft is based on a set of plain text file formats, making integration with external programs easy and convenient. This will be utilized heavily below.

One of the routinely generated gravity anomaly grids is shown in figure 2. This grid was generated to help evaluate field work results [Olesen et al., 1997] from the Skagerrak strait between Denmark and Norway. The grid was based on a set of 25377 individual gravity measurements, extracted from the KMS gravimetry data base. The data set included marine, as well as terrestic, gravimetry (see figure 1).

The initial visual inspection of the grid revealed a hitherto unknown structure: A narrow zone of anomalies of up to around -25 mgal, splitting the area around 58°N, 8.5°E, which was believed to have rather uniform negative anomalies of around -40 mgal. This sudden jump of +15 mgal (indicated by a white polygon on figure 2) was believed to be a computational artefact originating from erratic gravimetry from one of the ship profiles. But tracking down the right profile manually from a data set of 25377 observations is a tedious task, so before resolving to manual methods, it was decided to try developing a less demanding method, based on geographical information system (GIS) technology.

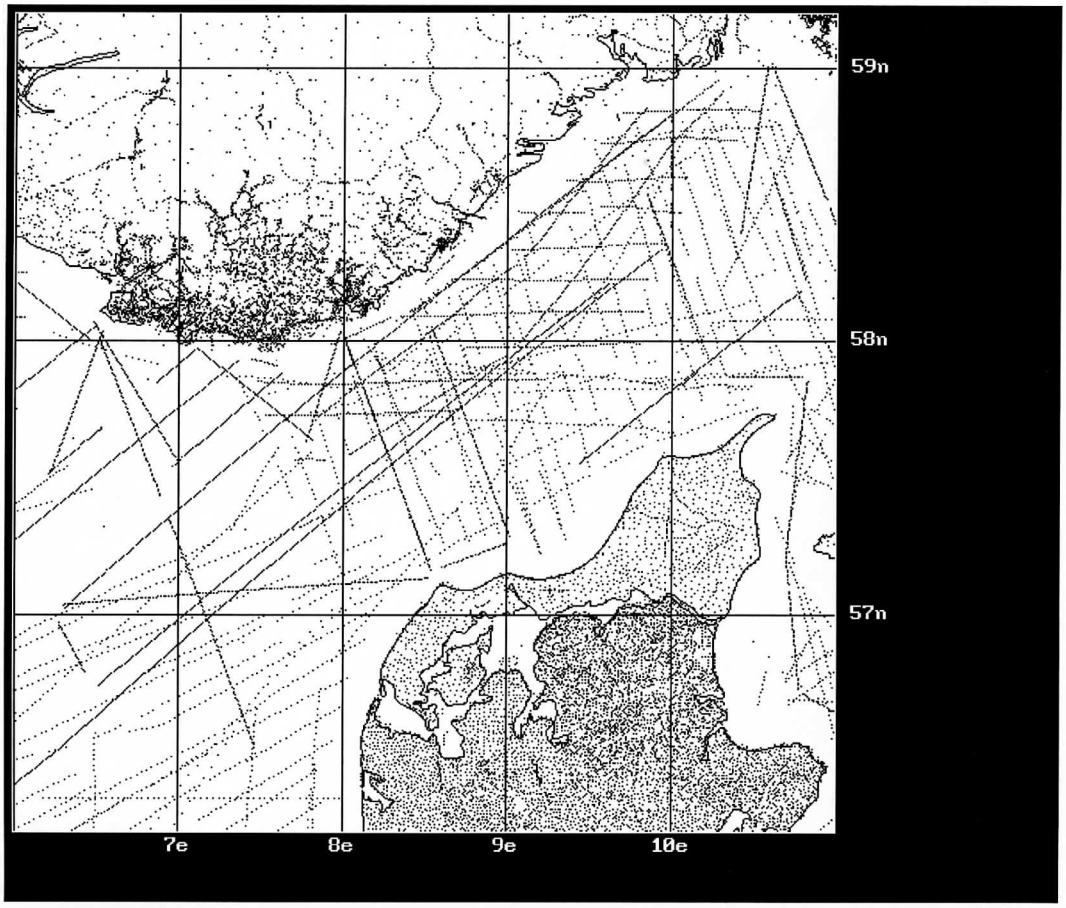

Figure 1: *The positions of the 25377 data points extracted from the gravimetry data base.*

3 The Busstop system

The Busstop system [Knudsen, 1997, Knudsen, 1998a] was selected for the ship profile hunt. Busstop is a prototype of an integrated system for handling, analysis and visualization of ocean data. It was developed with the main goal of facilitating the synergistic use of satellite based radar altimetry and ancillary data (e.g. satellite based radiometry, such as sea surface temperature and ocean colour observations) [Knudsen and Brandt, 1998, Knudsen, 1998b].

Busstop integrates functionality from Geographical Information Systems (GIS), image processing systems and data base management systems, and provides a smooth interface to user written programs (including the Gravsoft package). The traditional spatial GIS functionality has been extended with transparent support for temporal data. This enables the GIS functionality to work even as a tool for analysis of dynamic phenomena. Hence, Busstop is actually rather a *spatio-temporal* than a *geographical* information system. The temporal support is, however, not used in the present study.

Busstop uses an open architecture of cooperating stand alone programs [Knudsen, 1998c, Knudsen, 1998d]. The major components are the visualization program, *Reveal*, and the BUsstop SHell, *Bush*. Reveal generates static and animated visualizations of (primarily) gridded data. Bush provides a spatio-temporal version of the *map algebra* analysis method which, in its traditional spatial-only incarnation, is well known from traditional raster based GIS [Tomlin, 1983, Tomlin, 1990, Shapiro and Westervelt, 1992, Larson et al., 1991]. Additionally, Bush serves as the integration platform for the Busstop system, by providing a rudimentary scripting language, suitable for chaining simple components into solutions for more complex tasks.

The Busstop components access data indirectly using metadata sets to indicate the physical and logical structure of the data at hand. This means that a large number of data formats can be accessed simply by providing the system with a metadata description of the data to be accessed. The Gravsoft package uses a data format which fits into this access model, so the gravity anomaly grids and the point data file extracted from the gravimetry database could be readily analyzed using Busstop.

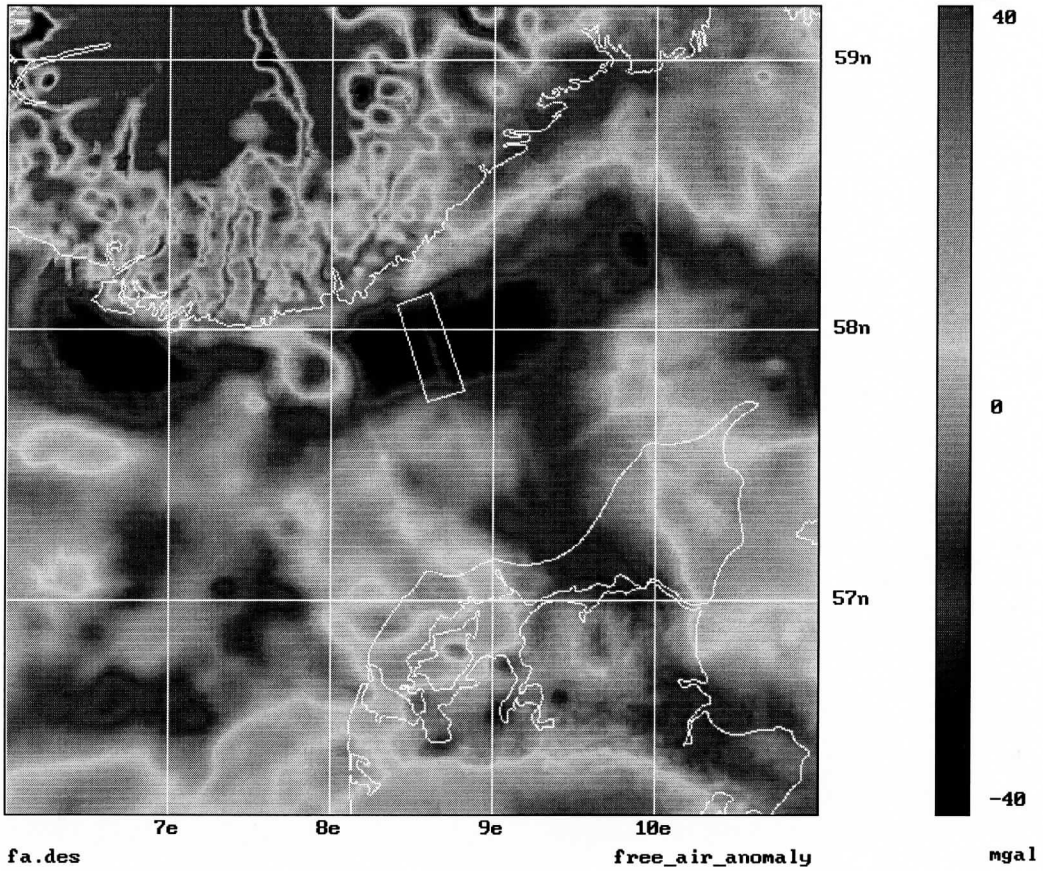

Figure 2: *The original free air anomaly grid. The suspicious +15 mgal jump is indicated by the white box located around 58°N, 8.5°E*

4 Tracking down the profile

The first thing done was to compute the spatial gradient of the original grid, using the Busstop component *hshade*: Flawed data are most likely to show up as high frequency components, and the gradient operation accentuates the high frequency part of the signal. Hence, it was expected to be a lot easier to determine the positions of the flawed data from the gradient field, than from the original field.

4.1 Visual tracking

Visual inspection with Reveal confirmed this expectation (see figure 3): Grid nodes affected by flawed data were centered around a sharp line of zero gradient, i.e. a local extremum. The local extremum occurs because the flawed data, in the area where they are dominating, drag the grid values away from the "true" value, while, outside of this area, the grid values rapidly fall back towards the "true" value.

Reveal supports the use of vector overlays. This means that point and line information can be overlaid on a grid in a "non-destructive" manner: graphically, the overlaid data are handled entirely independently, and can be toggled on and off interactively. Additionally, separate overlays can be used for on-screen digitizing, where the points, lines and polygons digitized are simultaneously stored in a disk file.

During the Reveal session, the 25377 positions of the input data points were stored in an overlay. By toggling the overlay on and off in rapid succession, the points falling closest to the zero-gradient line were easily identified, and actually seemed to stem from one particular ship profile. Upon closer inspection, a neighbouring profile, presumably a part of the same survey, showed to introduce similar effects, albeit of smaller magnitude.

After zooming in on the profiles, the on-screen digitizing feature was used to digitize two polygons enclosing the profile data points in a tight envelope: the zoom-level made it possible to digitize very close to the profiles, and hence to avoid having more than a few points from other

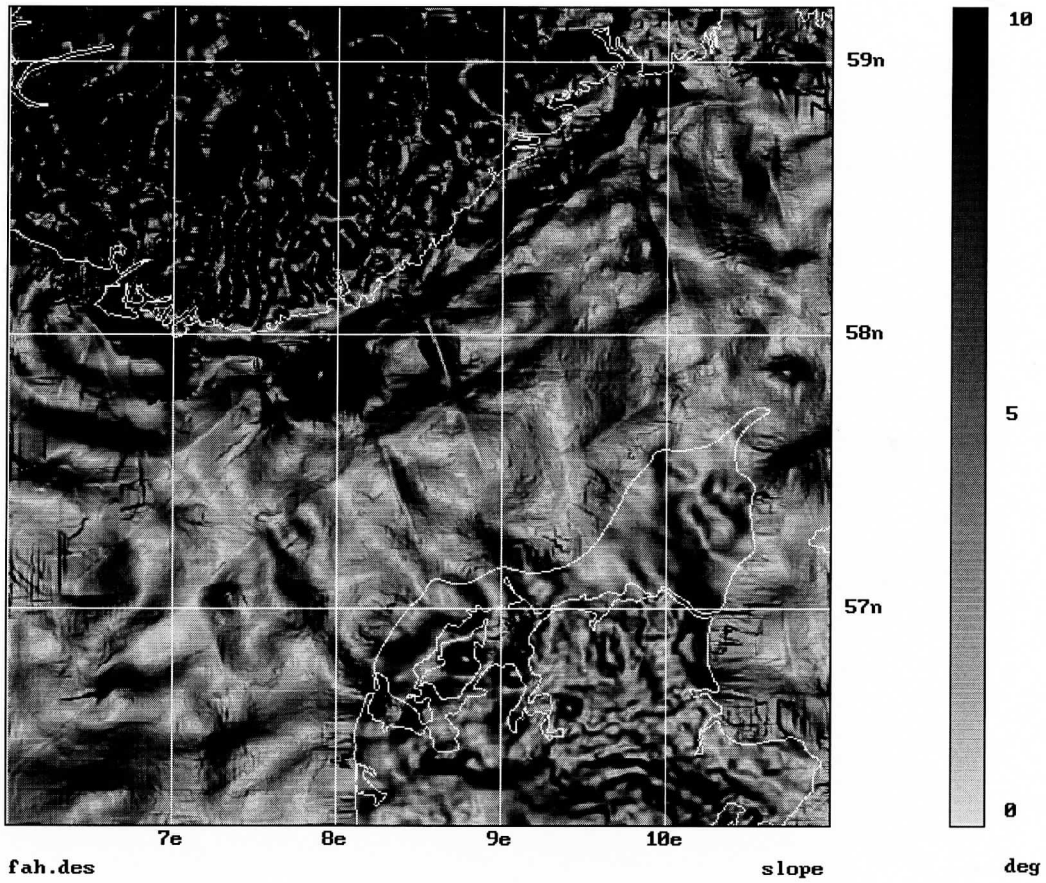

Figure 3: *The slope (gradient) of the original free air anomaly grid. The suspicious area now stands out clearly as a line of zero gradient, and can be traced into a much larger area than for the original data set.*

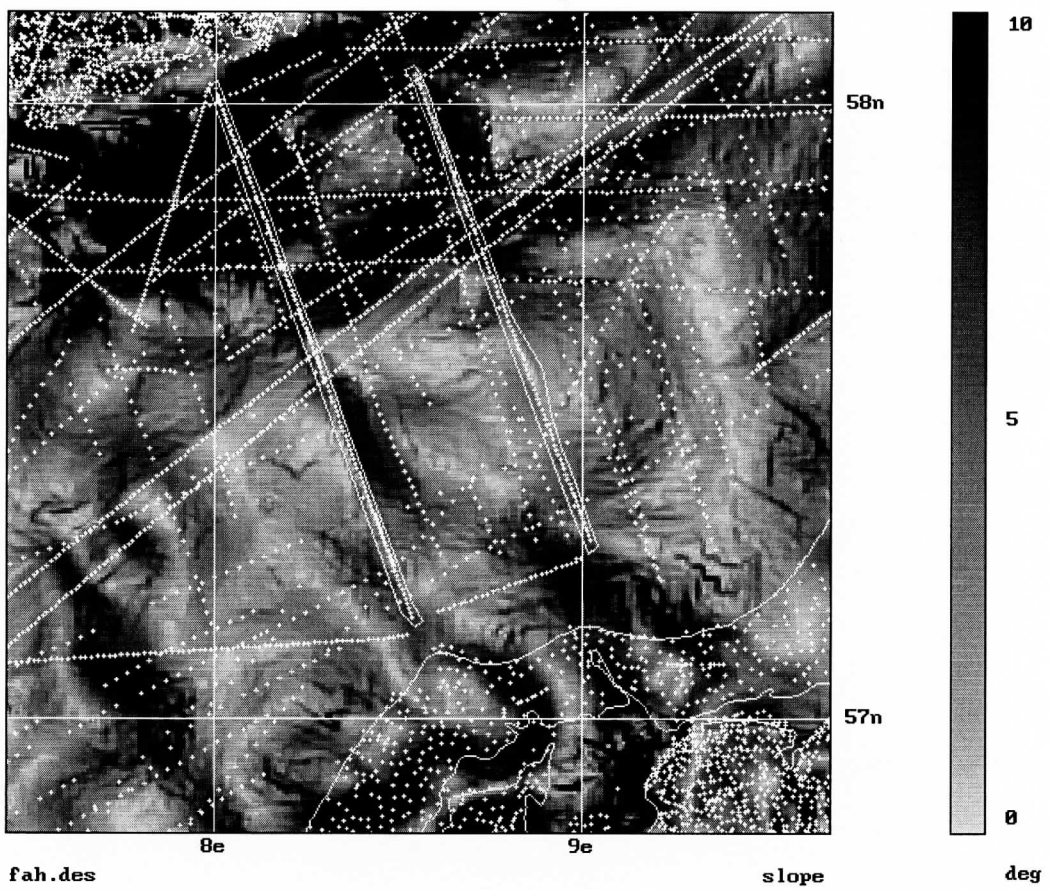

Figure 4: *After zooming in on the two suspicious ship profiles, their enclosing polygons can be digitized precisely enough to distinguish between the profiles and other nearby data.*

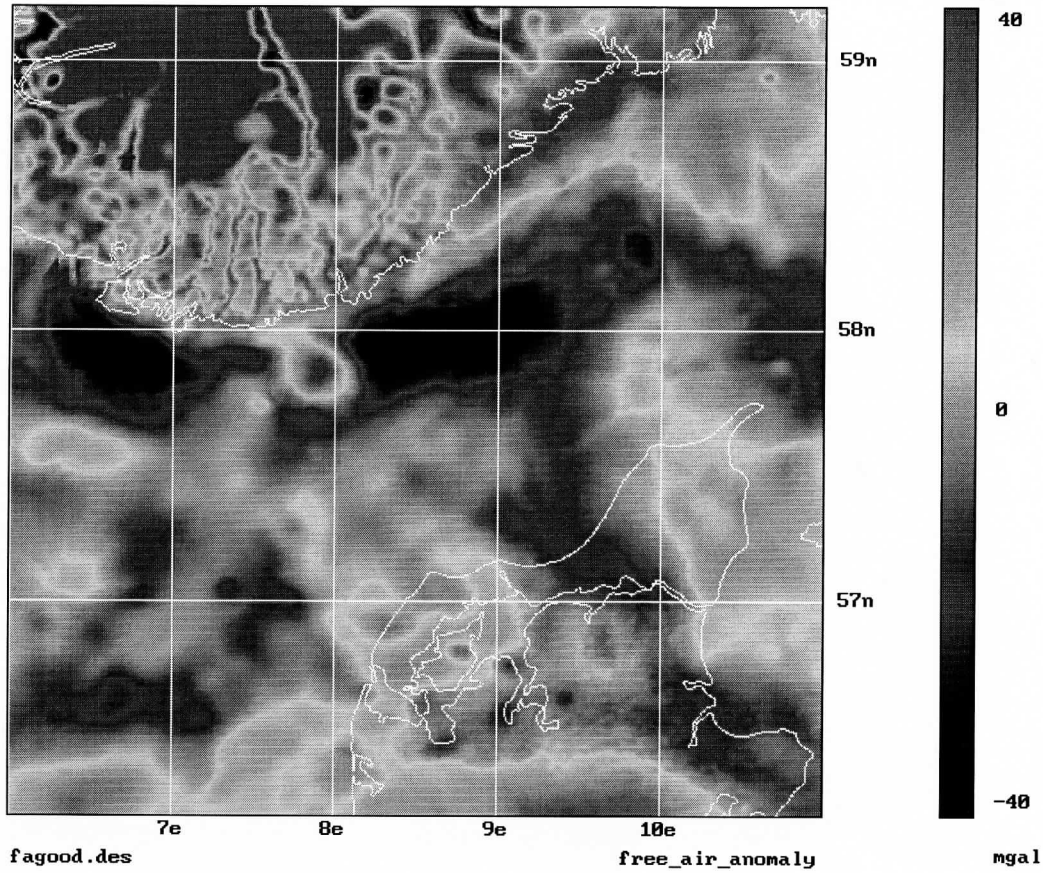

Figure 5: *The version of the free air anomaly grid, computed after exclusion of the suspicious data. The +15 mgal jump, splitting the area of negative anomalies with a barrier around 58°N, 8.5°E, has now disappeared.*

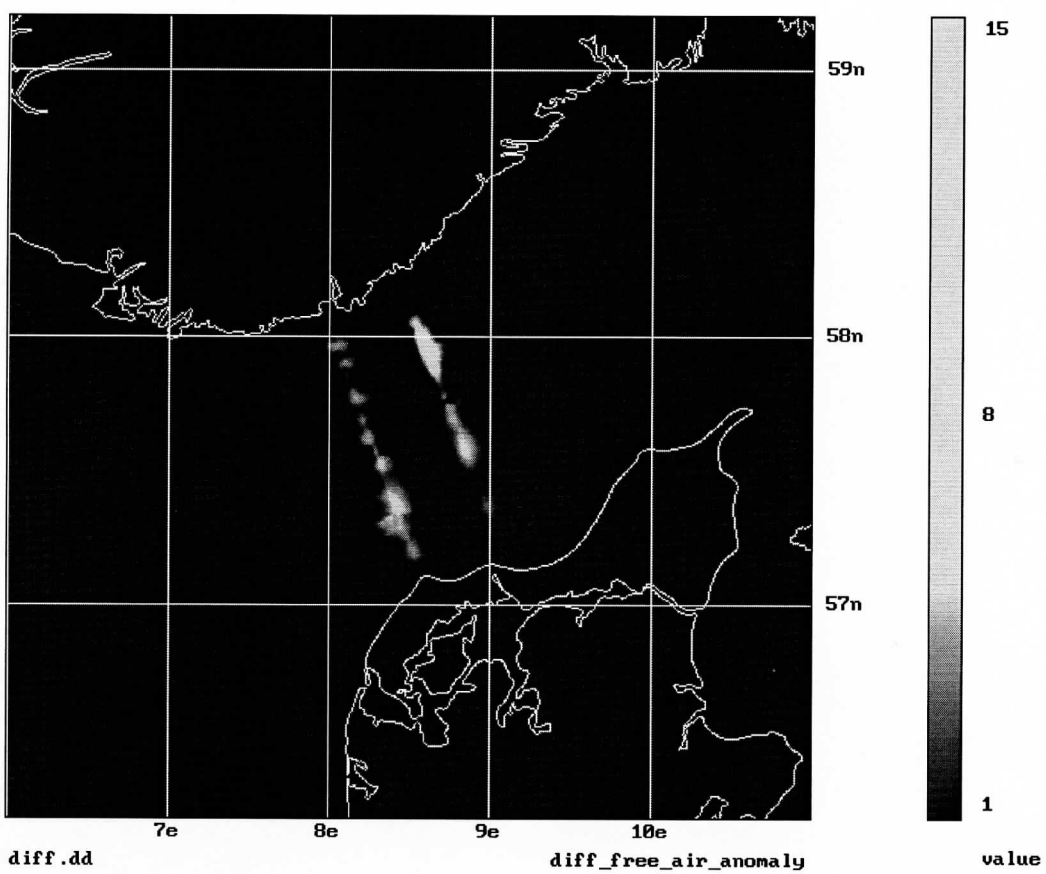

Figure 6: *The difference between the old and the new free air anomaly grid. Except for the zones, where changes were wanted, the difference in general stays below 1 mgal.*

```
// Generate original free air anomaly grid.
// Output goes to fa.grd & fa.err.
// Descriptor file fa.des, describing fa.grd,
// is assumed to exist
geogrid <fa.in

// Compute the internal statistics of fa.grd
basta fa.des

// Take a look
reveal fa.rev

// Compute the (scaled) gradient
hshade fa.des fah.des free_air_anomaly --scale 100


// Take a look, and digitize enclosing polygons
// for suspicious data
reveal fah.rev

// Convert the polygons to Idrisi format
dig2idr fah.dig bad.vec

// Split the input data set into the points falling inside
// and the points falling outside the polygons
if exist inside.db  del inside.db
if exist outside.db del outside.db
if exist bad.dat    del bad.dat
if exist good.dat   del good.dat
pip skagerak.dat bad.vec
move inside.db  bad.dat
move outside.db good.dat

// Generate the new free air anomaly grid, based on
// "good" data only
geogrid < fagood.in

// Take a look
reveal fagood.rev

// Compute the difference, and take a look at it
set f=free_air_anomaly
diff.dd{diff_$f} = fa.des{$f} - fagood.des{$f}
basta -v diff.dd
reveal diff.rev
```

Figure 7: *The Bush script for the whole detection-correction cycle. Although perfectly possible, it is not intended for direct execution by Bush. Rather as an operator's documentation of the steps included in the turnkey solution*

profiles fall within the polygons (see figure 4).

Having determined the enclosing polygons for the suspicious data, the Reveal session was terminated.

4.2 Spatial sorting and regridding

To pick the suspicious data, the digitization file from the Reveal session was passed on to the Busstop component *pip*. Pip, an acronym for "point in polygon" reads a number of polygons, then passes through all elements in a data file and splitting them into two output files: One containing the points falling inside one of the polygons, and one containing the points falling outside of all the polygons. The resulting files contained 324 and 25053 points respectively.

Now, the free air gravity anomaly grid was recomputed, using the outside data only. Visual inspection with Reveal (see figure 5) showed, that this simple remedy had worked: The 2 individually uniform areas from the first version, were now re-united into one.

4.3 Final check

To check for additional effects of throwing away the suspicious data, the absolute value of the difference between the old and the new version of the grid was computed, using Bush. Visual inspection of the result, using Reveal, showed (see figure 6) that the difference between the two grids remain far below 1 mgal, except for the small areas, where the effects of the flawed data were observed in the original data set.

As this result was quite encouraging, the steps involved in the detection/correction cycle were finally combined into a Bush script, documenting the process (see figure 7)

5 Conclusion

A quick-and-dirty, semi-automated, strategy for detection of residual erratic data from a gravimetry database was developed. The initial test was quite succesful in detecting and removing the erratic data. Throwing away data is obviously not a *solution*: Ideally, one should uncover what has happened during the survey providing the flawed data, and whether the error can be modelled and removed from the data. If that is the case, the corrected data can be re-introduced into the gravimetry data base. However, the first step of this process is to actually locate the data. Busstop showed to be able to provide a simple, and apparently efficient, solution to this piece of otherwise annoying geophysical everyday work.

Acknowledgements: This work was partially funded by the EU 4th framework program (AVO), the Danish Space Board and the Earth Observation Programme board of the Danish Research Councils (TK). The figures used originates from Thomas Knudsen's Ph.D. thesis [Knudsen, 1997]

References

[Gudmandsen, 1998] Gudmandsen, P., editor (1998). *Proceedings, EARSeL symposium 1997: Future Trends in Remote Sensing*, Rotterdam, The Netherlands. A. A. Balkema.

[Knudsen, 1997] Knudsen, T. (1997). *Busstop—a spatio-temporal information system*. PhD thesis, University of Copenhagen.

[Knudsen, 1998a] Knudsen, T. (1998a). Adding GIS functionality to specialized analysis programs for remote sensing data: Gravsoft and the busstop project. In [Gudmandsen, 1998], pages 125–132.

[Knudsen, 1998b] Knudsen, T. (1998b). Busstop—an integrated system for handling, analysis and visualization of ocean data. *Physics and Chemistry of the Earth*. in press.

[Knudsen, 1998c] Knudsen, T. (1998c). Busstop programmers reference. URL: http://www.gfy.-ku.dk/ tk/busstop/libbs/index.htm.

[Knudsen, 1998d] Knudsen, T. (1998d). Busstop user's guide. URL: http://www.gfy.ku.dk/ tk/-busstop/usrguide/index.htm.

[Knudsen and Brandt, 1998] Knudsen, T. and Brandt, J. (1998). GIS and high resolution atmospheric modelling for corrections of sea surface observations from the TOPEX/POSEIDON satellite altimeter. In [Gudmandsen, 1998], pages 373–378.

[Larson et al., 1991] Larson, M., Shapiro, M., and Tweedale, S. (1991). GRASS tutorial: r.mapcalc. Technical report, U.S. Army Corps of Engineers, Construction Engineering Research Laboratories, Champaign, Illinois, USA.

[Olesen et al., 1997] Olesen, A., Meyer, U., Hehl, K., Gidskehaug, A., Forsberg, R., Bastos, L., and Timmen, L. (1997). Airborne geoid mapping system for coastal oceanography (AGMASCO). Presentation, AGU Fall 1997, San Francisco.

[Shapiro and Westervelt, 1992] Shapiro, M. and Westervelt, J. (1992). r.mapcalc: An algebra for GIS and image processing. Technical report, U.S. Army Corps of Engineers, Construction Engineering Research Laboratories, Champaign, Illinois, USA.

[Tomlin, 1983] Tomlin, C. D. (1983). *Digital Cartographic Modeling Techniques in Environmental Planning*. PhD thesis, Yale University.

[Tomlin, 1990] Tomlin, C. D. (1990). *Geographic information systems and cartographic modeling*. Prentice Hall, Englewood Cliffs, NJ, USA.

[Tscherning et al., 1992] Tscherning, C., Forsberg, R., and Knudsen, P. (1992). The gravsoft package for geoid determination. In *Proceedings, First workshop on the European Geoid, Prague.*

MEAN DENSITY MAP FOR THE ITALIAN REGION BY GIS TECHNIQUES

Valerio Baiocchi ([1]), **Mattia Crespi** ([1]) and **Federica Riguzzi** ([2])

([1]) DITS – Area di Topografia, Universita` *La Sapienza* di Roma, Roma, Italy

([2]) Istituto Nazionale di Geofisica, Roma, Italy

Abstract

The knowledge of the mean density of the masses between the earth surface and the geoid is remarkably interesting for several geodetic and geophysical investigations; in this respect, it is very useful to manage these data in digital form.*

At present the unique information available about the mean density of the Italian region is the 1:1.000.000 scale graphical map published by Vecchia in 1955. This map was drawn computing the mean densities on the basis of many geological maps and profiles, by grouping these values in 8 classes ranging between 1.8 and 3.4 g/cm^3, each class 0.2 g/cm^3 wide. An additional class includes the water density (1.0 g/cm^3).

Starting from the graphical map scanning, the raster file was georeferenced in the WGS84 reference frame, devoting a special care to model and removing the deformations due both to the paper and the scanning process.

Finally, ASCII files of the mean density values sampled on a 15" (latitude) ×20" (longitude) regular grid and a vector file for convenient data manipulation and representation were produced. The main steps of the data processing were performed in the Intergraph *MGE* environment and a Fortran77 service program was written in order to produce the ASCII files in a suitable form.

* This work has been performed in the framework of a general agreement of cooperation and support by Istituto Nazionale di geofisica with respect to the International Geoid Service.

1. Introduction

Italy is an extremely variable region from a geological and geomorphologic point of view. This fact implies a great variability of the local gravity field with high gravity anomaly (Bouguer and isostatic) values and variations over limited areas.

The precision of the gravity reductions needed to compute these gravity anomalies and also the geoidal undulation estimates is limited by the poor knowledge of the topographic mass densities. This effect is obviously strictly related to the height. In particular, it is possible to show that a density error of 10% may cause differences of about 1 mgal every 100 m of height in the gravity reduction computations (even excluding the classical topographic corrections).

In 1955 Vecchia realized a paper coloured map of the mean density of the topographic masses above the sea level of the Italian region, with the aim to lower these errors and to provide a useful tool to improve the quality of the gravimetric measurement reductions. This map was used to compute the isostatic reduction tables of the gravity measurements (Ballarin, 1960) and to draw the gravimetric map of Italy (Ballarin, Palla and Trombetti, 1972).

In this context it is useful to briefly recall the principal applications of the mean density of the topographic masses both in geodesy and in geophysics (Heiskanen and Moritz, 1967; Torge, 1989):

1) Estimation of a local quasigeoid by remove-restore technique (Barzaghi et al., 1997)

   a - computation of the contributes to free-air anomalies due to the residual topographic masses (terrain correction) in the remove step

   b - computation of the free-air anomaly gradient

   c - computation of the residual contribution to the anomalous potential in the restore step

2) Computation of a local geoid from a local quasigeoid

   a - computation of the mean gravity along the plumb line $\bar{g}$ by the Prey reduction, then:

$$N = \zeta + \frac{\bar{g} - \bar{\gamma}}{\bar{\gamma}} H \quad (1)$$

   b - computation of the Bouguer anomaly Δg_B, then:

$$N \cong \zeta + \frac{\Delta g_B}{\bar{\gamma}} H \qquad (2)$$

(N: geoidal undulation, ζ: height anomaly, $\bar{g}$: mean gravity along the plumb line, $\bar{\gamma}$: suitable value of normal gravity)

3) Investigation of the structure of the earth's crust and upper mantle

computation of the Bouguer Δg_B and isostatic Δg_I anomalies

4) Gravity inverse problem, applied gravimetry

a - removal of the influence of known masses

b - constraints on density contrast in the iterative solution according to the optimization method

5) Computation of curvature of plumb line and orthometric correction

computation of the mean gravity along the plumb line $\bar{g}$ by the Prey reduction

Note that it is possible to roughly evaluate the error in the geoidal undulation N due to the error in the mean density starting from (2); in fact if we put H = 1000 m and assume a 10% error in the mean density, we have an error of 10 mgal in the Bouguer anomaly and an error of 1 cm in the geoidal undulation. Moreover, it has to be underlined that the assumed 10% error in the mean density is not extreme if compared with the large variability of the density in Italy with respect the standard density value 2.67 g/cm^3.

2. The paper map

The mean density map was drawn at 1:1.000.000 scale according to the conical Lambert projection referred to the Italian datum (ROMA40 ellipsoid).

A large effort was done by Vecchia to inspect all the existing geologic maps (about 300), profiles, papers, field reports and rock density tables. From these tables he established a density scale from 1.8 to 3.4 g/cm^3 divided in 8 classes, each class 0.2 g/cm^3 wide, being this interval in agreement with the mean precision achievable by the analysis of the profiles. Moreover, an additional class for the water (density 1.0 g/cm^3) was considered.

Densities were estimated as weighted means of the densities relative to each formation thickness belonging to the same geologic series along the vertical, from the surface to the sea

level. The 9 mean density classes were represented in the map by 9 different colours contoured by 0.2 mm black lines; with similar lines was drawn the geographic grid.

3. The procedure

The density values of the paper map obviously become simply usable if they are converted into digital files. The procedure adopted to obtain these files is based on the use of GIS techniques (Burrough and McDonnel, 1998), according to the scheme of figure 1.

First, we carried out a black/white instead of a colour scanning of the map, in order to strongly limit the memory requirement and to avoid that constant density areas (homogeneous areas) were represented by more than one colour, due to lack of uniformity in the colour of the paper map. Two raster files were created, since the map has dimensions greater than A0. Great care was devoted to control the resolution obtained passing from colours to black and white and to calibrate the threshold value in order to memorize as black only the pixels of meridians, parallels and boundary lines between different density fields. The two files were saved in the binary raster format *cit*, which is the Intergraph georeferenciable format.

These files were georeferenced and unified by the *Iras B* module of *MGE* with a mean error (30 m) lower than the standard graphic error for the considered paper map (200 m), following some well tested procedures. Particularly, a contemporary georeferencing and coordinate transformation according to a latitude and longitude regular grid was performed by a five degree affine transformation as a rectangular grid is more convenient than a conical one to perform the subsequent operations:

$$x' = a_0 + a_1y + a_2x + a_3x^2 + a_4xy + a_5y^2 + \ldots.$$

$$y' = b_0 + b_1y + b_2x + b_3x^2 + b_4xy + b_5y^2 + \ldots.$$

Where $a_0 \ldots a_{20}$, $b_0 \ldots b_{20}$ are the parameters; x', y' are the coordinates in the output georeferenced raster file and x, y are the coordinates in the input raster files.

The transformation parameters were estimated using the known coordinates of all the intersection points between meridians and parallels (Table 1).

EQUATIONS	216
PARAMETERS	84
RMS OF TRANSFORMED COORDINATES (m)	30

Table 1 - Affine transformation parameters estimation features

After this step, the homogeneous areas were bounded by long and generally continuous stripes of black pixels. Therefore, it was easy to assign them a colour similar to the original by an image processing commercial software (*Paintshop*); we chose a 16 colour palette to limit the memory storage.

The georeferenced raster colour file was processed by the *Iras C* module of *MGE* in order to obtain automatically an ASCII file with the density codes (one code for each density class).

This last step implied a discretization of the raster file according to the required resolution (15" × 20"), so that a density code could be assigned to each finite element (pixel) stemming from the discretization. Note that the adopted resolution (approximately corresponding to a 450 m × 450 m area) was chosen taking into account the standard graphic error, the requirements of the geodetic and geophysical investigations and the memory requirements.

The number of pixel exceeded 4 millions, so that it was necessary to split the map into 11 zones in order to overcome storage problems during the processing (Table 2); correspondingly, 11 files containing density codes were produced automatically.

A suitable Fortran77 program was implemented to clean these files from spurious code values (0 and 1) and to convert them into 11 ASCII files with density value (density class) and position of each pixel (Table 3).

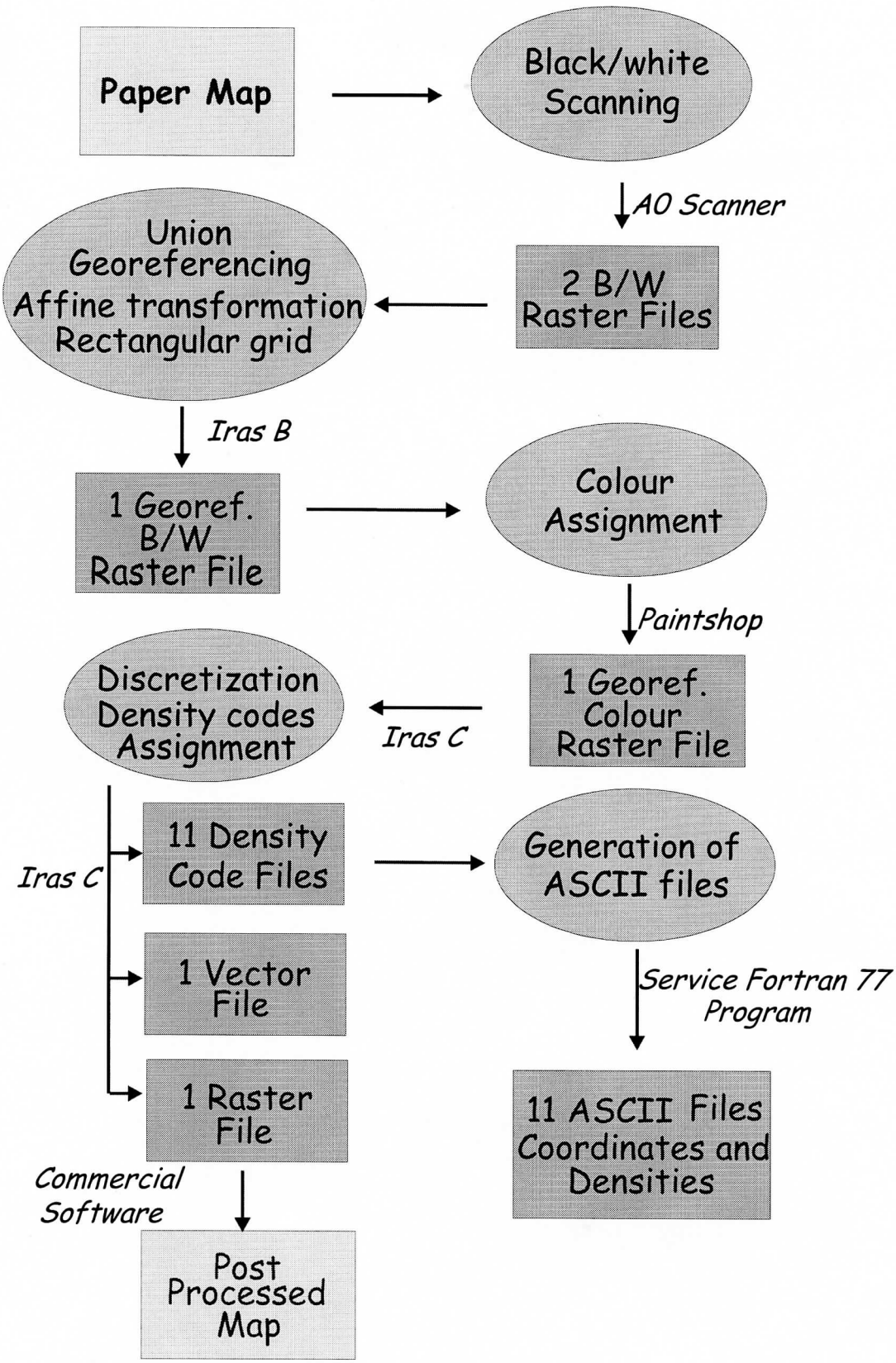

Fig.1: Scheme of the procedure used to achieve data files from the paper map.

ZONE	LOCATION (ROMA40 DATUM) LATITUDE LONGITUDE	PIXEL NUMBER
1	44°00'00" ÷ 47°00'00" - 6°00'00" ÷ - 3°00'00"	378000
2	44°00'00" ÷ 47°00'00" - 3°00'00" ÷ 0°00'00"	388800
3	44°00'00" ÷ 47°00'00" 0°00'00" ÷ 3°00'00"	288800
4	41°00'00" ÷ 44°00'00" - 5°00'00" ÷ - 2°00'00"	388800
5	41°00'00" ÷ 44°00'00" - 2°00'00" ÷ 1°00'00"	388800
6	41°00'00" ÷ 44°00'00" 1°00'00" ÷ 5°00'00"	518400
7	38°00'00" ÷ 41°00'00" - 5°00'00" ÷ - 2°00'00"	388800
8	37°00'00" ÷ 41°00'00" - 2°00'00" ÷ 1°00'00"	518400
9	38°00'00" ÷ 41°00'00" 1°00'00" ÷ 4°00'00"	388800
10	38°00'00" ÷ 41°00'00" 4°00'00" ÷ 6°04'06"	266400
11	36°38'45"÷ 41°00'00" 1°00'00" ÷ 4°00'00"	175500

Table 2 - Zones and corresponding locations

MEAN DENSITY OF THE MASSES FROM THE EARTH SURFACE
TO THE SEA LEVEL IN ITALY (VECCHIA, 1955)
ON A 15" (LATITUDE) x 20" (LONGITUDE) REGULAR GRID WITHIN
THE AREA:

WGS84 ELLIPSOID : LATITUDE 47.0007 - 44.0007
LONGITUDE 6.0452 - 9.0452

ROMA40 ELLIPSOID: LATITUDE 47.0000 - 44.0000
LONGITUDE -6.0000 - -3.0000

P.N.	WGS84 ELLIPSOID		ROMA40 ELLIPSOID		DENSITY
	LATITUDE (deg)	LONGITUDE (deg)	LATITUDE (deg)	LONGITUDE (deg)	INTERVAL (g/cm3)
1	46.9986	6.0480	46.9979	-5.9972	2.4 2.6
...	.....	.....	.....	.....	....
...	.....	.....	.....	.....	....

Table 3 – Header and beginning of the output ASCII file

In particular, both the ROMA40 and the WGS84 geographic coordinates were indicated, the latter derived by adopting a mean shift with respect to the former according to the values estimated in the frame of IGM95 GPS campaign adjustment (Surace, 1997) (Table 4).
Note that both for latitude and for longitude the shifts are smaller than the standard graphical error, provided the global longitude shift from Greenwich to Roma-Monte Mario (12° 27' 08.40") is removed.

	LATITUDE SHIFT WGS84 - ROMA40	LONGITUDE SHIFT WGS84 - ROMA40
RANGE	2.20" ÷ 2.50"	- 1.65" ÷ 0.35"
MEAN	2.35" (≅ 70 m)	- 0.65" (≅ - 15 m)

Table 4 - Shift between ROMA40 and WGS84 geographic coordinates

Finally, the automatic vectorizator of the *Iras C* module of *MGE* was used to make a vector file for convenient data manipulation and visualization on the basis of the cleaned density codes files.

The post processed map with the 11 zones is reported in figure 2.

4. Technical information and data retrieval

The ASCII files were named ZONE_1.DAT to ZONE11.DAT and were compressed together in the DENSITY.ZIP file by *Winzip* (v. 5.6 - default compression); the raster file of the post processed map is named DENSITY.TIF (TIFF format); the vector file was made according to two different formats: DENSITY.DGN (DGN format) and DENSITY.DXF (DXF format).

The memory occupation of each ASCII file range from 12.6 Mb to 37.3 Mb (uncompressed) and from 1.5 Mb to 4.5 Mb (compressed); the DENSITY.ZIP file requires 36.0 Mb, the DENSITY.TIF file 0.25 Mb, the DENSITY.DGN file 1.3 Mb and the DENSITY.DXF 20.0 Mb.

It is possible to request this document and all the mentioned files at the Internet address riguzzi@ing750.ingrm.it. The density map is available at the Web site http://ing712.ingrm.it/data_www/Geodesy/geodesy.html of the Istituto Nazionale di Geofisica.

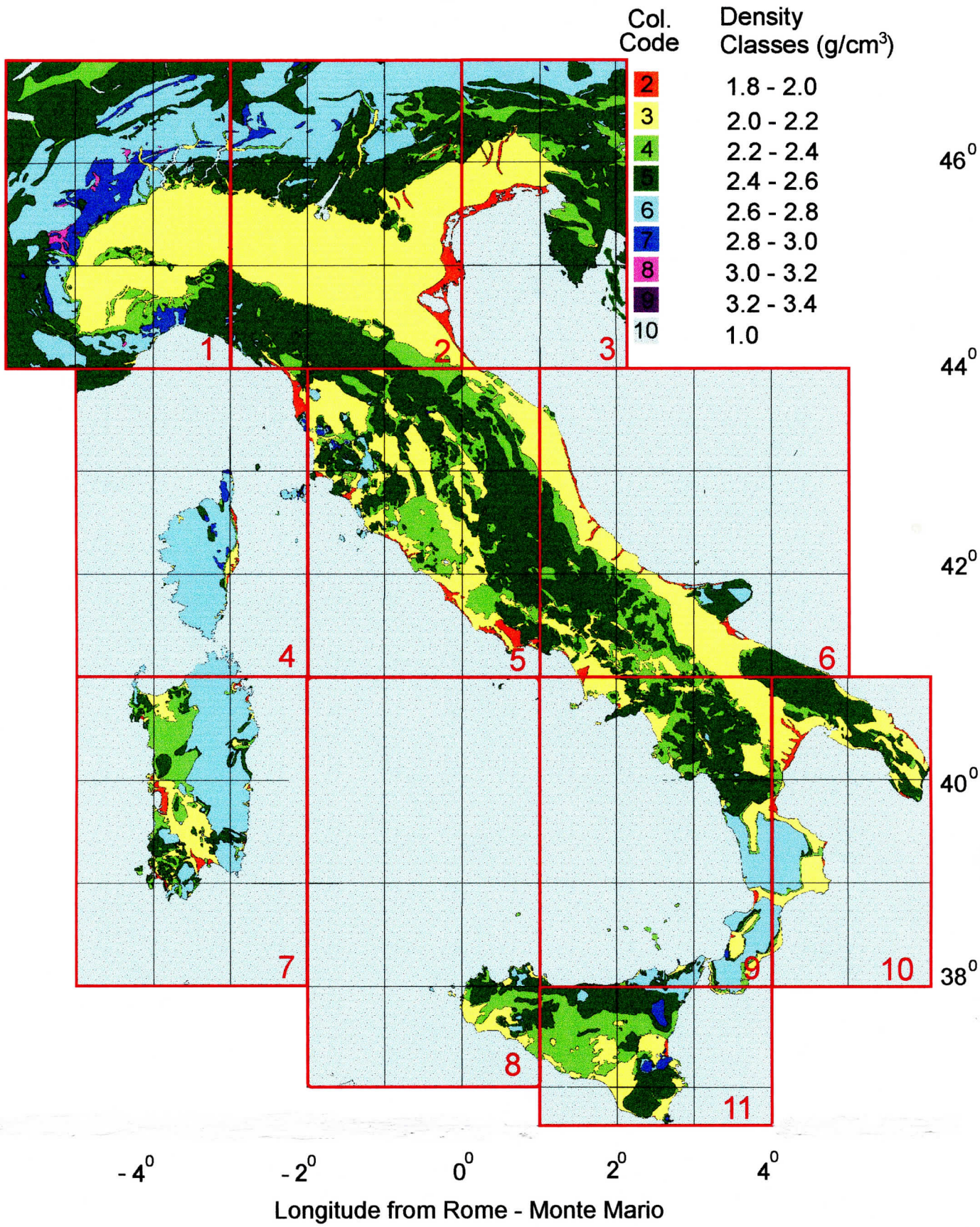

Fig.2: The post processed mean density map; red squares represent the 11 zones constituting each one an ASCII file of coordinates and density values.

Acknowledgments

The authors wish to acknowledge Fernando Sanso` for his helpful suggestions.

REFERENCES

Ballarin S. (1960). Introduzione alle tabelle per la riduzione isostatica delle misure di gravita`. Raccolta de *Il Bollettino Risponde* dal 1950 al 1995, Bollettino di Geodesia e Scienze Affini, XIX, I, 815-956.

Ballarin S., B. Palla, C. Trombetti (1972). The construction of the Gravimetric Map of Italy, Pubblicazioni della Commissione Geodetica Italiana, terza serie, memoria n. 19.

Barzaghi R., M. Brovelli, A. Manzino, F. Sanso`, D. Sguerso, G. Sona (1997). Il Geoide in Italia e le sue future applicazioni, Atti dello Workshop *La Geodesia Spaziale nel Mediterraneo*, Cagliari 27 e 28 febbraio 1997.

Burrough P. A. and R. A. McDonnel (1998). Principles of Geographical Information Systems, Oxford University Press.

Heiskanen W. A., Moritz H. (1967). Physical geodesy. Freeman, San Francisco.

Surace L. (1997). La nuova rete geodetica nazionale IGM95: risultati e prospettive di utilizzazione. Bollettino di geodesia e Scienze Affini, anno LVI, n. 3, 357-378.

Torge W. (1989). Gravimetry. Walter de Gruyter Editor, Berlino – New York.

Vecchia O. (1955). Carta della densita` media sino al livello del mare in Italia, Pubblicazioni della Commissione Geodetica Italiana, terza serie, memoria n. 9.

Gravimetric Geoid Modelling with GIS

S.D. Pagiatakis[1] and C. Armenakis[2]
[1]Geodetic Survey Division
[2]Centre for Topographic Information
Natural Resources Canada, Earth Sciences, Geomatics Canada,
615 Booth Street, Ottawa, ON, Canada, K1A 0E9

Abstract: The amount, complexity and diversity of data required for gravimetric geoid modelling continue to increase at an unprecedented pace and possess a variety of characteristics including coverage, distribution and accuracy. Integrated geodesy trends indicate that future heterogeneous data will require merging using more complex models. The use of Geographic Information Systems (GIS) technology offers an effective and efficient approach to higher level data processing, analysis, synthesis, retrieval, representation and mapping. Effective representation/visualisation of spatio-temporal data supports the user's interpretation and understanding. Operations such as data integration, planning and decision making can be effectively and efficiently supported by the GIS's spatial modelling capabilities. In this paper, we outline data requirements in gravimetric geoid modelling and emphasise the need for an integrated and methodical approach to their handling using GIS. A GIS/RDBMS combination is highly recommended for handling high volume, high level and diverse data sets, as shown in an example from the Canadian effort to generate the topographic mass density map of the Canadian landmass for the refinement of the geoid model.

1. Introduction

With the advent of space-based geodetic positioning techniques, geoid modelling has acquired a renewed and increased interest, particularly in combination with the Global Positioning System (GPS). GPS with its ever increasing accuracy, provides an alternative and cost-effective method to geodetic levelling for height determination at the centimetre level, for a suite of applications, including mapping, geodetic positioning, navigation, oceanography and geophysical exploration projects.

The volume and complexity of data required in gravimetric geoid modelling are increasing at an unprecedented pace. Such data include gravity observations on land and ocean surface, gravity observations from airborne systems, various digital terrain elevation data sets originating from map digitisation of various scales, projections and datums, as well as from photogrammetric and non-conventional techniques (e.g., interferometric synthetic aperture radar - InSAR data). These data sets possess a variety of attributes including coverage, terrain types distribution (e.g. ice caps and lakes) and accuracy. Furthermore, integrated geodesy trends indicate that future heterogeneous data will require integration using even more complex models.

In order to ensure high value information, we must exercise dedicated commitment to a program of dynamic data handling, management and processing with solid quality control/assurance and processing methodology procedures (data flow) for storage, maintenance, update, retrieval and visualisation of the data. Thorough procedures for evaluating potential data and information needs, as well as hardware and software

requirements, must be established to achieve systems compatibility and effective data sharing. Relational database management systems (RDBMS) represented for instance by MSAccess ORACLE, dBASE, INGRES and others, are only part of the solution. The use of Geographic Information Systems (GIS) technology, whether on their own, or as part of a larger RDBMS, offers an effective and efficient approach to higher level data processing, analysis, synthesis, retrieval and other similar operations (*Wellar*, 1993).

GIS appear to be a powerful *enabling technology* in geoid modelling, for they present us with a variety of new ways of perceiving the handling, processing, visualisation, analysis and use of data. Traditionally, geodesists have kept a distance from this technology, perhaps as "uninformed customers" due to the fact that GIS have their conceptual roots in management and land information systems. However, the unprecedented volume of data, variety of data sources, different accuracies and distribution of heterogeneous data combined with high accuracy requirements in geoid modelling, greatly supports the use of GIS combined with a database, where all data can be and are archived.

2. Data Sets in Gravimetric Geoid Modelling

In principle, regional gravimetric geoid modelling requires a) good gravity coverage and b) an accurate representation of the topographic masses (masses above mean sea level). The former data set includes point gravity values obtained by land, shipborne and airborne gravimetry, while the latter involves a digital elevation model along with a crustal density profile. Preprocessing procedures are used to convert these *spatial data* sets into a format suitable for geoid calculations, which include, among others, data validation, error detection and editing, as well as data reduction. Data reduction in gravimetric geoid modelling produces a wealth of data larger in volume than that of the original data.

2.1. Gravity

In Canada, the National Gravity Database (NGDB) contains more than 750000 gravity points irregularly spaced across the country and offshore. Eventually, gravity data holdings by the geophysical exploration industry and by the provincial and regional governments may be integrated into the NGDB. Foreign agencies from neighbouring countries (US and Denmark) provide gravity data under special agreements for geoid modelling purposes, while new emerging technologies, such as airborne gravimetry, promise a wealth of new gravity data.

Shipborne gravity measurements are subject to errors from many sources and their seamless integration with land gravity measurements is a challenge. With the emergence of *Low Earth Orbit* (LEO) satellite and satellite altimetry missions, we will be able to evaluate the quality of the marine gravity data from independent sources. Presently, the Geodetic Survey Division and the Universities of New Brunswick and Calgary are collaborating to validate and integrate such heterogeneous data sets using a GIS (*Pagiatakis*, 1996).

2.2. Digital Elevation Models (DEM)

Terrain elevation data are necessary for the reduction of the observed gravity to the mean sea level prior to calculating the geoid model. For a centimetre geoid, the terrain data must be dense, accurate and more importantly, consistent in datum and projection. In Canada, the most recent digital elevation model covering the entire country is the Canadian Digital Elevation Data (CDED) produced by the Centre for Topographic Information of the

Department of Natural Resources. This DEM consists of an ordered array of ground elevations at regularly spaced intervals[1] and it is equivalent to DTED Level I data and format. It has been derived from the digital contours of the 1:250000 scale National Topographic System (NTS) maps of Canada. At the time of writing CDED production is nearing completion. Other complementary sources of elevation data include photogrammetrically derived digital elevation data, aerotriangulation and geodetic control points (*Natural Resources Canada*, 1997b).

There exist other local and regional DEMs in Canada that have been produced from larger scale maps or from aerial photographs. These DEMs have denser coverage that varies according to the terrain and the accuracy of the elevations is higher than the CDED. Presently, the Geodetic Survey Division has access to the DEMs of the provinces of New Brunswick and Alberta. More data are expected to be available in the near future. The challenge is to produce a unique and coherent DEM for the reduction of gravity observations, which entails proper integration (*merging*) of the various DEM components in a consistent and seamless fashion (*edge matching*). The incorporation of *metadata* information will be an essential part of these DEM data sets. The use of GIS technology for this integration task is inevitable. Certain procedures and standards still need to be developed for integrating other DEMs in the future. Presently, the Geodetic Survey Division is working towards the merging of the various DEMs for the purpose of determining a new, highly accurate geoid model for Canada by the year 2000 (*Pagiatakis*, 1996).

2.3. Topographic Mass Density

One of the many factors posing hurdles in an accurate geoid model determination is the effect of variable topographic mass density. Current procedures assume an average density of 2.67 g/cm^3, which appears to be inadequate for geoid modelling at the centimetre level of accuracy. *Martinec* (1993) showed theoretically that the lateral density variations of the topographical masses are large enough to introduce a sizeable effect on the gravity reductions, which, in turn, have an effect on the geoid model that can reach the decimetre level in mountainous areas. Martinec's study was confirmed by *Pagiatakis et al.*, (1998) and by *Vanicek et al.,* (1998) using actual mass density values.

Assigning mass density to geological structures is a difficult, and at times, a formidable task. It is a complex activity that requires understanding how the spatial relationships, inherent in digital geological maps (and thus in the spatial data), can be used with other data sets, models and theories to produce the digital topographic mass density layer. In addition, it requires the input of a different expertise combined with the merging and integration of heterogeneous data sets, which can be performed more easily in a GIS. In Section 4, we present briefly a case study from Canada. More details can be found in *Pagiatakis et al.*, (1998).

3. GIS and Database Management

A GIS is a system that handles, manages, processes and visualises spatial (geometry) data and its attributes (non-geometric characteristics). A GIS typically consists of computer software, hardware and peripherals that transform geographically referenced spatial data into

[1] The spacing varies with latitude. For latitude 45° to 68° the spacing is 3"x3", from 68° to 80° is 3"x6" and from 80° to 85° is 3"x12".

information on locations, spatial interactions and geographic relationships of the fixed and dynamic entities that occupy space in natural and built environments. GIS support the effective and efficient move to higher level data/information environments. The software components are (*i*) data acquisition, input and editing, (*ii*) data storage and database management, (*iii*) applications software, including database management systems, (*iv*) data analysis/modelling/synthesis and (*v*) data visualisation, output and dissemination of data and information, and the associated user's interfaces. As such, a GIS increases the information productivity by integrating multiple databases while minimising both the amount of redundant data and the amount of processing time involved in retrieval operations.

The impact of using a GIS system is best seen mainly in three functions: a) data visualisation, b) database management, and c) data analysis and modelling.

a) Data Visualisation

One very important capability of a GIS lies with data representation and data mapping. Effective representation/visualisation of spatio-temporal data supports the user's interpretation and understanding (*Armenakis*, 1996). Data visualisation, a term coined by NSF in 1987, provides a holistic approach to the entire data exploration process by integrating the human's synthetic and analytic abilities. Visualisation can be considered as a combination of computations, motion, interaction, computer graphics, electronic mapping, digital image processing and cognitive inference. In short, visualisation allows the user to display and explore data in a variety of ways. Functions may include 2-D and 3-D representations, both vector and raster data, zoom-in/out, panning, animation for dynamic phenomena, and a variety of data representations, symbology and colours.

b) Database Management

A database not only is concerned with the storage of information, but also includes the relationships among the stored data as opposed to a set of unrelated flat data files. A database management system (DBMS) resides between the applications software and the database (or data files). The major advantages of a DBMS are data independence from the applications programs, data integrity, data sharing, control of data redundancy, and complex data query, access and retrieval functions. There are four types of DBMS data models: hierarchical, network, relational and object-oriented (O-O) (e.g., *Aronoff,* 1989; *Scholl & Voisard*, 1991). The most widely used data model is the relational one, or Relational DBMS (RDBMS), while the O-O models are still emerging. Relational database management systems are based on matrices or tables for each entity in the database. Associated links based on topological, or other relationships are designed into relation tables such that, in principle, everything in the database can be related to everything else in the database.

c) Data Analysis and Modelling

The strength of GIS lies with their ability to process the original data to answer specific queries based on the spatial analysis and modelling functions (*Burrough*, 1993). These mathematical functions use both spatial and attribute data. They are complex activities and require an understanding of how the spatial relationships that are inherent in maps can be used with other models and theories. Operations such as data integration, planning and decision making can be effectively and efficiently supported by GIS spatial modelling capabilities.

Examples of functions include (Table 1): geometric transformations, geometric computations, data classification, data integration, overlay and intersection of spatial layers, neighbourhood analysis, connectivity operations, statistical analysis, data errors and quality and data search and retrieval.

Functions (examples)	Operations (examples)
Geometric transformations	Map projections, registration, rotations
Geometric computations	Distance, perimeter, area, slope
Data classification	Land use, soil type layers, values into classes
Data integration	Data conflation, edge matching, editing of graphics, generalisation
Overlay and intersection of spatial layers	Logical and arithmetic operations between the digital map layers
Neighbourhood analysis	Line-in-polygon, point-in-polygon operations, spatial search
Connectivity Operations	Proximity, network analysis
Statistical analysis	Spatial errors propagation, histograms, principal component analysis, spatial interpolations
Data search and retrieval	Spatial, attribute, temporal and conditional queries

Table 1. Examples of GIS functions and operations.

4. Case Study – The Topographic Mass Density Map of Canada

In early1997, the Geodetic Survey Division initiated a study to develop a prototype GIS-based system in order to assign rock density values to rock types present in the Skeena region of British Columbia, an area of considerable varying relief and relatively complex geological structure (*Fraser et al.*, 1998). This prototype system involved the integration of density values with bedrock geology maps, digital elevation data and gravity observations in a GIS. After the prototype system was tested and validated, the study was extended to include the whole Canadian landmass *(Pagiatakis et al.*, 1998). In this latter effort, the digital geological map of Canada (*Natural Resources Canada*, 1997a) was used as the base map, along with various detailed geological studies and in-situ rock density values from the National Gravity database (NGDB). Details of the development, as well as of the design issues can be found in *Pagiatakis et al.*, (1998).

The digital geological map of Canada contains 43 different categories of rocks based on sedimentary, metamorphic and volcanic processes. Density values were assigned to the geological units using existing geological studies. Where not available, theoretical density values were used (*Clark*, 1966). Table 2b shows a subset of the geological units from the Skeena region, B.C., their rock type [i.e. igneous (I), sedimentary (S) and metamorphic (M)], their rock composition and the assigned density values. The density values of only the major rock constituents in a unit were used to determine its representative density. Table 2a, as extracted from the digital geological map of Canada, was joined with the "*Rock and Density Data*" component to produce the final Table 2c for use in gravity data reduction. Table 2c can be easily shared in various formats to suit the needs of the user. For example, the table in its fully expanded form representing the whole Canadian landmass, was extracted as an MS Excel file and used by the University of New Brunswick to calculate the effect of topographic mass density variations on the Canadian geoid (*Vanicek et al.*, 1998).

Quality control/assurance procedures will be particularly useful for the future expansion of the system, merging of new data sets, establishment of procedures for evaluating the quality of the data sets and conduct, analysis and evaluation of the system tests vis-à-vis the design specifications.

Spatial Data ***(a)***

Unit ID	Rock Unit	Area (km^2)	Perimeter (km)
729	MLJm	0.021	1.241
936	EO	0.057	1.623
1028	EKgb	0.020	1.020
1206	MJi	0.030	1.238

Rock and Density Data ***(b)***

Rock Unit	Domain	Composition	Type	Density Range g/cm^3	Assigned Density g/cm^3	Source
EKgb	onshore	Gabbro	I	2.80-3.13	2.98	Sobczak et al. Gibb
EO	onshore	Undivided sedimentary rocks	S	****	2.56	Sobczak et al.
MJi	onshore	Granodiorite, quartz diorite	I	2.50-2.78 2.69-2.82	2.69	Gibb
MLJm	onshore	Mafic intrusive rocks-diorite, gabbro	I	2.64-2.89 2.80-3.13	2.88	Gibb

Spatial Data joined with and Rock and Density Data (result of join operation) ***(c)***

Unit ID	Rock Unit	Area (km^2)	Perimeter (km)	Density Range gr/cm^3	Assigned Density gr/cm^3
729	MLJm	0.021	1.241	2.64-2.89 2.80-3.13	2.88
936	EO	0.057	1.623	****	2.56
1028	EKgb	0.020	1.020	2.80-3.13	2.98
1206	MJi	0.030	1.238	2.50-2.78 2.69-2.82	2.69

Table 2. Spatial Information and Bedrock Geology Attribute Data. 'Unit ID' is a unique number assigned to each geological unit. 'Rock Unit' signifies the geological unit according to geological age and rock composition.

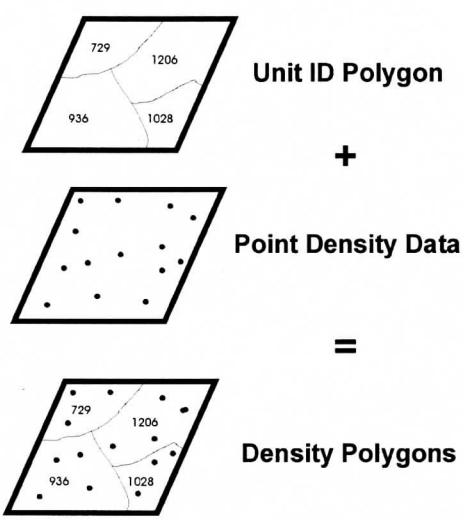

Fig. 1. Overlay and point-in-polygon analysis

After the assignment of density values to the various rock categories, the density tables were imported to the polygon layer of the geological map using the ArcView GIS-based software package. In a second stage, over 14000-point density values, determined from actual rock samples *(D.B. Hearty*, 1998; pers. com.), were overlaid according to the schematics of Figure 1. The comparison of the point densities with the assigned values was realised with a *point-in-polygon* analysis for all geological structures and showed a good agreement in spite of the fact that the assigned densities (first step) referred to general rock types.

The task of producing the topographic mass density layer from the geological map of Canada and from numerous general and detailed geological studies proved to be very challenging indeed. The amount and diversity of information available was impossible to handle via the usual route of creating many flat files and writing numerous pieces of software to edit, analyse, model, synthesise, store and retrieve the data. Most importantly, all spatial and attribute information encompassed in the geological map of Canada could not be used effectively and efficiently outside a GIS environment. In fact, most of the functions we performed to produce the density map, such as data analysis/modelling/synthesis, join operations, point-in-polygon analysis, visualisation and others would not be possible without a GIS.

5. Discussion

Further refinement of geoid modelling requires the inclusion and integration of data from a number of heterogeneous data sets. The access, retrieval, processing and normalisation of these masses of data can be greatly supported using spatial/attribute modelling and exploration tools available in current GIS and RDBMS systems. A prototype GIS system has been designed and successfully implemented to assign rock density values to the rock type for the Canadian landmass (*Fraser et al.*, 1998; *Pagiatakis et al.*, 1998). This system integrates density values with bedrock geology digital maps, digital elevation data and gravity observation data for improving the determination of the Canadian geoid (*Pagiatakis et al.*, 1998; *Vanicek et al.,* 1998).

The capabilities of current GIS and RDBMS systems to effectively and efficiently handle and process large volumes of heterogeneous spatial data indicate that their use will be inevitable in the further refinement of the geoid modelling.

Acknowledgements: This project was supported in part by the Earth Sciences Sector of the Department of Natural Resources Canada, through the Geomatics Professional Development Program (GPDP). Dave Fraser and Karen McEwen accepted the challenge to produce the geological map of Canada using GIS technology. We thank Alan K. Goodacre for providing his expertise in assigning density values to geological units and Bryne Hearty for providing all point density values from the archived density tables.

References

Armenakis, C. (1996). "Mapping of Spatio-Temporal Data in an Active Cartographic Environment,"*Geomatica, Vol. 50, No. 4*, pp. 401-413.

Aronoff, S. (1989). *Geographic Information Systems: A Management Perspective*, WDL Publications, Ottawa, Canada, 294p.

Burrough, P.A. (1993). *Principles of Geographic Information Systems for Land Resources Assessment*, Oxford Science Publications, 194p.

Clark, S.P. Jr, (Ed.), (1966). *Handbook of Physical Constants*. The Geological Society of America, Inc., New York.

Fraser, D., S.D. Pagiatakis and A.K. Goodacre (1998). Using In-situ Rock Density to Calculate Terrain Corrections to Gravity Observations. Proceedings of the 12th Annual Symposium on Geographic Information Systems; 6-9 April, 1998, Toronto, Ontario, Canada.

Gibb, R.A., (1968). "The densities of Precambrian rocks from northern Manitoba." *Canadian Journal of Earth Sciences, 5*, 433.

Martinec, Z., (1993). "Effect of Lateral density variations of topographical masses in view of improving geoid model accuracy over Canada.." Energy, Mines and Resources, Geomatics Canada, Geodetic Survey Division, Ottawa. Contract Report #93-002, 111 p.

Natural Resources Canada, (1997a). Geological Map of Canada – Map D1860A (CDROM, ver. 1:0; Jan. 97). Geological Survey of Canada ,Ottawa, Canada.

Natural Resources Canada, (1997b). Digital Elevation Model – Standards and Specifications. Centre for Topographic Information , NTDB Customer Support Group, Sherbrooke, Québec, Canada.

Pagiatakis, SD., (1996). "Towards a refined gravimetric geoid model for Canada, 1996-1999." *International Geoid Service Bulletin, 5*, 31-39.

Pagiatakis, SD, D. Fraser, K. McEwen, A.K. Goodacre and M. Véronneau (1998). Topographic Mass Density and Gravimetric Geoid Modelling. Proceedings of the 2nd Joint Meeting of the International Gravity Commission (IGC) and the International Geoid Commission (IGeC), 7-12 September 1998, Trieste, Italy. Università di Trieste (in preparation).

Sobczak, L.W., J.R. Weber and E.F. Roots, (1970). "Rock densities in the Queen Elizabeth Islands, Northwest Territories." Proceedings of the Geological Association of Canada, 21, 5-14.

Scholl M., A. Voisard (1991) "Object-Oriented Database Systems for geographic Applications: An Experiment with O_2", in Proceedings of the Workshop on Geographic Database Management Systems, G. Gambosi, M. Scholl, H.-W. Six (Eds), Springer-Verlag, DG XIII Commission of the European Communities, pp.103-137.

Vanicek, P., J. Huang, W. Brink and P. Novak, (1998). Preliminary investigation of the effect of topographical mass density variations on gravity and geoid in the Canadian Rocky Mountains. Progress report on Contract "Theoretical and Practical Refinements of Precise Geoid determination Methods. Natural Resources Canada, Geodetic Survey Division, Ottawa, Canada.

Wellar, B (1993). "GIS Fundamentals." In *Profiting from a Geographic Information System*, G.H. Castle (ed.), GIS World Inc. Colorado, pp. 3-21.

Geodetic Data Management with GIS and DBMS Techniques

L. Biagi (*), M.A. Brovelli (**), G. Salemi (***)

(*) Politecnico di Milano, IGeS, Facoltà di Ingegneria di Como
(**) Politecnico di Milano, Facoltà di Ingegneria - DIIAR
(***) Università di Udine, Dipartimento di Georisorse e Territorio

INTRODUCTION

The application of spatial geodesy techniques in topography and cartography often needs the knowledge of the accurate geoid estimate. In fact, as well known, the processing of GPS observations allows the determination of the geodetic coordinates in the WGS84 reference frame, while the height coordinate that interests the cartography is the orthometric height H. Therefore, for the transformation between orthometric H(P) and ellipsoidal h(P) height in a point P, the geoid undulation N(P) has to be known:

$$H(P) = h(P) - N(P)$$

So, in order to get homogeneous heights on the whole territory to be investigated, it is desirable to have as reference surface only one standard precision geoid. In the Italian area the ITALGEO95 geoid (Barzaghi et al., 1996), developed and calculated by the International Geoid Service (IGeS), could be used. ITALGEO95 is a gravimetric and geocentric geoid, estimated on a regular grid of 3'x 3' resolution, characterized by a general precision of 20 cm on all the national territory.

Therefore the problem arises for the people involved in the calculation, management and updating of the geoid, to have a system that allows a reliable and optimized search, analysis and visualization also of big amount of geodetic data. In order to overcome these problems we hypothesize to use the GIS techniques for the management and the visualization of the geodetic data (either raw or preprocessed): these systems may be customized to automate frequently performed actions and to create new commands allowing the estimate of the geoid in a specific and interesting area and the axtraction of auxiliary information as those, for instance, related to the data quality.

In the choice of the GIS, the examination of the methodological aspects for some key points (data structures and models, hybrid and object-oriented techniques, geomatics algorithms implementation, datum representation) suggests, up to now, the use of already consolidated techniques in almost-standard approaches.

DATA BASE MANAGEMENT SYSTEM

The variety of the needed information for the geoid computation and management suggests the use of a DBMS (Data Base Management System) storage method, rather than a file approach; indeed DBMS method allows for a simpler and better structured technique (Chiarandini & Salemi, 1998) of implementing the actions more frequently used (the data updating and the records extraction). Moreover the data represent one of the fundamental components of a GIS: therefore the tools used

for the file creation, the information manipulation, the data maintenance and updating must be carefully evaluated.

A database can be thought as a collection of one or more files or data tables stored in a structured format; in such way, the relations between the different columns or all the data can be coded and used by the DBMS software to manipulate, to extract and to recover the data. A database must satisfy the applications of several users with different requirements; thus it must be planned so that:

- the data storage method is independent from the programs that access the data base;
- a standard method, associated with validation tests, is imposed for the data input/output, in order to ensure the data integrity and the files consistence;
- some safety restrictions are applied for the access to specific data subsets;
- robust methods are adopted for the data reading and updating operations when several users can concurrently access to the files.

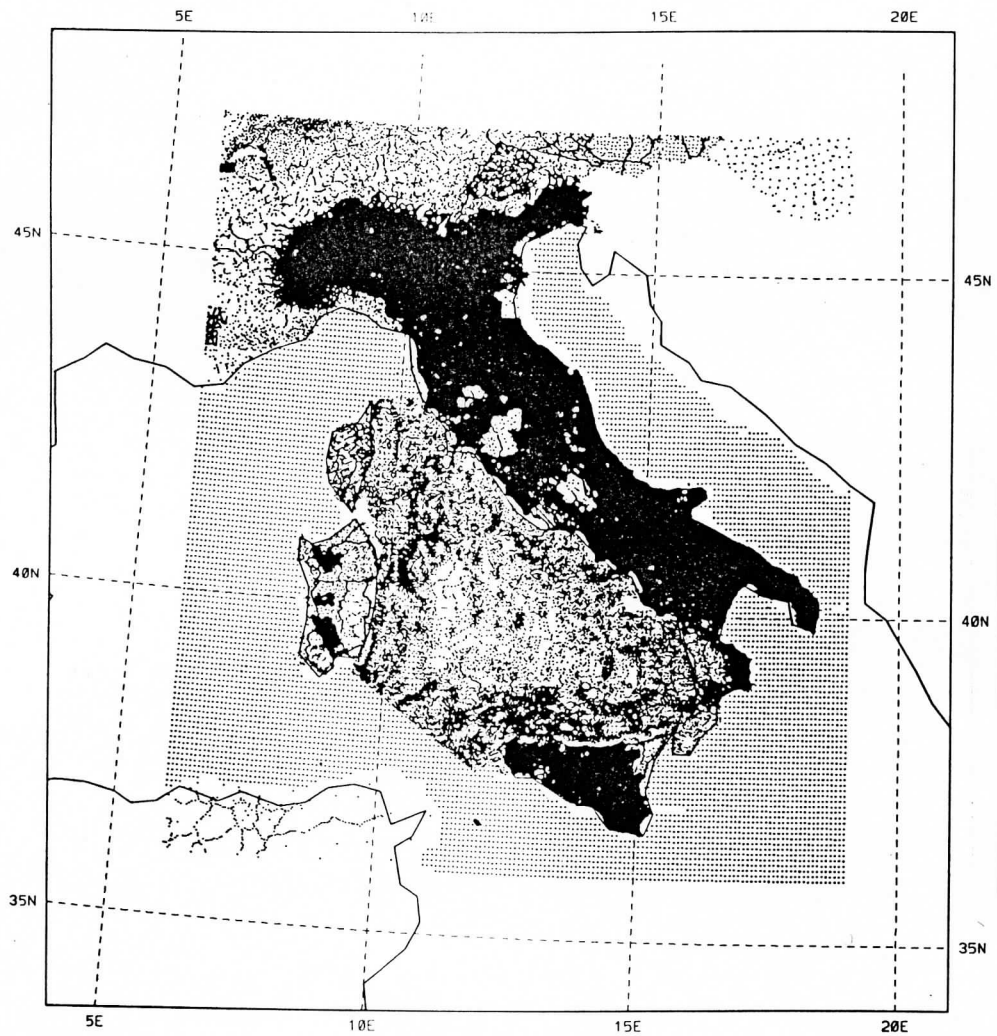

Fig. 1 – Observed gravity anomalies used for ITALGEO95 geoid computation (after Barzaghi et al., 1996)

GIS EVALUATION FOR GEODETIC APPLICATION

In the evaluation of the GIS to use in the geoid data management, the following items must be considered:

- price: both in monetary terms and in hardware requirements terms (standard and not devoted);
- diffusion: number of installations and types of hardware platforms;
- personalization: possibility of interaction with other products (either standard or personalized) through a high level programming language as C++ ;
- flexibility: both management of raster data and site point data (according to the data models more used in the geodetic community)

On these aspects, the GRASS software (Geographic Resources Analysis Support System), developed by U.S. Army Corps of Engineers Construction Engineeering Research Laboratory Office of GRASS Integration (USACERL-OGI), allows, with a non trivial installation, a very high level of customizing (USACERL, 1993) and has the capability to fulfil the urgent demands of not yet mature technologies (at least regarding to the available products).

On the subject of the database of the project ITALGEO-GIS, it must contain all the raw data needed to the geoid calculation, the computed estimates (ITALGEO90, ITALGEO95) and all the information that can be useful for the validation and the comparison of the estimates. Referring to the data model necessary to describe in a GIS environment the features or entities relavant to the geoid estimation, we can distinguish three data typologies: vectorial, site point and raster; therefore the data can be classified according to the following table:

TYPE	**DATA**
Vectorial	Coast lines
Site point	Observed gravity anomalies
	Vertical deviations
	Sea surface heights (SSH) from radaraltimetry data
	Ellipsoidal heights computed with GPS measurements
	Orthometric heights derived from levelling measurements
	Digital terrain models derived from stereoscopic tecniques
	Batimetry
	Coefficients of the geopotential global models
Raster	Gravity anomalies (model)
	Gravity anomalies due to the residual terrain corrections (RTC)
	Geoid estimated by RTC
	Geoid residual calculated via Fast Collocation
	Geoid (model)
	ITALGEO95 model
	ITALGEO90 model
	Digital terrain models
	Crustal density models
	Moho depth models
	Collocation solutions

Tab. 1 – Examples of vectorial, site point and raster data.

Every data type needs associated information about its quality and its use. For instance, the file of observed gravity anomalies (composed by 296.244 value on site points) should be characterized by:

- the geographical position of the datum;
- its source:
  - Italian file (4 original files);
  - BGI file;
  - digitized maps by the Salonicco University from gravimetric maps compiled by Morelli;
  - digitized maps by Milan Polytechnic from gravimetric maps compiled by Morelli;
- a validation code;
- its use [in the calculation of the ITALGEO95 model an integrated file has been derived from the original data set; the derived file on earth-sea is 1'x1' pseudo-gridded, on sea is 5'x5' gridded (Fig. 1)]

Fig. 2 - The Italian digital terrain model (raster data)

The Italian DTM is an example of raster data (Fig. 2), obtained by integration of several DTM's coming from different sources, with different resolutions and spatial characteristics. This is a binary file containing 7202x6122 heights on a geographical 7.5"x10" grid; to this file a "source DTM's" file, with the encodded information about the original DTM source, is associated.

Of course, the database must be built so that the integration both of new data and new information (e. g., the reference datum of the observed height anomalies and the possible use in the database for the calculation of the next Italian gravimetric geoid) are allowed.

Moreover, similar data types are obtained by different kinds of measurements and need different storage methods. For instance, the ITALGEO95 geoid computed by Remove-Restore and by Fast Collocation (Fig. 3) has a raster data format, corresponding to the geoid undulation values on a geographical grid; nevertheless, the geoid calculated on sparse points by local collocation or by combination of GPS measurements and geometric levelling must be managed remembering the different data model (site point type) as well as the different estimate methodologies.

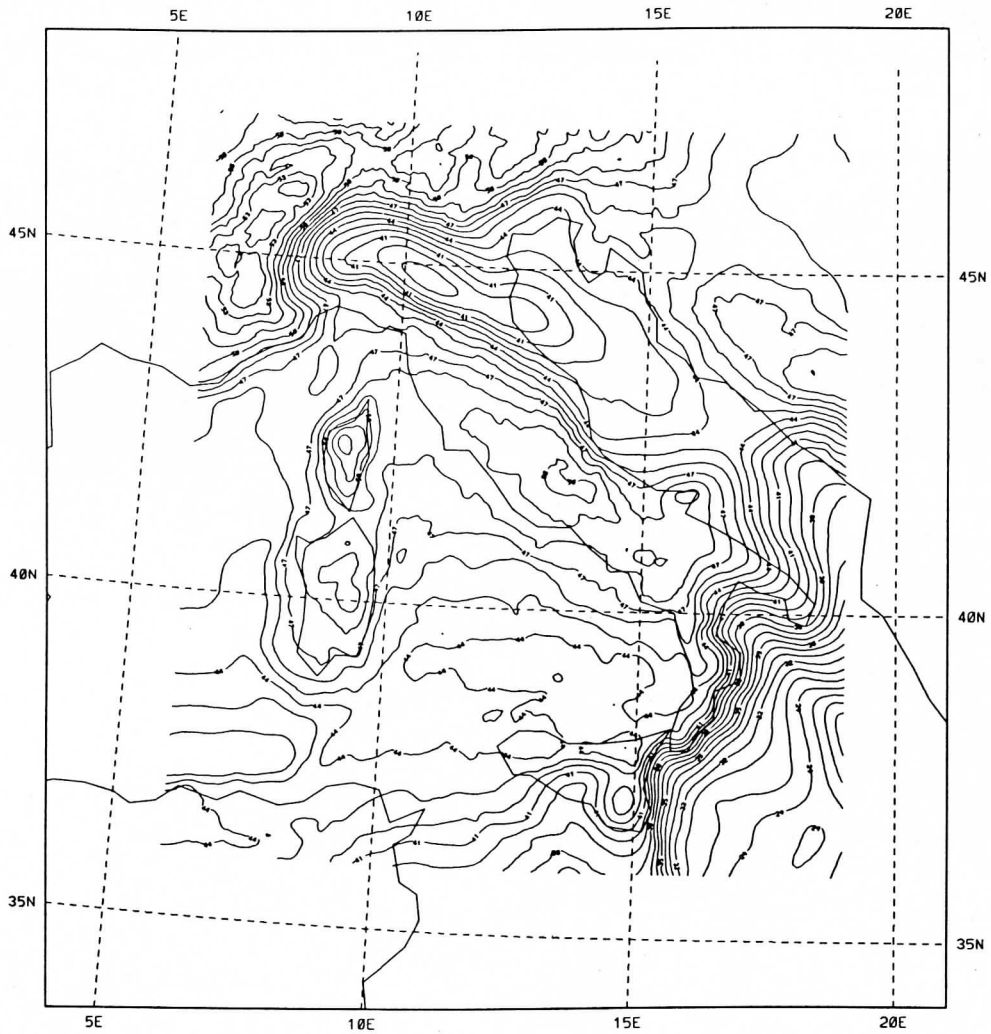

Fig. 3 – The ITALGEO95 geoid (Barzaghi et al., 1996).

In the evaluation of the GIS data management kernel, the fact that the dataset can be rather articulated and large (for the raw data files dimensions), has to be considered with attention. For example, the file describing the gravity anomalies data for the Italian area contains the observed values for 296.244 sparse points and the Italian DTM, used for the residual terrain correction in the ITALGEO95 computation, is composed of 44.090.644 values. These values are numerically massive; however they don't constitute a valid presupposition for the use of techniques related to the

VLDB (Very Large Date Base); indeed, in this case a specialized hardware and a specific software would be required.

SPATIAL DATA MODELS

In the gravimetric geoid management the possibility of accessing different data types (i.e. arcs, polygons, site points and raster data) is needed; this is true not only for the raw data evaluation, but also for the pre- and post- processing phases. In general terms, the data contained in a GIS database are composed by two components:

- the geographical attribute, that is the spatial reference of the datum (i. e. the coordinates of the datum point);
- the statistic or textual attribute, that contains the qualitative information associated to the datum.

The geometric component can be vectorial (the points coordinates which describe the geometric form of an object) or raster (a set of pixel corresponding to the particular object). The textual component is given by the set of the different attributes (numerical, string,...) associated to the geometric component of the datum.

The vectorial representation of an object is an attempt of as much as possible exact representation; the coordinates space is supposed continuous and therefore all the concepts of position, distance and dimension are those ordinary. If we consider the bidimensional case, the fundamental entities for such structures are:

- points (all the geographical and graphics entities that can be defined with a couple of coordinates (x,y); besides the coordinates, other data must be filed that describe the point type and eventually some relative information);
- line (in the simplest case, the initial and the ending points and the symbol used for the display must be filed; a chain is a set of couples of coordinates which describe a continuous complex line). Simple lines and chains don't include information on the topology; in order to introduce topology in the lines nets we need to build specific pointers in the data structure. This is often realized through punctual entities with topologic structures, the so called nodes);
- area (the polygons areas, said also region, can be represented by different approaches. The purpose of a polygonal data structure is to describe the topologic of areas, like form, nearness and hierarchy. This is for instance possible through the complete topologic structuring, based on the description with nodes and arcs).

In the raster data type structure, the basic element is the cell (pixel); the representation isn't continuous, but discrete; this weighs in a substantial way if the estimate of lengths or surfaces is required. Every cell in the bidimensional matrix can contain only one value: therefore, if different geographical attributes exists, they must be represented by matrices set, that are called overlays. Such concept is entirely equivalent to the overlapping of different separate cartographic types used for producing a map. In the simplest form, the concept of overlay is realized in the raster data structure superimposing bidimensional matrices and getting in such way a three-dimensional structure.

Comparing the two different data models, we can note that a data structure of vectorial type allows a good representation of the data entity model; moreover it is a compact data structure, in which the topology can be described expressly. Besides, the graphic representation is accurate at all the scales and the coordinates transformation is an easy operation. Opposite, it possesses a complex data structure, where the combination of nets of many polygons (by intersection and overlay) is difficult and requires notable resources of calculation.

The raster data type structure (that is mostly used for the data set which are at our disposal) is quite simpler; moreover it allows an easy mathematical modeling since all the spatial entities have a simple and regular form. The main objection to the raster model (Fig. 4) is that this one, compared to vectorial model, is penalized in terms of hardware problems (memory usage and computation resources); today this fact has no more reason because of the achieved technological developments; so the final user has the maximum choice freedom, according to other considerations.

The vectorial model is more functional in the GIS softwares finalized to planning, nets management and to administration (Intergraph, ARC/INFO, ArcView, MapInfo). In general such software implement also some functions for the raster data analysis, even if the major part of the analyses are developed on the vectorial model. The raster model, instead, has its principal application in the analysis of natural phenomenons, like the geophysics, the atmospheric and the environmental modeling (GRASS, Idrisi). In the raster GIS, some functions for vectorial data management are implemented, although the functionalities for the raster data analysis are mostly emphasizes (for instance, in GRASS the function r.mapcalc is available, which is an algebra for the raster data management and allows to perform complex operations on grids with simple commands).

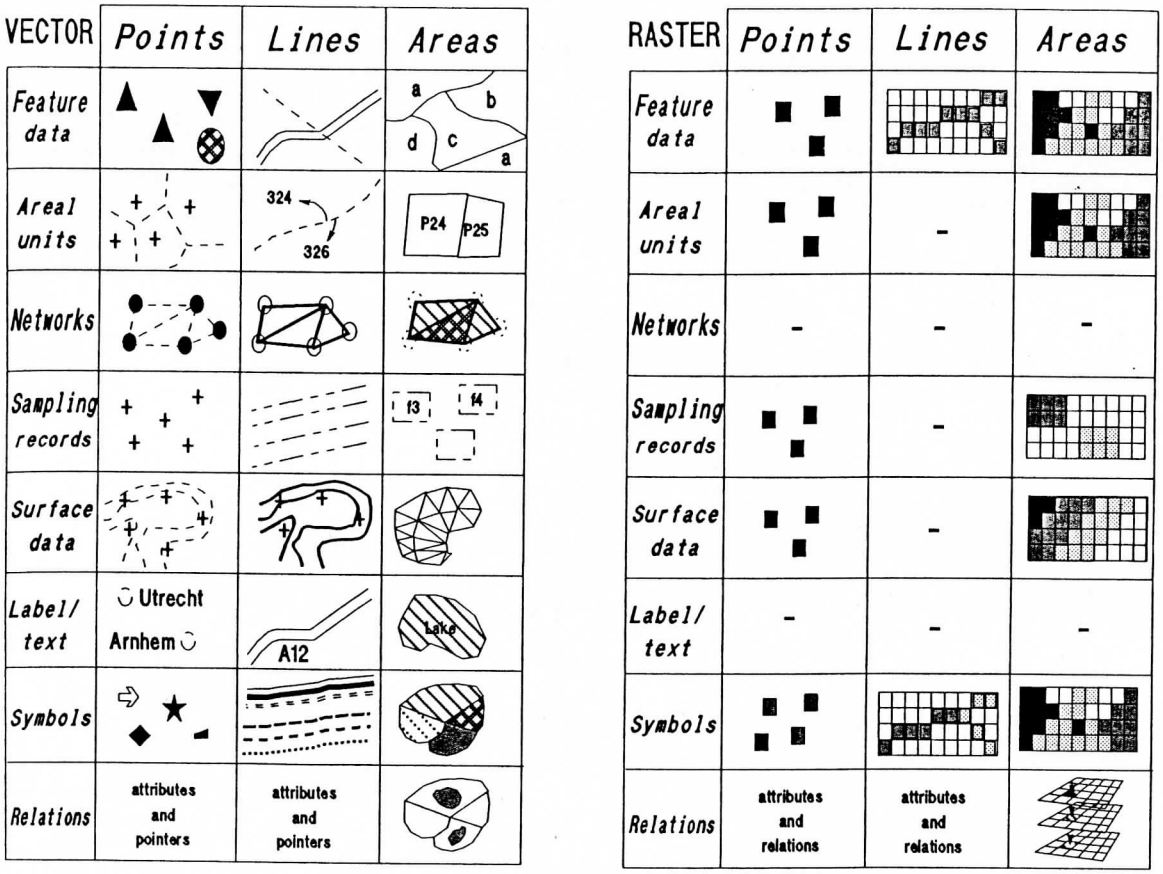

Fig. 4 – The two different approaches to manage and to display data using vector entity models and raster models (after Burrough & McDonnell, 1998)

HYBRID AND OBIECT-ORIENTED ARCHITECTURES

Regarding the information management, a hybrid architecture is currently priviliged in the GIS: the textual part is structured using a relational data model (Codd, 1970) and is managed by a RDBMS (Relational Data Base Management System); the geometric part is managed by a proprietary system, in order to obtain a more efficient storage of the spatial component of the data. The choice of a spatial database is quite different from that concerning traditional DBMS like, for example, a business administration one: in fact the spatial databases are characterized by the spatial aspects that must be considered while planning the archive itself. In particular the relational database management systems, that support the most used GIS-engine interfaces (Pennywitt et al., 1992), must have extra features such the spatial extensions and the spatial indexing methods, in order to optimize the spatial data management (Chiarandini & Salemi, 1997).

The quad-tree structures for raster data and the k-d-tree for site point type are an example in such sense. When many topological information coming from vectorial data must be stored (in the indexes) the B-tree structures result extremely useful; such structures are realized with "internal nodes" and "leaf nodes" and remember the structure of a tree. Furthermore, structures exist that allow to include the geometric properties of the database in the index structuring; in this case, the reference is to the R-tree model and to the MBR (Minimal Bounding Rectangles) model, in which the space is divided in "minimalis" rectangles that contain, in the their intern, the geo-referenced objects.

Another possible approach is the use of integrated systems, in which the spatial component (the files containing the points coordinates and the topology of the geometric elements) coexists with the textual component (the attributes files); the different data types are in relationship, so that a geometric-statistic database is created. However, the implementation of such a system is complicated because it is realized extending an already existing system (i. e. adding to a RDBMS graphics features like the graphic management of the data and the possibility of operations on spatial data).

Finally the last possibility is offered from the object oriented systems, that have been developed beginning from the end of the '80 for the UNIX environment (and now available for the PC too); these systems can operate on a client-server architecture and can be used for implementing a GIS with integrated architecture (because the object oriented structure allows to treat in the same way the modeling and management both of the textual part and of the geometric part of the same entity).

So, in DBMS research field, there are two different approaches:

- the integration of a RDBMS with the structures typical of the object paradigm;
- the construction of a new system which is independent from the architecture of the RDBMS.

In the object oriented systems an object, that is a real entity (e. g. a natural or artificial feature), is specified by:

- the object status, as attributes set (instance variables);
- the object register: methods that operate on the value of the attributes (instance methods).

The procedures implemented for acting on the attributes value are integral part of the object and they don't belong to the application that manages the data base. So, the spatial and the statistic part of the data are treated in the same way. In the comparison between these possible systems, the diffusion of the geo-relational models, or the hybrid data structures, connected to the possibilities offered by some actual commercial RDBMS (Oracle, Informix, Ingres, Info) which allow, either to represent the geometry and the topology of the spatial objects, either to manage their attributes. The

advantages are manifold: for instance, the data attributes don't need to be memorized in a spatial data base and can be managed (expansion, access, cancellation, updating) without modifying the spatial data base. Besides, the data structures can be defined by standard methods using the data dictionaries; the data themselves can be recovered using common and RDBMS independent methods as the SQL (Structured Query Language).

On the contrary the GIS based on object oriented database are characterized by little differences between the objects from the real world and the concepts and their representation. It is possible, then, to integrate in the same database raster and vectorial data structures, with a disk space occupation smaller than that involved by the relational entities model: indeed it is necessary to memorize a small number of index files. Unfortunately, today one oriented model (O-O) doesn't exist which is universally approved; in such case, products different with different standards could aim to an only O-O language. Besides, working with continuous spatial surfaces, it is difficult to identify the "objects" and the complexity of the objects types in the system doesn't allow the use of standard as the SQL as general interrogation language or as system for the queries optimization.

Today, therefore, the GIS systems based on relational hybrid techniques have a great diffusion for the use facilities, for the possibility to easily integrate the attributes of the data coming from different systems and for the possibility to modify the spatial data after their insertion in the system. A lot however has still to be developed. In fact, in all the existent systems, the management of the temporal data is rather limited; Postgres software is an exception because foresees the concept of time travel that allows an easy management of the historical series. Besides, usually the coordinates data are managed from the DBMS in a less rigorous way (obviously this depends from the implementations) and this involves safety and integrity data problems.

GEOID UPDATING

Regarding the geoid model updating (Barzaghi & Borghi, 1998), the project foresees the calculation of the geoid in points which do not belong to the collocation grid. There are three levels of increasing precision which are proportional to the CPU time consuming:

A. Simple interpolation using generic programs and algorithms;
B. Interpolation through spectrum analysis of the signal and calculation on the three frequencies:

$$\hat{N}(P) = \hat{N}^{M}(P) + \hat{N}^{RTC}(P) + \hat{N}^{r}(P)$$

where:

- $\hat{N}^{M}$ is the contribute of the anomalous potential model, estimated in the point P: $\hat{N}^{M} = R\sum_{n=2}^{N_{max}}\sum_{m=0}^{n}[C_{nm}\cos m\lambda_P + S_{nm} sinm\lambda_P]P_{nm}(sin\varphi_P)$,
- C_{nm} = geopotenzial normalized coefficients of the anomalous potential,
- P_{nm} = associated Legendre functions,
- n_{max} = maximum degree of the geopotential global model;
- $\hat{N}^{RTC}$ is the effect of the residual terrain correction;
- $\hat{N}^{r}$ is the collocation solution: $\hat{N}^{r} = C_{N\Delta g}[C_{\Delta g\Delta g} + \sigma^2 I]^{-1}[\Delta g_r + n_r] = C_{N\Delta g}\hat{s}$,
- $\hat{s}$ = solution vector obtained in the calculation of the collocation estimate (e.g. ITALGEO95),

- $C_{N\Delta g}$ = covariance to be estimated between the point P and the points of the collocation grid.

C. More refined interpolation based on the introduction of additional local information as:
- new gravity anomaly observations;
- digital terrain models more refined;
- geoid ondulations obtained by GPS observations and levelling.

The estimated geoid should be integrated with additional information obtained from the database: these allow to fully evaluate the result quality (density of observations in the calculation area, source of the data used,...). As examples we can hyphotize the production of reports, in which the following information are given:
1) about the gravity anomaly data:
- density of the original data in the area where the geoid has been locally estimated;
- density of the data used for the construction of the grid for the collocation solution;
- source of the data in the selected zone;
- presence of outliers;

2) about the residual anomaly data:
- statistic in the considered area;
- covariance local function;

3) about the estimated geoid:
- comparisons with geoid determined by GPS and levelling;
- statistics in the selected area.

What's more, on the selection criterions for the GIS to be used, it is necessary to remember that the system must not only allow the objects positioning in the space but also the study of continuous variations in the space; in other words, a "good database" which furnish thematic maps or contours maps is not enough.

Another aspect connected to the data is the implementation of sophisticated algorithms for their analysis in the GIS. For instance the exact splines functions are commonly used in the GIS for curves and contour lines regularizing. However, in the case that the data have been sampled in two or three dimensions, the effects due to the natural variation or to the measurement errors can be so large to produce locally anomalies which can be too much little or, on the opposite side, too much large. These anomalies can be removed using the "thin plate" spline functions, where the surface obtained by an exact spline is replaced by a locally regularized average. In this case the spline p(x) would have to pass not too far from the observed values: so the regularization spline is the function f that minimizes the following expression:

$$A(f) + \sum_{i=1}^{N} w_i^2 [f(x_i) - y(x_i)]^2$$

where the term A(f) represents the regularity of the function f; the second term represents its proximity or fidelity to the data; the weights w_i must be inversely proportional to the error variance:

$$w_i^2 = p / Var[\varepsilon(x_i)] = p / s_i^2$$

where the value of p reflects the relative importance assigned by the user to every characteristic of the regularization splines.

This type of approach, frequently used for interpolating quotas from a DEM (Digital Elevation Model) in a fast and efficient way for wide areas, has been experimented in GRASS for the interpolation of attributes from a spline, function of the longitude, of the latitude and of the height (Hutchinson, 1995; Mitasova et al., 1995).

DATA HETEROGENEITY

In research organizations, as IGeS, the access to scientific and statistic data stored in heterogeneous and multidisciplinary databases (SSDB: Scientific Statistics Data Base) is often necessary. This operation is sometimes performed by the technique of the cross reference linkage, by using keys that could reveal itself inaccurate. Particularly, between agencies afferent to one structure, often happens that common conventions do not exist on the naming, the description, the formatting, the representation and the structure of the data. Straight, data that contain the same information can have different representations either logic or physic, and sometimes different values. This involves the necessity to apply scientific techniques and statistics to identify record that are similar but not necessarily identical (Fig. 5).

A generalized model was proposed for resolving these data heterogeneity problems, which is based on the use of a probabilistic framework to recover data that are the same or similar and that are identified differently in the same or in different databases. Particularly, the comparison and the probabilistic matching of the records are possible, when the values of their attributes are near or similar, but not necessarily identical. This approach allows, besides, to somehow model the uncertainty in the data retrieval for an heterogeneous environment.

Two types of incompatibility for data representation have been distinguished: semantic and structural incompatibilities. For the first type, the problems concern specifically the synonyms, the homonyms, the codes, the errors of recording, the incomplete information, the asyncronous updatings. These problems are not resolvable with pure unsupervised methods, because the data specificity requires the presence of the human operator. However, this presence can be minimized by rigidly applying some "behavior rules" or by rigidly codifying data between the data suppliers and the data users. Recording errors, which are due to typographical mistakes, must be resolved using more attention by the human operator; synonyms problems can be worked out using the same identifiers for the same entity in different databases; homonyms are represented by different entities which share the same identifier in different databases. It's obvious that the last two problems don't exist if the same codifying rules are applied by different agencies.

We analyze, therefore, the types of structural incompatibility that are verified when the attributes are differently defined in different database:

- Type mismatch: the same attribute can be defined as character in a database and numerical in another one; or multidimensional in a DB and single-valued in another one.
- Fully grown: for instance, the use of a different format for the same element (day/month/year vs month/day/year).
- Unity: the use of different measurement units for the same element in different databases.
- Granularity: the measures that represent the given elements differ to level of granularity: for example a dose per month or per year.

Different approaches were used to resolve these conflicts and also were compared (Chatterjee & Segev, 1991). Just two examples: the rules approaches (Wang & Madnick, 1989) which use non-unique attributes to identify istance; the storing of possible synonyms of a particular object in a table for conflict resolution (Markowitz, 1991). More problems arise when the missing and incomplete information must be represented using null values in standard relational databases. In

fact some databases don't allow null values and the meaning of null can vary ranging from unkonw to unavailable to not applicable.

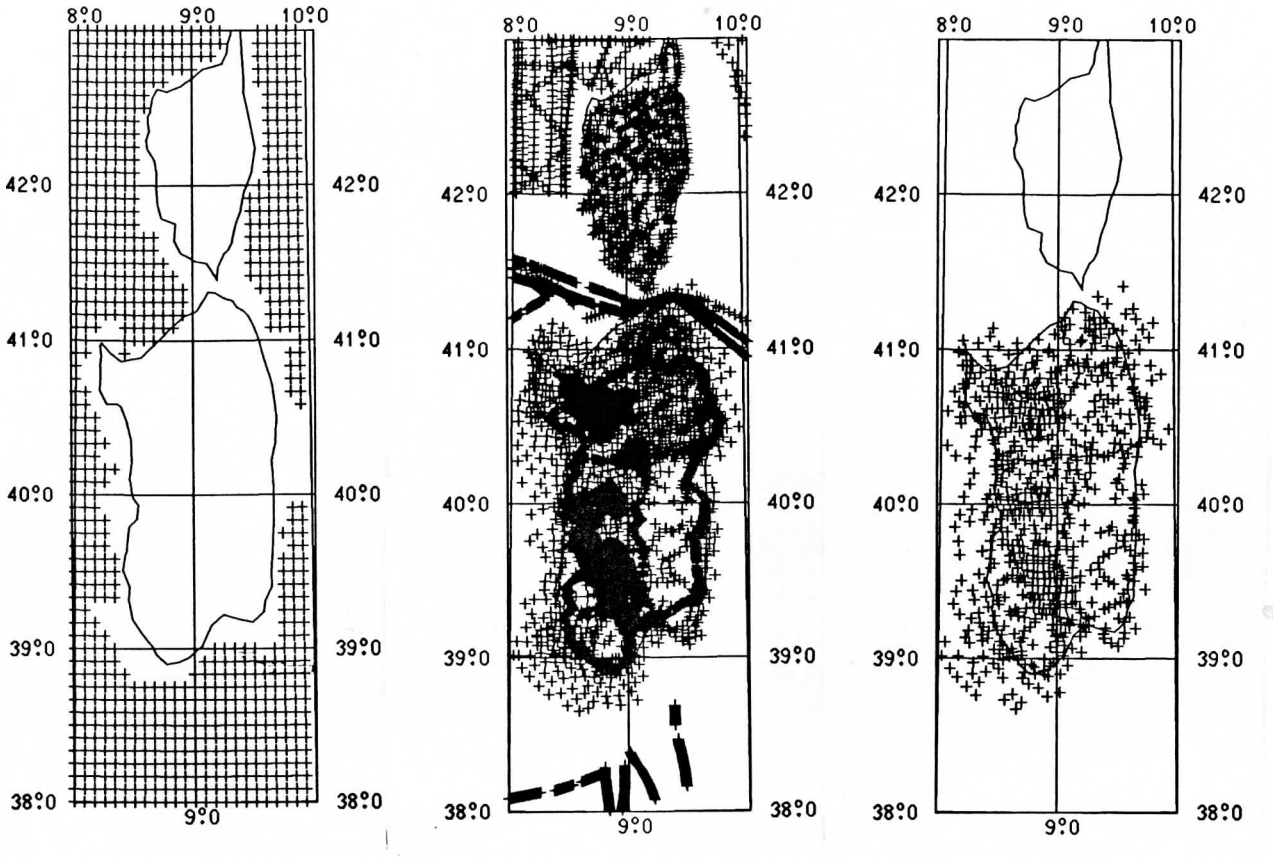

Fig. 5 – Sardinia experiment: different data coming from different databases.
(Left: the bathymetric data file. Center: the gravimetric D.M.A. data file.
Right: the gravimetric Italian data file).

CONCLUSIONS

It is obvious the importance of developing systems able to manage different and similar data coming from different agencies with different data storage approaches. The solution seems to be provided by the GIS systems, both in the data base management and in the visualization tools. In this paper the first topic was explored and the approach based on the RDBMS with spatial extensions seems to be the most promising. At the present we propose the use of GRASS software for the geodetic data management; moreover we are evaluating the possibilities of interfacing this GIS with the Postgres data base, in which index structures like the R-trees are implemented.

REFERENCES

AA.VV. (1994) - International School for determination and use of the geoid - Lecture Notes International Geoid Service - DIIAR - Politecnico di Milano.

Barzaghi, R.; Borghi, A. (1998) - The definition of a regional geopotential field for precise gravity field modelling, I.Ge.S. Bulletin, 7: 52-67.

Barzaghi, R.; Brovelli, M. A.; Manzino, A.; Sguerso, D.; Sona, G. (1996) - The new Italian quasi-geoid: Italgeo95, Bollettino di Geofisica e Scienze Affini, anno LV, 1: 57-72.

Barzaghi, R.; Guzzetti, F.; Pinto, L. (1998) - Problemi connessi all'utilizzo di reti GPS per l'inquadramento altimetrico della cartografia a grande scala, Bollettino della Sifet, 1: 17-36.

Biagi L., Brovelli M.A., Salemi G., 1998, Tecniche GIS per la gestione e rappresentazione dei geoidi, Atti della II conferenze nazionale ASITA, Novembre 1998, pp. 317-322.

Burroghs P. A. , 1986, Principles of Geographic Information Systems for land resources assesment, Oxford University Monographs on Soil and Resources Survey, n. 12, Oxford, Uk:Clarendon Press.

Burrough P. A., McDonnell R. A., 1988, Principles of Geographical Information Systems, Oxford University Press.

Chatterjee A., Segev A. (1991), Data manipulation in heterogeneous databases, ACM SIGMOD Record, 20 (4): 64-68, December 1991.

Chiarandini A., Salemi G. (1997), Estensione della Tecnologia delle Basi di Dati Relazionali per Sviluppare Applicazioni G.I.S. Integrate, Bollettino della Sifet, 1: 83-100.

Chiarandini A., Salemi G. (1998), A Database Approach for Geodetic Data Management, I.Ge.S. Bulletin, 7: 84-88.

Codd E. (1970), A Relational Model for Large Shared Data Banks, Communications of the ACM, vol. 13, n. 6, June 1970.

Healy R.G. (1991) - Database Management System in Geographical Information Systems (M.F.Goodchild, D. Maguire, D. Rhind eds.), Longman Scientific & Technical, vol. 2, pp. 251-267;

Hutchinson, M. F. (1995) - Interpolating mean rainfall using thin plate smoothing splines, International Journal of Geographical Information Systems, 9:385-404.

Jones C. ,1997, Geographical Information System and Computer Cartography, Addison Wesley Longman Limited, Essex, England.

Knudsen, T. (1996) - Geophysical Use of Geographical Information Systems, Technical Report n.8 - National Survey and Cadastre - Denmark.

Laurini R. and Thomson D. , 1992, Fundamental of Spatial Information Systems, The Apic Series,San Diego, Ca.

Markowitz, V. M. (1991) – An architecture for identying objects in multidatabses, in Proceedings of the First International Workshop on Interoperability in Multidatabases Systems, Kyoto, Japan, pp. 294-301.

Mitasova, H.; Mitas, L.; Brown, W. M.; Gerdes, D. P.; Kosinovsky, I.; Baker, T. (1995) - Modelling spatially and temporally distributed phenomena: new methods and tools for Grass GIS, International Journal of Geographical Information Systems, 9: 433-446.

Pennywitt K.E., Barrett P.J., Ray M.M. (1992) – GRASS-to-DBMS interfacing : a survey of current research effort with recommendations for future GRASS enhancements, Report of the Project no. A-9110-000, Computer Science and Information Technology Laboratory Georgia Tech Research Institute.

USACERL (1993) - GRASS 4.1 User's Reference Manual, Champaign, Illinois, United States Army Corps of Engineers Construction Engineering Research Laboratories.

Wang Y. R., Madnick S. E. (1989), The inter-database instance identification problem in integrating autonomous systems, in Proceedings of the Fifth International Conference on Data Engineering, Los Angeles, California, February 1989, pp. 46-55